Predicting the Effect of Solvents and Impurities/Additives on Crystal Shape and Growth Kinetics

A Proposal to IFPRI

Michael F. Doherty*
Department of Chemical Engineering
University of California
Santa Barbara, CA 93106-5080 USA

May 20, 2017

Abstract

The goal of this research is to develop a practical engineering tool for predicting the relative growth rates (growth kinetics) and morphology of solution-grown faceted crystals, including the effects of solvent, and impurities/additives. The underlying crystal growth methodology (i.e., without the presence of additives) will be tested on a variety of solute-solvent systems, including: L-cystine, paracetamol, olanzapine, and sodium chloride, all grown from aqueous solution. Organic crystals will also be tested on non-aqueous solvents, e.g., ethanol, ethyl acetate, etc. We will extend our models to account for the effect of additives/impurities for which some new models will be developed, and some existing ones will be re-deployed. Test systems will include L-cystine grown from aqueous solution in the presence of L-cystine dimethyl ester, adipic acid grown out of aqueous solution in the presence of hexanoic acid, and octanoic acid additives; naphthalene grown from hexane (solvent) in the presence of biphenyl (additive), paracetamol (acetaminophen) grown from aqueous solution in the presence of p-acetoxyacetanilide impurity; and potassium chloride grown from aqueous solution in the presence of lead chloride. All these systems have ample experimental data available in the literature.

1 Introduction

The choice of solvent is perhaps the most critical design decision in crystallization from solution, with implications for solubility and impurity rejection as well as growth kinetics and crys-

*Phone: 805-893-5309; Fax: 805-893-4731; E-mail: mfd@engineering.ucsb.edu

tal morphology. Understanding and being able to predict solution effects (solvents and impurities/additives) on crystal habit is valuable from an engineering perspective, so the optimum morphology can be achieved. When coupled with the other growth conditions the design space becomes very large, so screening through it using a crystal growth model is preferable and will lead to a more targeted application of experimental resources[1].

My research group has developed[2–4] a mechanistic solid-state chemistry growth model that predicts the crystal habit of organic molecular compounds under defined growth conditions, through consideration of established mechanisms such as spiral and two-dimensional (2D) nucleation & growth. These mechanistic modeling techniques have since been successfully applied by others to various crystalline explosives, where accurate morphological predictions have been obtained for 1,3,5-Trinitroperhydro-1,3,5-triazine (RDX)[5], β-Octahydro-1,3,5,7-tetranitro-1,3,5,7-tetrazocine (β-HMX)[6] & 2,2-Dinitroethene-1,1-diamine (DADNE or FOX-7)[7].

Accounting for the interaction energetics at kink sites on crystal surfaces is critical to the model, and the presence of a solvent alters the relevant surface interactions due to solvation of the crystal surface. To correctly predict this effect one must determine how these interactions are modified by the presence of a solvent and/or additives in solution. The most accurate method for obtaining the relevant free energies, kink densities and kink rates used in the model (see section on Background) would be molecular simulations. This might be practical for simple crystal systems where there are few types of kink sites, but even so it would be computationally lengthy. For more complicated crystal systems there can be many distinct kink sites (the $(10\bar{1}4)$ surface of calcite has 32 kink sites[8], while aragonite has 112 distinct kinks[9], RDX has 8), which further multiplies the necessary number of molecular simulations to obtain the input parameters required by the model, rendering this approach impractical for engineering purposes. The challenge is to find a practical method to estimate solvent-modified surface interactions that offers an improvement upon previous methodologies adopted within the mechanistic model[2,10–12]. As explained later in this proposal, we do intend to employ molecular simulation, but strictly for the purpose of understanding surface interactions so that we can develop a general analytical model that replaces the molecular simulations in the overall methodology. We believe we have a way of accomplishing this feat.

We propose the development of a new generation of models for *predicting* relative growth rates for faceted crystals of non-centrosymmetric (noncentric) compounds (both organic and ionic crystals, i.e., crystals of realistic complexity) grown from solution. This proposal outlines the key kinetic

and thermodynamic quantities and we propose practical ways for calculating them reliably. The main objectives of this research are (others are mentioned throughout):

1. Develop methods to determine the free energy landscape and the energy barriers for solute incorporation (including solvation/desolvation effects) at different types of kink sites using rare-event simulation. The methods will be tested on the following selection of compounds which are chosen because of the ample existing experimental data: L-cystine, paracetamol, olanzapine, sodium chloride, all grown from aqueous solution. The organic compounds will also be tested on non-aqueous solvents, e.g., ethanol, ethyl acetate, etc.

2. Develop an analytical model for growth unit attachment rate at crystal surfaces *without* the need for molecular simulation.

3. Extend the model/approach to include impurities/additive molecules in solution.

4. Test our models at nanoscopic length scales through atomic force microscopy experiments on the above test systems.

The structure of the proposal is as follows. First, we provide some background for the basis of our mechanistic growth models for predicting crystal shape. This is followed by the proposed research, where new concepts for generalizing our models to noncentric growth units are described along with a brief description of the experimental methods and facilities.

2 Background and Preliminary Results

At low levels of supersaturation (typical of many crystallizations) the dominant growth mechanism is layered growth on crystal faces by the spiral mechanism. Under these conditions diffusion of solute molecules to the crystal interface is rapid, and the rate controlling step is the surface integration of solute growth units at kink sites along the flowing steps.[13]

2.1 Growth Mechanisms

Our model is based on detailed mechanistic theories of crystal growth – the 2-D nucleation, and the screw dislocation mechanism of Burton, Cabrera and Frank (BCF)[14] – in which relative face growth rates depend on face-dependent parameters. These parameters include the number and orientation of the periodic bond chains (PBC's) on each face (these are the step directions), the

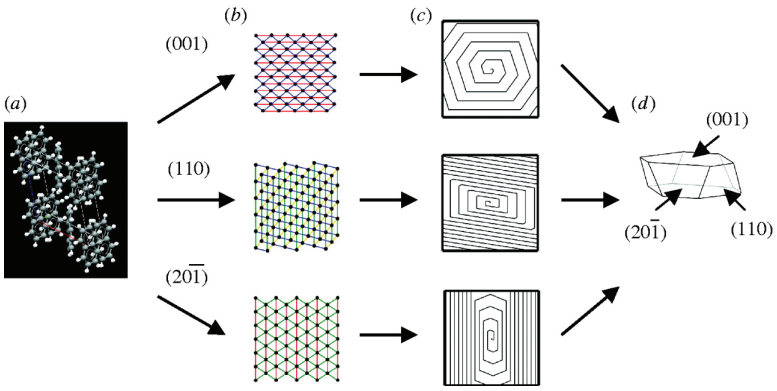

Figure 1: The crystal shape prediction methodology.

number of different types of kink sites/growth units along those PBC's, the density of kink sites, the net rate of solute incorporation into each type of kink site, and the solvent-mediated kink energy at each kink site. Note that we will use molecular models for the solid and continuum models for the solvent to correct for solvent surface energy effects at kink sites and molecular models to account for the activation barriers associated with attachment and detachment kinetics at kink sites (although we believe we have a way of simplifying these calculations so that they can be executed rapidly - that remains to be confirmed). Chernov[15,16] developed the BCF model for simple centrosymmetric growth units.

The steps involved in implementing the growth model are demonstrated in Fig. 1. The first step (a) is to input the crystallography for the solute molecule; step (b) involves specifying a force field for the solute molecule in the solid state with sufficient fidelity to determine the bond directions and strengths between all the atoms/groups in the solid. This information is used to determine the periodic bond chains (PBC's) that run throughout the solid using the rules developed by Hartman and Perdok.[17] These PBC's correspond to the edges/steps of the spirals on each crystal face. Interfacial kink energies are also calculated at this point using a molecular model for the solid and a continuum model for the solvent; step (c) involves the determination of the spiral dynamics according to the rules of Snyder and Doherty[2] which allows for the calculation of all the face relative growth rates. Note that these rules provide non-obvious relationships between the number of PBC's on a face and the number of sides on the corresponding spirals. All three faces shown in the figure happen to have three PBC's, which leads to six-sided spirals on faces (001) and (20-1), but only four-sided spirals on the (110) face; in step (d) all this information is assembled and a growth shape is *predicted*.

2.2 Recent Advances: Noncentric Growth Units and Ionic Crystals

Almost all mechanistic models of crystal growth that have been developed to date have been restricted to centrosymmetric growth units, which means that for all practical purposes they do not apply to crystals of real interest. The main difference between crystals of centrosymmetric and non-centrosymmmetric growth units is the isotropic driving force experienced by centrosymmetric growth units to incorporate into the solid state structure. Non-centrosymmetric growth units have more than one type of kink site, thus each edge on each face differs in terms of how many different types of kink sites it can have. Hence, the driving force for the incorporation of solute growth units within the kink sites is no longer isotropic. The velocity of the step needs to have a specific term which describes the net rate at which solute growth units incorporate within the different types of kink sites. Thus the step velocity is the product of the distance of propagation ($a_{p,i}$), density of the kink sites (ρ_i) and the net rate of incorporation of growth units into the kink sites (u_i). Hence,

$$v_i \propto a_{p,i}\rho_i u_i \tag{1}$$

The kink rate term, u_i, accounts for the non-isotropic behavior of the noncentric growth units (for centrosymmetric systems u is independent of the specific edge and face and hence is the same for all step fronts on all faces and does not influence the relative face growth rates). This approach of using the kink rate to estimate the step velocity has been adopted and justified by Chernov et al.[18,19] and by Zhang and Nancollas[20] to describe Non-Kossel crystal growth of ionic crystals in which there are at most two independent growth units (nominally corresponding to the two dissociated ions). However, many more independent growth units can and do exist for noncentric systems (paracetamol has 4, calcite has 4, aragonite has 16, some organic explosives such as RDX have 8, etc.). We have formulated the problem of finding a general expression for u_i in terms of a steady-state master equation which balances rates and probabilities of interchangeable events. We have successfully used such an approach to find new exact mechanistic expressions for the kink rate, which leads to the following equation for n different growth units (Kuvadia and Doherty[3])

$$u_i = n[(j^+)^n - \prod_{k=1}^{n} j_k^-]/[\sum_{\ell=1}^{n}(j^+)^{n-\ell}(j^-)^{(\ell-1)}] \tag{2}$$

where j^+ is the attachment flux of growth units into the kink site and j_k^- is the detachment flux from the kink site k. j^+ is independent of the specific kink site and depends only on supersaturation and solution composition, whereas j_k^- depends on the solution chemistry and the local bonding energies for the kink site k. Both rate expressions depend on a solvation activation energy barrier, which will

be calculated by rare event simulation as part of this program of research. For molecular crystals, all the growth units are a single chemical species so it has been customary to assume that the solvation activation behavior is the same for all of them and can be eliminated from the calculations. This assumption has never been tested but it will be tested as part of this research program. For inorganic crystal growth, the growth units are ions and will experience *different* solvation barriers and attachment/detachment kinetics. These barriers must be individually calculated for ionic systems, which is a *major difference between molecular and ionic crystals*, see the section Attachment Kinetics in Proposed Research. The quantity $(j^-)^{(\ell-1)}$ in Eq. 2 is given by

$$(j^-)^{(\ell-1)} = \sum_{k=1}^{n} j_k^- \, j_{k+1}^- \, j_{k+2}^- \cdots j_{k+\ell-2}^- \tag{3}$$

By inserting values for n, we can generate the kink rate expression for any number of different kink types in series. Further generalization of this expression for u_i for multiple ionic growth units has been accomplished recently (Dandekar and Doherty[21]).

Modeling surface integration-limited crystal growth from solution requires understanding the solid-state interactions as well as the surface growth mechanisms that govern the growth process. The importance of the interactions between the crystal and the solvent in modeling inorganic crystal growth from solution is highlighted by the comparable magnitudes of the lattice energy and the hydration energy for most inorganic solids (both energies have magnitudes typically > 100 kcal/mol). The lattice energy is dominated by the interionic long-range electrostatic interactions in the solid state, while the hydration energy depends on the interactions between the solvated ions and the water molecules present in the solvation shell. For example, the lattice dissociation enthalpy for cubic NaCl crystal is 188.1 kcal/mol while the combined hydration enthalpy for Na^+ and Cl^- ions is -187.2 kcal/mol. As a result, the dissolution enthalpy for NaCl crystal in aqueous solution is only 0.9 kcal/mol. Thus, the interactions of the surface growth units with the solvent play a *huge* role in determining the kinetics of the individual processes involved in growth on inorganic crystal surfaces.

In a recent pair of papers, Dandekar and Doherty[9,21] have developed some of the needed solid-state modeling infrastructure for inorganic crystal growth which is only summarized here for brevity. This includes (a) a method to identify the building units within the unit cell and the corresponding PBC's in the bulk material, (b) identification of edge structures on every face, including the identification of all the different types of kink sites, (c) calculation of the solid-state bond valencies at all the surface sites from the bulk partial charges and the coordination shell information of the

surface atoms (note, we have found that the Bond Valence Model is a perfectly adequate and simple method for finding these partial charges suitable for crystal growth theories and is much faster than using DFT calculations), (d) a space partitioning method for long-range energy calculations (note that Ewald sums will not work for crystal growth because the atomic partial charges are different from each other on the terrace, along an edge and at a kink site and from their bulk values), (e) generalized kink rate expression for ionic growth units, (f) a generalized kink density expression for multiple ionic growth units.

All this clears the way to focusing on the last remaining major obstacles to a comprehensive modern theory of crystal growth described below. These include, the need to know the free energy landscape and the energy barriers for different kink sites, the need to know the solution structure around each kink site to establish the solvent-mediated kink energies, as well as the correct partial charges on each surface atom.

3 Proposed Research

3.1 Attachment kinetics

Solute incorporation at kink sites in both organic and ionic crystal growth[22] is thought to be desolvation limited.[23–25] Theoretical models[22] show that kink attachment rates are the critical parameters for predicting crystal growth rates and shapes. Piana and Gale found that desolvation controls the rate of BaSO4 growth,[24] and proposed that the anions on some surfaces can assist the desolvation of cations. To the best of our knowledge, there have been no simulation studies on solute incorporation at kink sites for any organic crystal systems. We propose to develop the first such studies as part of this research program.

Stack et al. demonstrated the current state of the art in simulations to understand kink nucleation. Specifically, they used metadynamics to investigate ion attachment in the creation (1D nucleation) of kink sites in $BaSO_4$ growth. The big disadvantage of their approach is that it only uses solute coordinates, even though solvents were found to be involved in some way: "It is likely that there is a shift in the interfacial water structure with temperature ... creating the non-Arrhenius nature of this reaction."[26] Our method, which is capable of precisely identifying the role of solvent degrees of freedom in the mechanism will have many advantages:

1. Free energy barriers from projection onto an accurate solvent coordinate would more accurately correspond to the kinetics and provide improved explanations for the observed temper-

ature dependence.[27] Additionally, features on free energy surfaces constructed from accurate coordinates neatly coincide with known metastable states and transition states. Thus solvent coordinates will provide more easily interpreted free energy landscapes like those sketched in Figure 2.

2. Stack et al.[26] recognized the importance of dyanmical corrections to transition state theory in their rate calculations and used a rigorous, albeit arduous, procedure to obtain accurate rates. Accurate reaction coordinates result in free energy barriers that maximize the accuracy of transition state theory and minimize the importance of more expensive dynamical corrections.[27,28]

3. Identifying and understanding the role of key solvent degrees of freedom will point toward *analytical theories* to make predictions across a range of solutes and solvents. Ultimately, these advances will replace the need for large scale computer simulations for each new system, much like classical nucleation theory provides an analytical model for finding critical-sized nuclei and the corresponding free energy barrier.

The challenge in achieving these goals is that solvent coordinates are notoriously difficult to identify.[29–31] Peters et al. developed the state of the art simulation approaches for optimizing solvent coordinates.[32–34] He used these methods to identify an accurate solvent coordinate for ion-pair dissociation[35,36] - a seemingly simple reaction that eluded mechanistic understanding for many decades.[29,31,37–39] Actually, ion pair dissociation has much in common with attachment of ions at kink sites. For example, both processes are limited by desolvation and both processes would appear to be barrierless within a continuum electrostatics description. Based on prior experience with ion-pair dissociation, we will investigate two types of coordinates for ion-attachment kinetics:

- (**solute coordinate**) This may be distance between the kink site and a tagged ion, or a coordination number between the kink site and all ions in solution which could fill the kink. The coordination number coordinate prevents us from having to specify which ion will become part of the kink site.

- (**solvent coordinate**) We will examine energy gap coordinates which measure the degree of solvation around select ions. We will also try coordinates that measure the local water density in the vicinity of the kink site.

A central goal of the proposed work is to develop analytical models that can predict ion attachment rates without large scale simulations. Ultimately, we seek quantitative analytical models that can predict trends in crystal growth kinetics across a series of different ionic compounds and solvents. Thus we have restricted our coordinate optimization to relatively simple (but accurate) solvent coordinates that lend themselves to analytical theories.

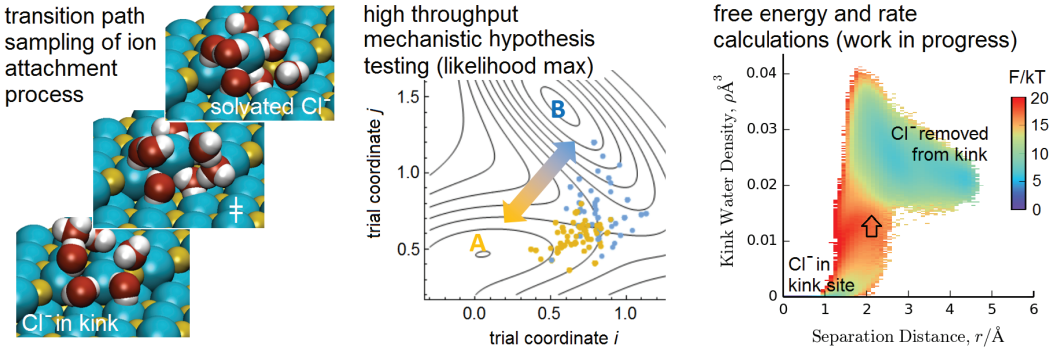

Figure 2: (a) Transition path sampling simulations of Cl- attachment to an NaCl crystal in contact with water. (b) Likelihood maximization considers several solute and solvent coordinates and identifies the optimal combination. (c) Free energy calculations identify the transition state location and activation barrier along the ion attachment/desolvation pathway. At the transition state, the reaction coordinate is entirely associated with movement of the water molecules into the kink site. This explains why transmission coefficients in the work of Piana and Gale were so small. In contrast, finding an accurate reaction coordinate will allow us to construct reasonably accurate transition state theories that are simple and (hopefully) generalizable.

After constructing a model of the free energy barrier we will compute rates using transition state theory. The free energy barrier from this model gives a rate $j^+ = k^+ S[ion]_{eq}$, with rate constant

$$k^+ = (1/2)\kappa \langle|\dot{q}|\rangle_\ddagger \, exp[-\Delta F^\ddagger / k_B T] \tag{4}$$

where $\langle|\dot{q}|\rangle_\ddagger$ is the absolute average velocity along the reaction coordinate at the transition state. Again coordinates with a simple physical interpretation allow us to easily estimate effective masses and thereby obtain accurate prefactors. (Note that the $k_B T/h$ formula is not applicable for collective variable reaction coordinates.) ***We hypothesize that this approach will yield simple analytic models for the rate in which geometry and electrostatics of the kink site, sizes and charges of ions, and the sizes and dielectric constants of the solvent are the only inputs.*** Such a model will be a major breakthrough in the theory of crystal growth.

Although this section has emphasized ionic crystals, the same reasoning will be applied to organic crystals in order to identify a suitable solute coordinate and a suitable solvent coordinate that can be used to derive analytical models to predict the energy barrier for attachment of organic growth units at kink sites.

3.2 Influence of Additives and Impurities

Previous modeling efforts in addressing the effects of additives on crystal morphology fall mainly into two broad categories- non-mechanistic and mechanistic. Non-mechanistic models such as the modified attachment energy approach[40,41] are useful in detecting which faces are capable of recognizing an impurity, but give no mechanistic insights on how the growth rate of the face is inhibited. Kink density reduction models of Chernov,[42] and Cabrera and Coleman[43], the step-pinning model of Cabrera and Vermilyea[44] and the "spiral pinning model" of Sizemore and Doherty[45] are the main mechanistic models. The kink density reduction model reasons that some of the kink sites are killed because of additive locking in those sites, however, it does not explain the effect of a supersaturation dead zone (i.e., the stop-start behavior of growth rate) seen at low additive concentrations. The step-pinning model proposed that the immobile impurities partition the edge into multiple segments, arresting the growth of those segments whose length is less than or equal to some critical length, thus decreasing the overall velocity of that edge. However, some experimental papers[46,47] contradict the step-pinning model and show convincingly that it cannot explain growth rate reduction of some faces on paracetamol crystals.

According to the spiral pinning model, additives have no effect on fully developed spiral edges, since they have already reached their critical lengths and move with a constant velocity. The effect is seen only on the first turn of an emerging spiral where the sides are yet to reach their critical lengths. The additive, if present on that particular face, increases the rotation time of the spiral by increasing the critical lengths of all edges, i.e, causing the edges to take a longer time to reach constant normal velocity. Thus, it reduces the growth rate of that particular face. According to theory, the step pinning model should dominate at low levels of additive concentration, and the step pinning model should dominate at higher levels.

We propose to build on and extend the spiral pinning model introduced by Sizemore and Doherty[45] and to connect the models as the additive concentration increases from low levels. Our main focus is on crystal shape evolution in the presence of structurally similar additives. A structurally similar additive is a foreign molecule present in solution that has many of the same atoms in much

the same chemical structure as the host molecule. Such an additive usually differs from the host molecule by only one or two functional groups. Structurally similar additives are also called "tailor made additives" or "imposters" and often arise as reaction byproducts from the chemical synthesis steps. The main goal of our method is to develop a rapid estimate to screen additive candidates (in conjunction with experiments) to engineer crystal morphology. The method is designed to give results in minutes rather than days. To achieve this we employ a mechanistic model which requires only very modest all-atom molecular mechanics and energy minimization calculations. The theoretical concepts used to develop these models rely on a mechanistic understanding of relevant surface phenomena governing the crystal growth process as well as knowledge of bulk solid-state chemistry. We propose to develop a quantitative impurity recognition method on each crystal face using a combination of mean field theory and configurational energy minimization. Based on this recognition, we will compute modified crystal growth rates of all facets and hence modified steady-state crystal shapes. We describe the challenges for non-centrosymmetric growth units and the methodology to overcome these challenges, and generalize the methodology to all molecular crystals. The first step is to extend this model to the general case of noncentric solutes. Once we have developed such a general model we will then test and refine it on several additional crystal–solvent–additive systems. Candidates include L-cystine (noncentric) grown from aqueous solution in the presence of L-cystine dimethyl ester, adipic acid (centric) grown out of aqueous solution in the presence of hexanoic acid, and octanoic acid (noncentric) additives, and naphthalene grown from hexane (solvent) in the presence of biphenyl (additive). The L-cystine system is described in detail by Ward and coworkers[48], the adipic acid system is described in the Klug and van Mil patent (1994) (US patent US5296639) who report a significant effect of the hexanoic acid additive on the crystal shape. Succinic acid (additive) is known to have very little influence on the evolving shape of adipic acid, and this too can be used to test our models. In this system, the kink energies & bond chains are expected to be dominated by molecular charge distributions and hydrogen bond effects. The naphthalene system is comprised of nonpolar molecules where dispersive interaction are expected to dominate.

A more challenging test system that we will study is paracetamol (acetaminophen) grown from aqueous solution in the presence of p-acetoxyacetanilide impurity (solute and impurity are both noncentric). This system has been experimentally studied in detail by Shekunov et al.[47] using laser interferometric measurements of the growth rates of several crystal faces as a function of both supersaturation and of impurity concentration. The experiments are superb (this is one of the

best experimental papers ever written on the effect of impurities on crystal growth rates) and it will provide us with all the necessary data to test our modeling approach. Another valuable set of experimental data was published by Botsaris, Mason and Reid[49] on the effect of lead chloride on the growth rates of potassium chloride faces grown from aqueous solution. These data report a significant effect even at very low impurity concentrations (e.g., 100 ppb).

3.3 Surface Morphology Experimental Methods

Students in the Doherty Lab have long ago mastered ex-situ atomic force microscopy (AFM) to image surface morphology of crystal faces. This has allowed us to directly observe spirals and 2D nuclei on the surfaces of many crystals, e.g., paracetamol, pentaerythritol, the anatase polymorph of titanium dioxide, and many others. The video-microscope apparatus in the Doherty Lab is shown in Fig. 3 (a), and an adipic acid crystal grown in it is shown in Fig. 3 (b). In Fig. 3(c) we show asymmetric spirals on the (001) face of paracetamol as measured by our students. As can be seen from the scale bars in panel (c), the step height is 0.6 nm (6Å), which is exactly one interplanar spacing in the c-direction - corresponding to a one molecule thick monolayer. We believe this is the first image of asymmetric spirals to be reported. UC Santa Barbara is the birthplace of AFM and our local shared facilities in the NSF-sponsored MRSEC are excellent. Moreover, the Doherty group has developed close collaboration with scientists at Asylum Instruments, located near the university, which gives us access to their ultra-high resolution prototype AFM instruments before they are released to the market. We will use all the AFM instruments at our disposal to image crystal faces on all the systems we investigate in order to test the morphological fidelity of our models at the nanoscopic as well as the microscopic (i.e., overall crystal shape) level of resolution. The crystals that we plan to grow experimentally and image in this research program include, paracetamol, olanzapine, and sodium chloride.

4 Leveraging Existing Resources

IFPRI funding will be leveraged by existing funding for my group from a Swiss multinational pharmaceutical company as well as new funding expected from a multinational name-brand US pharmaceutical. The students and postdocs supported with those funds will be available to train the IFPRI-funded student on the theoretical, computational and experimental methods required to conduct the research described in this proposal. All the state-of-the-art experimental facilities in

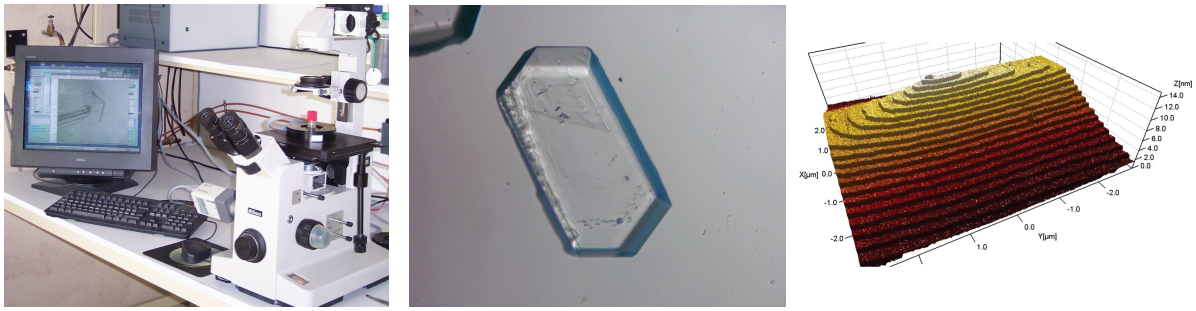

Figure 3: (a) Video-microscope apparatus in the Doherty Lab, (b) Adipic acid crystal, (c) AFM image of the 3-dimensional asymmetric spiral on the (001) face of paracetamol grown from aqueous solution (Kuvadia and Doherty[50]).

the UCSB MRSEC/MRL will also be available. The molecular simulation aspects of this research will be carried out in collaboration with my colleague, Baron Peters, who is a world leader in rare event simulation.

Timeline

This proposal describes an ambitious program of research that will transform the field of crystal growth and morphology engineering. The work will be completed in phases, as listed below.

Phase 1. Years 1-3. Develop modeling infrastructure for solvent and impurity effects.

1. Prepare and execute rare event molecular simulations for solute incorporation at kink sites for sodium chloride crystals grown from aqueous solution (now completed by Mark Joswiak who graduated May 2017. The new IFPRI-funded student will prepare her/his own simulations as a training exercise to compare against the known results.) Repeat for potassium chloride.

2. Identify good reaction coordinates that lend themselves to physical interpretation (now completed, but will be repeated as a training exercise) and to the development of analytical models of the attachment process (not done).

3. Develop an analytical model for the attachment process and use it to predict the growth shape of sodium chloride crystals grown from aqueous solution (first two quarters of 2018).

4. Test the model predictions (shape of the growth spirals, etc.) against AFM experiments performed by my students at UCSB.

5. Extend the model to other systems, starting with two test systems, (a) succinic acid grown from aqueous solution, and (b) paracetamol grown from a simple solvent.

6. Extend the existing spiral pinning model to noncentric solutes and additives.

7. Apply the model to L-cystine grown from aqueous solution in the presence of L-cystine dimethyl ester, and to paracetamol grown from aqueous solution in the presence of p-acetoxyacetanilide impurity.

8. Apply the model to potassium chloride grown from aqueous solution in the presence of lead chloride.

9. Merge the spiral pinning and step pinning models to create a single model that covers a wide variety of situations.

If the project is extended for a further period there is plenty of research to be done continuing the development of these methods.

References

(1) Schmidt, C.; Ulrich, J. Morphology prediction of crystals grown in the presence of impurities and solvents - an evaluation of the state of the art. *Journal of Crystal Growth* **2012***353*, 168.

(2) Snyder, R. C.; Doherty, M. F. Predicting crystal growth by spiral motion. *Proc. R. Soc. A* **2009***465*, 1145.

(3) Kuvadia, Z. B.; Doherty, M. F. Spiral Growth Model for Faceted Crystals of Non-Centrosymmetric Organic Molecules Grown from Solution. *Cryst. Growth Des.* **2011***11*, 2780.

(4) Lovette, M. A.; Doherty, M. F. Predictive Modeling of Supersaturation-Dependent Crystal Shapes. *Crystal Growth & Design* **2012***12*, 656.

(5) Shim, H.-M.; Koo, K.-K. Crystal Morphology Prediction of Hexahydro-1,3,5-trinitro-1,3,5-triazine by the Spiral Growth Model. *Crystal Growth & Design* **2014***14*, 1802.

(6) Shim, H.-M.; Koo, K.-K. Prediction of Growth Habit of β-Cyclotetramethylene-tetranitramine Crystals by the First-Principles Models. *Crystal Growth & Design* **2015***15*, 3983.

(7) Shim, H.-M.; Kim, H.-S.; Koo, K.-K. Molecular Modeling on Supersaturation-Dependent Growth Habit of 1,1-Diamino-2,2-dinitroethylene. *Crystal Growth & Design* **2015***15*, 1833.

(8) Dandekar, P.; Doherty, M. F. A mechanistic growth model for inorganic crystals: Solid-state interactions. *AIChE Journal* **2014***60*, 3707.

(9) Dandekar, P.; Doherty, M. F. A Mechanistic Growth Model for Inorganic Crystals: Solid-State Interactions. *AIChE J.* **2014***60*, 3707.

(10) Winn, D.; Doherty, M. F. A new technique for predicting the shape of solution-grown organic crystals. *AIChE J.* **1998***44*, 2501.

(11) Winn, D.; Doherty, M. F. Predicting the shape of organic crystals grown from polar solvents. *Chemical Engineering Science* **2002***57*, 1805 .

(12) Lovette, M. A.; Doherty, M. F. Needle-Shaped Crystals: Causality and Solvent Selection Guidance based on Periodic Bond Chains. *Crystal Growth & Des.* **2013***13*, 3341.

(13) Lovette, M. A.; Browning, A. R.; Griffin, D. W.; Sizemore, J. P.; Snyder, R. C.; Doherty, M. F. Crystal Shape Engineering. *Industrial & Engineering Chemistry Research* **2008***47*, 9812.

(14) Burton, W. K.; Cabrera, N.; Frank, F. C. The Growth of Crystals and the Equilibrium Structure of their Surfaces. *Phil. Trans. Roy. Soc. A* **1951***243*, 299.

(15) Chernov, A. A. *Modern Crystallography III. Crystal Growth*. Springer-Verlag: Berlin, **1984**.

(16) Chernov, A. A.; Nishinaga, T. *Morphology of Crystals, Part A*, chap. Growth Shapes and Their Stability at Anisotropic Interface Kinetics: Theoretical Aspects for Solution Growth. Terra Scientific: Wiley, Tokyo, **1987**.

(17) Hartman, P.; Perdok, W. G. On the relations between structure and morphology of crystals. I. *Acta Crystallogr.* **1955***8*, 49.

(18) Chernov, A. A. Notes on interface growth kinetics 50 years after Burton, Cabrera and Frank. *J. Cryst. Growth* **2004***264*, 499.

(19) Chernov, A. A.; Rashkovich, L.; Vekilov, P. Steps in Solution Growth: Dynamics of Kinks, Bunching and Turbulence. *J. Cryst. Growth* **2005***275*, 1.

(20) Zhang, J.; Nancollas, G. H. Kink Density and Rate of Step Movement during Growth and Dissolution of an AB Crystal in a Nonstoichiometric Solution. *Journal Of Colloid And Interface Science* **(1998)***200*, 131145.

(21) Dandekar, P.; Doherty, M. F. A Mechanistic Growth Model for Inorganic Crystals: Growth Mechanism. *AIChE J.* **2014***60*, 3720.

(22) Dandekar, P.; Kuvadia, Z. B.; Doherty, M. F. Engineering Crystal Morphology. *Ann. Rev. Mater. Res.* **2013***43*, 359.

(23) Nielsen, A. E. Electrolyte crystal growth mechanisms. *J. Crystal Growth* **1984***67*, 289.

(24) Piana, S.; Jones, F.; Gale, J. D. Assisted desolvation as a key kinetic step for crystal growth. *J. Am. Chem. Soc.* **2006***128*, 13568.

(25) Vekilov, P. G. What Determines the Rate of Growth of Crystals from Solution? *Crystal Growth & Design* **2007***7*, 2796.

(26) Stack, A. G.; Raiteri, P.; Gale, J. D. Accurate rates of the complex mechanisms for growth and dissolution of minerals using a combination of rare-event theories. *J. Am. Chem. Soc.* **2012***134*, 11.

(27) Peters, B. Recent advances in transition path sampling: accurate reaction coordinates, likelihood maximisation, and diffusive barrier-crossing dynamics. *Molec. Sim.* **2010***36*, 1265.

(28) van Erp, T. S. Dynamical rare event simulation techniques for equilibrium and nonequilibrium systems. *Adv. Chem. Phys.* **2012***151*, 27.

(29) Geissler, P. L.; Dellago, C.; Chandler, D. Kinetic Pathways of Ion Pair Dissociation in Water. *J. Phys. Chem. B* **1999***103*, 3706.

(30) Bolhuis, P. G.; Dellago, C.; Chandler, D. Reaction coordinates of biomolecular isomerization. *Proc. Nat. Acad. Sci. USA* **2000***97*, 5877.

(31) McCormick, T. A.; Chandler, D. Grid-Flux Method for Learning the Solvent Contribution to the Mechanisms of Reactions. *J. Phys. Chem. B* **2003***107*, 2796.

(32) Peters, B.; Trout, B. L. Obtaining reaction coordinates by likelihood maximization. *J. Chem. Phys.* **2006***125*, 054108.

(33) Peters, B.; Beckham, G. T.; Trout, B. L. Extensions to the likelihood maximization approach for finding reaction coordinaes. *J. Chem. Phys.* **2007***127*, 1.

(34) Peters, B. Inertial likelihood maximization for reaction coordinates with high transmission coefficients. *Chem. Phys. Lett.* **2012***554*, 248.

(35) Mullen, R. G.; Shea, J.-E.; Peters, B. Communication: An existence test for dividing surfaces without recrossing. *J. Chem. Phys.* **2014***140*, 041104.

(36) Mullen, R. G.; Shea, J. E.; Peters, B. Transmission Coefficients, Committors, and Solvent Coordinates in Ion-Pair Dissociation. *J. Chem. Theory and Comp.* **2014***10*, 659.

(37) Karim, O. A.; McCammon, J. A. Rate constants for ion pair formation and dissociation in water. *Chem. Phys. Lett.* **1986***132*, 219.

(38) Ciccotti, G.; Ferrario, M.; Hynes, J. T.; Kapral, R. Dynamics of ion pair interconversion in a polar solvent. *J. Chem. Phys.* **1990***93*, 7137.

(39) Ballard, A. J.; Dellago, C. Toward the mechanism of ionic dissociation in water. *J. Phys. Chem. B* **2012***116*, 13490.

(40) Clydesdale, G.; Roberts, K. J.; Lewitas, K.; Docherty, R. Modeling The Morphology Of Molecular-Crystals In The Presence Of Blocking Tailor-Made Additives. *Journal Of Crystal Growth* **1994***141*, 443.

(41) Berkovitch-Yellin, Z. Toward An Abinitio Derivation Of Crystal Morphology. *Journal Of The American Chemical Society* **1985***107*, 8239.

(42) Chernov, A. The Spiral Growth of Crystals. *Soviet Physics Uspekhi* **1961***4*, 117.

(43) Cabrera, N.; Coleman, R. Theory of Crystal Growth from the Vapor. In *The Art and Science of Growing Crystals*, J. Gilman, ed. John Wiley & Sons, Inc., **1963**.

(44) Cabrera, N.; Vermilyea, D. The Growth of Crystals from Solution. In *Growth and Perfection of Crystals*, R. Doremus; B. Roberts; D. Turnbull, eds. John Wiley & Sons, Inc., **1958**.

(45) Sizemore, J. P.; Doherty, M. F. A New Model for the Effect of Molecular Imposters on the Shape of Faceted Molecular Crystals. *Crystal Growth & Design* **2009***9*, 2637.

(46) Ristic, R. I.; DeYoreo, J. J.; Chew, C. M. Does Impurity-Induced Step-Bunching Invalidate Key Assumptions of the CabreraVermilyea Model? *Crystal Growth & Design* **2008***8*, 1119.

(47) Shekunov, B. Y.; Grant, D. J. W.; Latham, R. J.; Sherwood, J. N. In situ optical interferometric studies of the growth and dissolution behavior of paracetamol (acetaminophen) crystals. 3. Influence of the growth in the presence of p-acetoxyacetanilide. *J. Phys. Chem. B* **1997** *101*, 9107.

(48) Rimer, J. D.; An, Z.; Zhu, Z.; Lee, M. H.; Goldfarb, D. S.; Wesson, J. A.; Ward, M. D. Crystal Growth Inhibitors for the Prevention of l-Cystine Kidney Stones Through Molecular Design. *Science* **2010***330*, 337.

(49) Botsaris, G. D.; Mason, E. A.; Reid, R. C. Growth of potassium chloride crystals from aqueous solutions. I The effect of lead chloride. *J. Chem. Phys.* **1966***45*, 1893.

(50) Kuvadia, Z. B.; Doherty, M. F. Reformulating Multidimensional Population Balances for Predicting Crystal Size and Shape. *AIChE Journal* **2013***59*, 3468.

IFPRI Research Project Brief

Deliquoring of Wet Filtration Cakes

The International Fine Particle Research Institute wishes to fund a project in the area of pressure filtration, specifically the deliquoring of wet filter cakes. IFPRI has had an enduring interest in this area, dating back to a 1991 IFPRI-sponsored project on prediction and scale-up of pressure filtration lead by Lee White. Interest in solid-liquid separations has increased in recent years, particularly with regard to deliquoring of solids which interact strongly with their mother liquors.

The goal of this project is a first-principles based prediction of the limit of deliquoring a particle slurry in filtration, optionally combined with washing. That is, given particle morphology distributions and wetting properties, predict:

1) Bed property evolution during dead-end filtration
2) Liquid flow patterns during deliquoring and washing of filter cake
3) Final filtration performance

The project should consider cake formation and deliquoring in pressure or compression filtration. Both aqueous and non-aqueous systems are in scope, as are viscous liquids. The project should consider the impact of impurities in the mother liquor. Particle formation and/or dissolution during filtration are out of scope, as the driving interest is that of predicting filtration performance from particle properties.

Detailed insight into microscopic phenomena using 3D-tomography data to develop a better model for dead-end filtration

Urs A. Peuker, Freiberg
Institut für Mechanische Verfahrenstechnik und Aufbereitungstechnik
TU Bergakademie Freiberg
Agricolastraße 1
09599 Freiberg / Sachsen
Tel: 03731 39-2916
Fax: 03731 39-2947
E-mail: urs.peuker@mvtat.tu-freiberg.de

---

1 Introduction to the topic

This proposal addresses the key question of cake filtration, which is the estimation of the filtration parameters directly form the information available on the particles. In this context the main fields of interest are:

- Particle shape (distribution)
- Particle size distribution
- Particle interaction (distribution)

The filtration process needs.

- The specific cake resistance
- The (integral) porosity
- The pore size distribution (in case of mechanistic models)
- The de-watering behavior

Until it is not possible to access detailed information on the inner cake structure and the particle properties in the same time, an increase in the insight will not be possible. Thus we are proposing to use µ-CT (computer tomography) measurements to create the information needed. The data acquisition becomes even more efficient and accurate, when the filtration is performed directly in the CT, which is possible when an in-situ filtration cell is used.

On the basis of both macroscopic lab-scale work with a nutsch filter as well as microscopic work using in-situ experiments a joint approach is developed to connect particle properties with pore properties. The insight given by the experiments will also guide the way what kind of filtration model has to be applied and further developed to describe de-saturation process.

1.1 Short review on the fundamentals

Filtration

The description of filtration processes typically bases on the Darcy-equation and the Carman-Kozeny-equation (equation1). The specific cake resistance is correlated to the particle properties using the so called hydraulic diameter, which is connected to the specific surface (equation 2), as well as the porosity. The Carman-Kozeny-equation has been modified since its first publication, but

these modifications mainly address the dependency from the porosity. Thus in a general form the interaction of resistance and particle properties can be expressed using equation 4.

$$\frac{\Delta p}{\Delta L} = K_1 \cdot \frac{(1-\varepsilon)^2}{\varepsilon^3} \cdot S_V{}^2 \cdot \eta_L \cdot u \qquad \text{Equation 1}$$

$$S_V = 6 \cdot f \cdot \frac{\sum \overline{x}_i{}^2 \cdot \Delta Q_{0,i}}{\sum \overline{x}_i{}^3 \cdot \Delta Q_{0,i}} \qquad \text{Equation 2}$$

$$r_c = K_1 \cdot \frac{(1-\varepsilon)^2}{\varepsilon^3} \cdot S_V{}^2 \quad \text{with} \quad 3{,}5 < K_1 < 5{,}5 \qquad \text{Equation 3}$$

$$r_c = f(\varepsilon) \cdot S_V{}^2 \quad \text{as a general form of Equation 3} \qquad \text{Equation 4}$$

Summarizing, how particle properties are connected to the filtration properties we can state:

- Particle size distribution is represented via the specific surface S_V (scalar parameter)
- Particle shape is represented via the form factor f (scalar parameter)
- Pore structure is represented by the porosity (integral, scalar parameter)

Even though porosity is not independent from particle properties, the porosity used here is an experimental (or average) value. Looking to the application these interdependencies are not suitable to predict filtration directly from particle properties. Looking at some own experimental work it can be stated that the filtration properties strongly depend on the structuring of the particles when building up the cake. With the same macroscopic porosity different specific cake resistances have been measured (Table 1).

Table 1 Cake resistance for a model product surface modified alumuosilicate (S_V=1,25 m²/m³) using different mother liquids and thus varying the wetting properties, the contact angle respectively (data partly taken form [1])

poroosity	Spec- filtration resistance in 10^{15} 1/m²	Surface modification (@ S_V const.)	Mother liquid
0,4	2,67	hydrophilic	water
0,4	5,10	hydrophobic	acetone
0,4	5,21	hydrophobic	iso-propanole
0,4	6,40	hydrophobic	ethanol
0,4	7,14	hydrophobic	n-butanole
0,4	7,52	hydrophobic	methanole

Cake formation - estimation of r_c

On the basis of the Darcy-equation it is possible to make a differential balance of liquid and solids during the cake filtration process, which finally leads to the well-known *t*/*V* vs. *V* plot, or *dt/dV vs. V* respectively (Equation 5). This plot is used to estimate both cake resistance form the slope of the straight line and medium resistance form the interception with the y-axis. Several assumptions have to be respected during the balance, e.g. homogeneous cake structure, no compressibility as well as no de-mixing (segregation) of the particle system during the process.

$$\frac{dt}{dV} = \frac{\kappa \cdot \eta \cdot r_c}{A^2 \cdot \Delta p} \cdot V + \frac{\eta \cdot R_M}{A \cdot \Delta p} = b \cdot V + a \qquad \text{Equation 5}$$

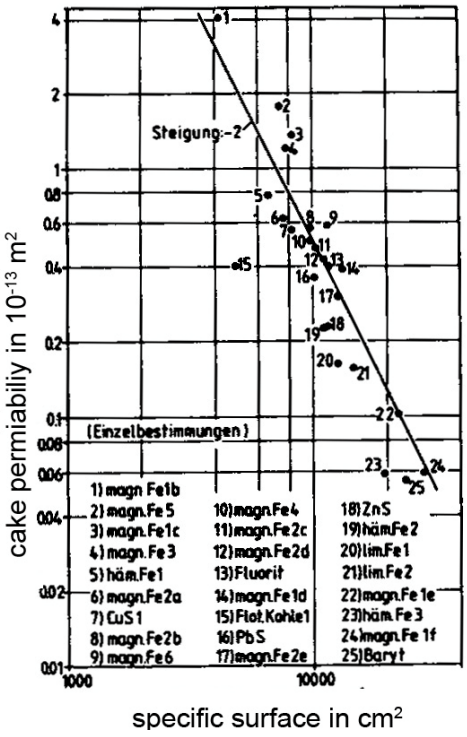

Figure 1 Overview on the principle validity of the Carman-Kozeny approach (data taken form [2]) - the cake permeability is the inverse of the specific cake resistance.

The plot (Figure 1) shows the principle trend following the Carman-Kozeny law, but on the other hand the data points scatter around the trend line. Thus additional parameters are necessary to obtain a more precise and predictive description of the specific cake resistance. Comparing the data point 1 (iron ore) with data point 15 (coal), the permeability and thus the cake resistance differs about one order of magnitude at approximately the same specific surface. The precision of a forecast of filtration properties from PSD-data on the basis of the Carman-Kozeny equation still has an average error of more than 100% for typical materials.

1.2 Own scientific work (selection)

Prof. Peuker works since more than 20 years in the field of mechanical separation processes, especially in the flied of dead-end filtration.

Investigating the influence of PSD on filtration properties and process behavior.

In several studies, research projects, industrial services and PhD-thesis the influence of different parameters on the filtration parameters have been evaluated. One focus was on bi-modal suspensions, which derive form clay containing minerals, selective comminution or crystallization processes. It was shown that a homogeneous cake only can be formed at high solids concentrations (e.g. c_v = 0.4). At lower concentrations segregation occurred, leading to a dense covering layer at the top of the cake.

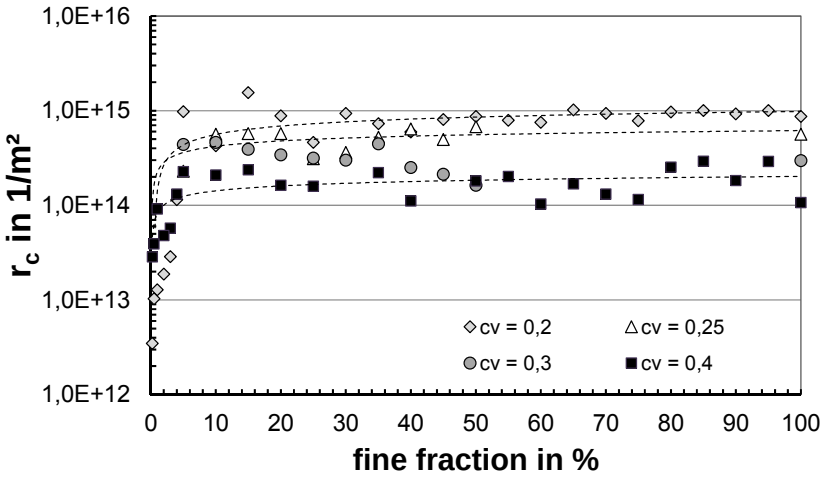

Figure 2 Process data of lab-scale experiments (average values) using *t*/*V* vs. *V* method with an sand-clay mixture ($x_{50,coarse}$ = 10 $x_{50,fine}$) - development of the cake resistance as a function of the feed concentration c_v.

A deeper look in the individual experiments shows the reliability of the experiments (Figure 3). Due to segregation, the experiments show a low reproducibility until the fine fraction has reached a certain value, which amounts to about 40 %. At low concentration of fines the pore volume built up by the large fraction exceeds the volume of all fines. Thus all fines can be trapped within these pores. The scattering of the experimental data is then due to the stochastic distribution of the fines within the pores. This comes to an end when the inner structure of the cake is inverted, above about 40-50 % of fines the inner structure can be described as large particles enclosed in a bed of fines.

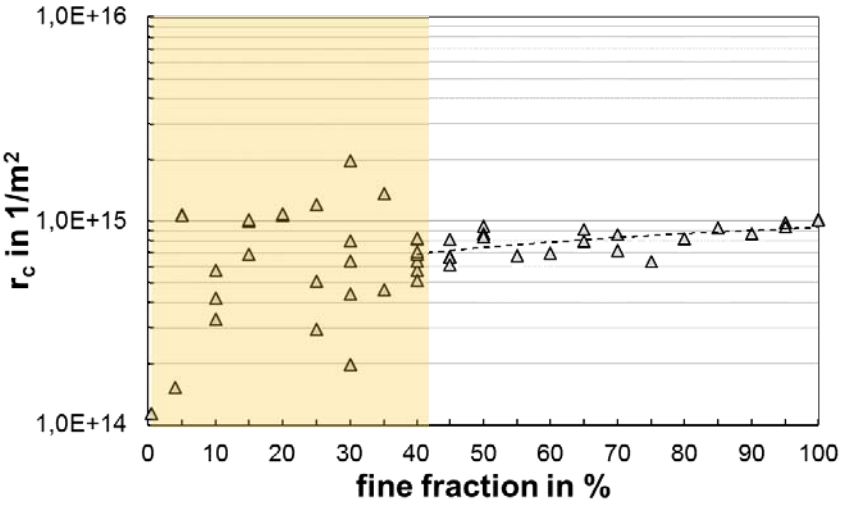

Figure 3 Process data of lab-scale experiments using *t*/*V* vs. *V* method with an sand-clay mixture ($x_{50,coarse}$ = 10 $x_{50,fine}$) feed concentration c_v = 0,2 - 0,25 - marked area depicts large scattering in the data due to heterogeneous cake formation.

Investigating the influence of wetting properties on filtration and washing properties

In several studies [3-7] the filtration properties of solvent based suspension have been investigated. During these research activities methods to modify particle surfaces have been established. All filtration data collected in this context shows a significant influence of the wetting angle on the cake structure and filtration parameters, which not only can be explained by porosity effects. An example

gives Figure 4, where the specific cake resistance (in iso-propanole) increases by approximately one order of magnitude the more hydrophobic the surface becomes. The iso-propanole shows in contradiction to water a sufficient wetting over the entire range of surface modification.

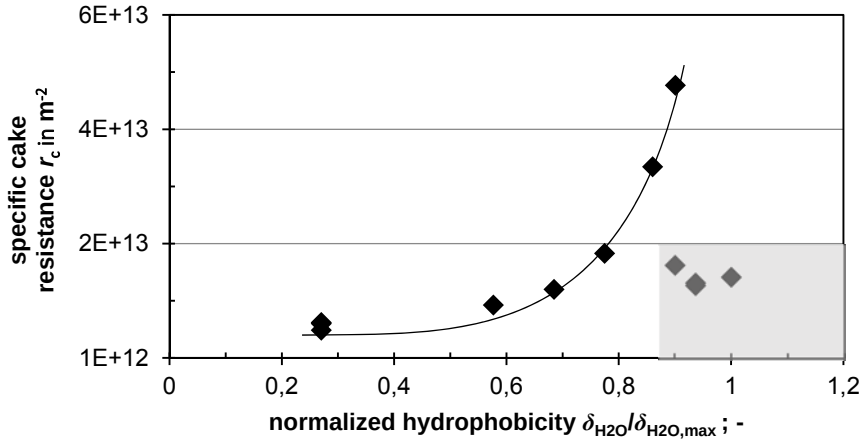

Figure 4 Cake resistance (glass spheres) for different silane based surface modifications measured with mother liquid iso-propanole.

3D-analysis of filtration processes in computer tomograph.

The Institute MVTAT owns since 09/2015 a computer tomograph (Zeiss Xradia Versa 510). This CT is equipped with a special device, which allows to supply liquid or gaseous media to the measuring chamber. With this supply it is possible to run an in-situ filtration cell within the CT. This cell has to respect the specifications of the measuring process, which are the spatial dimension as well as the characteristic time scales. The in-situ filtration cell itself is actually under development, several versions have been tested until now, which special focus on cake characterization during washing and de-saturation.

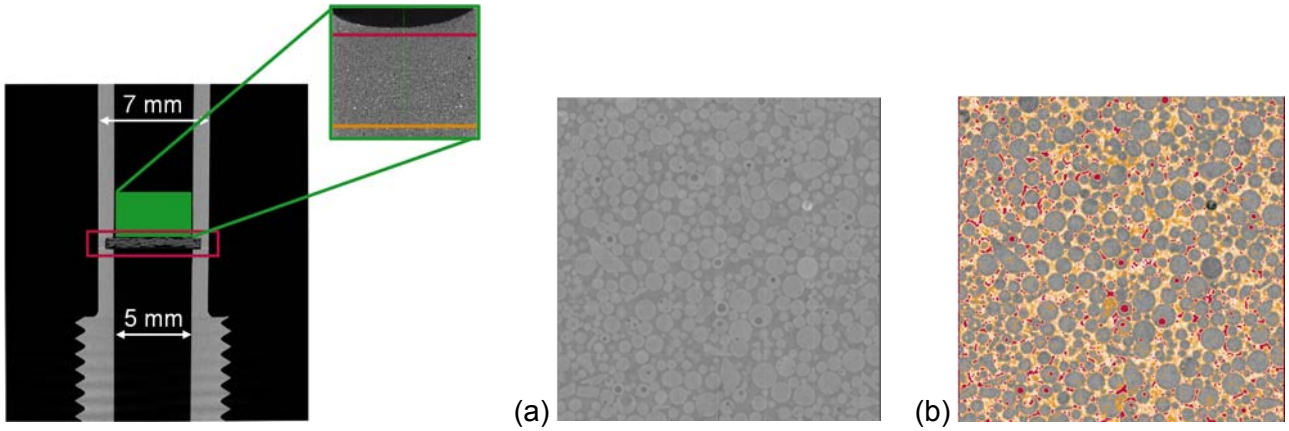

Figure 5 Actual development of an in-situ-filtration cell:
left: 2D - vertical projection through the cell body - green area in displayed in detail showing the filter cake (glass spheres 0-50 µm); right: characterization of the multiphase pore system - horizontal projection; (a) raw data; (b) processed image data to identify gas-filled volumes; grey: particles, orange: liquid, red; gas.

Development of de-saturation models

Pore size distribution can be used to model the de-saturation of a porous system [8]. This has the advantage that it is possible to describe a residence time distribution of the draining liquid and with that the tail of the de-saturation kinetics can be described quite well [9]. One the other hand more

information is needed to use the quantitative model. The pore size distribution can derive e.g. from capillary pressure measurements.

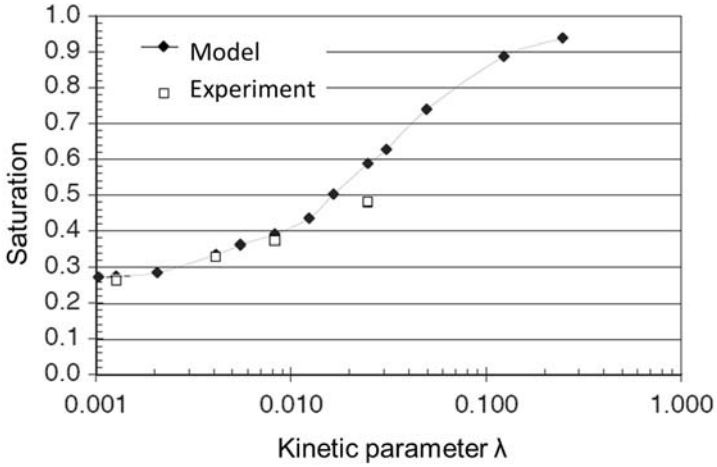

Figure 6 Quantitative modelling of the de-saturation during centrifugation (filter centrifuge) using 5 classes of pores with a pipe flow approach (Hagen-Poisieulle). The Kinetic parameter λ can be seen as a reciprocal time and derives from the theory of centrifugal de-watering.

2 General aims of the project (including Milestones - year 1-3)

In the first period of the project fundamental questions have to be answered, which allow a new concept to model filtration processes. On the basis of selected computer tomography results *the particle properties are linked to the pore properties*. The aim is to come to a better prediction of the hydraulic properties of the cake compared to the Carman-Kozeny approach.

The second outcome is an investigation *how de-saturation* with all mayor and minor phenomena *occurs*. This will guide us to the selection of a right mechanistic model approach.

The model approach itself is the third outcome, it uses both the predicted parameters of the pore system as well as right mechanistic approach. Due to the huge complexity the experimental work focusses on two different particle shapes and three different surface energies of the particle system. The model has to be capable to be fine-tuned in the future taking into consideration further properties of the particle system.

Outlook for years 4-6

To use the above mentioned model in a flow-sheet simulation the model has to be sufficiently simple and should also describe all relevant processes. Therefore filter cake washing and filter cake consolidation will be the focus of the work to create a unified robust mechanistic model.

2.1 Working Program

The general strategy of the working program is to use the in-situ experiments within the 3D-computer tomograph as effective as possible. Therefore a hybrid approach is chosen: Conventional lab-scale filtration experiments are used to map the influencing parameters. On the basis of these results the process parameters are chosen, with which the in-situ-experiments are conducted. The data exploitation aims at correlating the data sets of the lab-scale experiments with those of the in-situ-experiments and to use the in-situ data as a point of support. The in-situ experiments are supposed to provide a phenomenological insight into the microstructure of the cake. This implies the orientation and structuring of the particles as well as the local distribution of the fluids. The CT is capable to resolve between gas, aqueous phase and solids (Figure 5, right).

Since the field of particle properties, which are influencing the filtration process and especially the inner structure of the filter cake, is huge, it is not possible to investigate all variations. The choice of the model particle system therefore becomes quite important. The inner structuring within the filter cake depends on the particle shape. Particle shape can be described by integral or descriptive parameters. Looking at the latest generation of particle based products, needle shaped as well as sheet / flake shaped particles are the most frequent challenges especially concerning filtration in chemical and new-materials industry[1].

- Sheet / flake shaped particles: There are two model particle systems, with which we already have experiences. This is glimmer and molybdenum sulfide. Both particle systems have an aspect ratio above 3 showing a clear flaky or sheet like shape (green particles in Figure 7). They can be processed via wet grinding to generate different size fractions. The particle shape derives from the crystal structure of the material. In the selection process of the model system the x-ray extinction of the materials will be an additional criterion.
  In certain process windows of the particle interactions flaky particles are supposed to form card house structures. Especially when applying x-ray tomography this hypothesis can be highlighted.

[1] The suggested model materials have been chosen due to their advantages concerning availability, safety, x-ray properties and for being mechanically robust and chemically inert.

- Needle shaped particles: The generation of needle shaped particles is typically due to the crystallization thermodynamics. The majority of these products are organic materials. Thus, the stability of these needles in is quite low, making is problematic to use them as model product. But milled glass fibers are an alternative, which can be generated in larger quantity. The characterization of the grinding product uses image analysis to quantify the particle size and length, aspect ratio of the fiber fragments respectively.
  Needle shaped particles are supposed to form a kind of network structure during filtration.

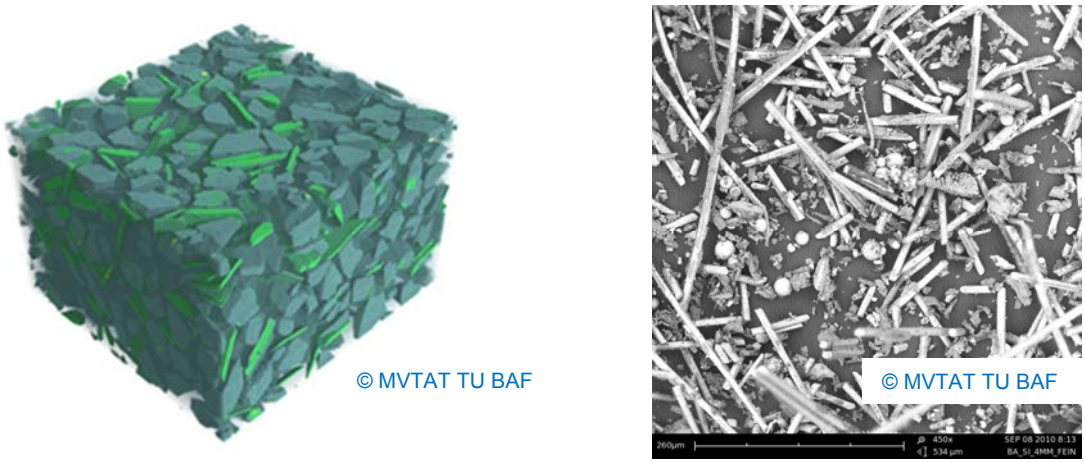

Figure 7 Possible model particle systems: left 3D computer tomography image of filter cake of mixture of *sheet shaped glimmer* (green) and quartz (petrol); right *needle shaped particles of milled glass fibers* (deriving from circuit boards).

The 3D-experiments are supposed to provide an insight into the microscopic behavior during one- and two-dimensional pore flow. On the basis of this understanding the type of model approach to describe the filtration process is selected. Possible model approaches are:

1. Integral black box model: An overall approximation function is correlated to the particle properties and thus directly linking particle properties (e.g. PSD, shape, wetting,...) to filtration properties (resistance, residual moisture, washing behavior,…).
2. Pore model: Particle properties are linked to a characteristic pore, in which a mechanistic model can be set up.
3. Pore bundle model: Particle properties are linked to a characteristic pore size distribution, in which a mechanistic model can be set up.
4. Material specific transport function: Particle properties are used to generate a continuous material model, in which the de-saturation and washing can be quantified using characteristic transport coefficients in the differential equation of the fundamental transport laws.

Deliverable 1 ***Construction of in-situ filtration cell for voxel size of approx. 2 µm***

General questions: The experiments in the CT need an adopted filtration cell, which allows the intended resolution of the measurements.

Based on the existing expertise (Figure 5) a filtration cell for in-situ as well as ex-situ experiments is designed and manufactured. The aim is to use a spatial resolution of about 2 µm, which is 1/10 of the lower (x_{16}) particle diameter. The cell needs to provide the same filtration properties when used in miniaturized experiments. Therefore one special focus is on minimizing any inhomogeneity in the filter cake due to particle-wall interactions.

The field of view during the tomography measurements is 1024 or 2048 times the voxel size, thus 2-4 mm at the desired resolution. Therefore the diameter of the cell will be about 4-5 mm. This allows

an acceptable handling during macroscopic experiments, e.g. cake formation as well a sufficient strength of the CT-signal, reducing the measurement times.

The bench mark for the development of the in-situ cell is quantified with filtration experiments. The in-situ cell has to provide in a t/V vs. V plot the same filtration parameters (Ɛ, r_c and R_m) than in the 50 mm lab-scale cell. The latter is the reference, which is specified relevant guidelines, e.g. VDI 2762 [10].

Deliverable 2 ***Phenomenological Filtration experiments focus on: cake structure (wetting properties)***

General questions: Data collection on filtration properties and their correlation to the inner cake structure.

The investigation on the filtration properties base on an experimental program in two scales. In the traditional lab-scale (50 mm nutsch filter) integral a process parameters (Ɛ, r_c and R_m), are collected. On the basis of the quantitative analysis of these experiments the 3D-tomography experimental program is designed. The number of complex and time-consuming experiments with the in-situ filtration are carefully selected to obtain the maximum output of the 3D-data.

Typical industrial materials are used for the study:

- Particle system with ideal PSD (log-normal or RRSB distribution) and compact particles / aspect ratio close to one
- Elongated particles (sheets or needles) with an aspect ratio above two (cf. Figure 7).
- Surface modified particles of both particle systems (surface modification using silane chemistry, changing the wetting: cos (δ) = 20 °; 50 °, 80 °)

The CT investigations on the samples of these experiments use the in-situ set-up. The cake is built up outside the CT and then the cell with the cake (S = 1) is inserted into the measuring chamber of the CT.

Deliverable 3 ***Data exploitation of CT measurements - cake formation***

The main work is the data exploitation which aims at the determination of the porosity parameters of the cake. Therefore a complex image analysis has to be performed. These calculations are time consuming, thus maximum 12-20 samples can be processed. The aim is a better understanding of the structuring as a function of the selected parameters of the particle system.

Milestone I **Year 1**

The first year establishes the in-situ filtration technique in connection with conventional lab work. It provides data sets on macroscopic filtration parameters, which can be correlated to microscopic structural information. Furthermore it is possible to link some particle properties to structural parameters of the filter cake.

Deliverable 4 ***Phenomenological Filtration experiments focus on: de-saturation***

General questions: Investigations on the liquid distribution during and at the end of a de-saturation process.

La scale experiments are conducted to determine the capillary pressure curve of the particle systems (Deliverable 2). From this the two pressure differences are chosen for the in-situ experiments:

1. Pressure difference, which leads to an equilibrium saturation of about S = 50%
2. Pressure difference, which corresponds to the vertical part of the capillary pressure curve.

The second set of lab scale experiments is performed focusing on the de-watering kinetics. From this process data, the point when the gas breakthrough occurs is chosen as a characteristic point during the de-saturation process.

The CT investigations on the samples of these experiments use the in-situ set-up. The cake is built up outside the CT and then the cell with the cake (S = 1) is inserted into the measuring chamber of the CT. It is connected to the internal media supply of the measuring chamber. The cake is processed (Δp, t defined by the lab scale experiments) - then the tomogram is recorded. A second process step and a second measuring phase can be foreseen, describing the progress of de-saturation[2].

Deliverable 5 ***Data exploitation of CT measurements - de-saturation***

The main work is the data exploitation which aims at the monitoring of the liquid distribution within the porosity. Therefore a complex image analysis has to be performed, which distinguishes between the three phases. These calculations are time consuming, thus about 12-15 samples can be processed. The aim is a better understanding of the liquid distribution within the cake during de-saturation.

Milestone II **Year 2**

The information on the liquid distribution will allow to choose the right model to describe the de-saturation process.

Deliverable 6 ***Modelling of cake formation and de-saturation***

The model has to respect the needs of a future industrial application, e.g. the use as a building block in a flow sheet simulation. It is necessary to use as little sophisticated input information as possible. Furthermore the model should not base on any parameter, which only can be measured by a CT. The model must use the data on particles, which can be provided by conventional and commercial analytics.

The 3D-shape analysis will be replaced by a 2D-shape analysis deriving form CCD-camera data and automated image analysis of the particle system. It has to be questioned, how detailed the pore structure has to be resolved in the model, since a connection of particle properties on one hand and finals process results like liquid load (residual moisture) on the other hand is needed. The detailed model approach cannot be defined yet, since it depends on the outcome of Milestone II.

Deliverable 7 ***Phenomenological Filtration experiments***
focus on: washing / viscous fingering

Beside the theoretical work first investigations looking at a washing step are conducted. A contrast between pure washing liquid and ion-loaded pore liquid occurs due the x-ray absorption of these ions. Diffusion as well as convective mixing during the long measuring times within the CT can lead to an uncertainty / haziness in the results. Therefore the characterization will focus on systems with a difference in viscosity, where convective mixing is suppressed.

With the same strategy lab scale and in-situ CT experiments are combined. The las scale experiments determine relevant points in the process, on which than the CT measurements are applied.

Milestone III **Year 3**

Based on the deeper insight into filtration processes provided by in-situ measurements with a CT, a model is presented, which brings together the information on particle properties and process behavior in filtration processes. It has a focus on de-saturation, yet.

[2] Please note that the measuring time for a tomogram with sufficient resolution needs about 4-6 hours.

2.2 Gant Chart of the working program

	1st year				2nd year				3rd year			
quarter	**Q1**	**Q2**	**Q3**	**Q4**	**Q1**	**Q2**	**Q3**	**Q4**	**Q1**	**Q2**	**Q3**	**Q4**
Construction of in-situ filtration cell for voxel size of approx. 2 µm												
Phenomenological Filtration experiments focus on: cake structure (wetting properties)												
Data exploitation of CT measurements - cake formation												
Phenomenological Filtration experiments focus on: de-saturation												
Data exploitation of CT measurements - de-saturation												
Modelling of cake formation and de-saturation												
Phenomenological Filtration experiments focus on: washing / viscous fingering												

3 Literature

[1] C. Perbandt, U.A. Peuker, Particle-particle interaction in non-aqueous liquids - effect on filtration properties, Filtech Europe, Wiesbaden, Germany, 2005.

[2] H. Anlauf, Entfeuchtung von Filterkuchen bei der Vakuum-, Druck- und Druck/Vakuum-Filtration, in, Universität Karlsruhe, 1986.

[3] S. Neubauer, U.A. Peuker, Filtration Properties in Solvent-Water Mixtures, World Filtration Congress, Leipzig, Germany, 2008, pp. 7.

[4] S. Neubauer, U.A. Peuker, Liquid mixtures as suspension liquids - Effective on the filtration parameter, Chemie Ingenieur Technik, 79 (2007) 1753-1758.

[5] M. Wilkens, U. Peuker, The modelling of washing processes under the influence factor of back mixing in two liquid systems, World Filtration Congress, Graz, 2012.

[6] M. Wilkens, U. Peuker, The Influence of Surface Energy on the Washing Quality of Filter Cakes, Advances in Chemical Engineering and Science, 1 (2011) 252-255.

[7] M. Burisch, U.A. Peuker, Influence of Wetting on Washing and Filtration Properties, Chemical Engineering and Technology, 39 (2016) 543-550.

[8] K. Zeitsch, New Theory for the Permeability of a Filter Cake Formed by Sedimentation, Tech. Mitt. KRUPP - Forschungsberichte, 42 (1984) 71-76.

[9] U.A. Peuker, Über die kombinierte Dampfdruck- und Zentrifugalentfeuchtung, in: Ph.D. Thesis Universität Karlsruhe, Karlsruhe, 2002, pp. 297.

[10] VDI, Filtrierbarkeit von Suspensionen Bestimmung des Filterkuchenwiderstands, in, VDI - Verein Deutscher Ingenieure, 1995.

4 Financial planning

All costs are calculated in US $. The costs are presented in yearly budgets. According the discussion in September 2016 with Timothy Bell at Dupont the financial frame has been set.

	1st year	2nd year	3rd year
Overall project costs / funding TU Bergakademie Freiberg Prof. Peuker	**38.000.-**	**37.000.-**	**40.000.-**

4.1 Labor costs

	1st year	2nd year	3rd year
PhD-student (50 % daily working hours)	32.000.-	33.000.-	33.500.-

4.2 Other costs

4.2.1 Consumables

	1st year	2nd year	3rd year
Consumables nutsch filter / filtration rig	1.000,-	1.000,-	1.000,-
Consumables instrumental analytics	500,-	500,-	500,-
Spare parts nutsch filter	1.000,-	-	-
Consumables tomography	2.000,-	2.000,-	1.000,-
Sum consumables	4.500,-	3.500,-	2.500,-

4.2.2 Traveling costs

	1st year	2nd year	3rd year
IFPRE Meeting	1.500,-	500,-	1.500,-
International conference	-	-	2.500,-
Sum travel costs	1.500,-	500,-	4.000,-

4.3 Available equipment

4.3.1 MVTAT-TU Bergakademie Freiberg (Prof. Peuker)

Method	Supplier	Measured parameter
Lab-scale nutsch filter according VDI 2762 (50 mm)	self-construction	filtration experiments
Lab-scale nutsch filter according VDI 2762 with washing unit (50 mm)	self-construction	filtration & washing experiments
Lab-scale nutsch filter according VDI 2762 with press piston unit (50 mm)	self-construction	filtration & consolidation experiments
Lab-scale nutsch filter according VDI 2762 with washing & press piston unit (50 mm)	self-construction	combined filtration, washing & consolidation experiments
Lab-scale nutsch filter nach VDI 2762 (70 mm)	self-construction	filtration experiments

laser diffraction	Sympatec Helos	particle sizing in the size range 0,1-875 µm
Automated image analysis	Sympatec QICPIC	particle sizing and shape analysis in the size range 5 -875 µm
Analytical centrifugation	Shimadzu L.U.M. Lumisizer	particle sizing in the size range 0,1-100 µm and sedimentation characterization
Analytical centrifugation with X-ray detector*	Brookhaven	particle sizing in the size range 0,1-100 µm and sedimentation characterization
Mercury porosimetry	Thermo Fisher Scientific	Pore size distribution
BET-analyzer	Micromeritics Flowsorb 2300	Direct evaluation of the specific surface of the particle system - integral value
Electron microscopy SEM	FEI - Phenom	Shape analysis and size analysis via image analyses
Computer tomograph	Zeiss Xradia Versa 510	3D-Characterization and in-situ experiments
Zeta-potential measurement	Malvern Zeta-Sizer Nano	Surface charge and particle interactions.
Potentiometric titration	Mütek - PCD-02pH, PCD-04	Surface load of particles
Tensiometer	Krüss - K12 Mk4	surface tension
Contact angle measurement	Krüss - G10	Wetting properties
* accessible due to co-operation TU Bergakademie Freiberg - HZDR		

Deliquoring of Wet Filtration Cakes: From Microfluidic Observations to Industrial Applications

Karin Schroën, Wageningen University, Food Process Engineering group, The Netherlands.
Professor in Food Microtechnology; karin.schroen@wur.nl, +31-317-483396.

Summary
To bring deliquoring of wet cake filtration to the next level, fundamental understanding of the process is needed. Currently, engineering equations are extended to comprise various aspects relevant to specific cases; however, this leads to highly specific solutions that can only applied to a limited range of process conditions.

In this proposal, microfluidic methods are used to systematically vary process conditions such as pressure, particle size (distribution) and particle interactions. Besides, special attention will be paid to the flow of liquids through labyrinths that are idealised particle beds. In this way, both the liquid and particle related aspects of cake filtration can be investigated individually, and in tandem.

Through this approach, scaling relations based on underlying mechanisms will be generated and tested for industrially relevant particles, both in microfluidic set-ups and and at larger scale. This will open the way to the identification of advanced process startegies that make cake filtration more efficient and less energy demanding.

Current approach to cake filtration
In every textbook, you will find the Darcy (eq 1) and Kozeny-Karman (eq 2a and b) equations used to describe cake filtration.

$$\frac{\Delta P}{L} = \frac{\mu}{k}\frac{dV}{dt}\frac{1}{A} \qquad 1$$

$$\frac{\Delta P}{L} = \mu\left(\frac{5(1-\epsilon)^2 S_v^2}{\epsilon^3}\right)\frac{dV}{dt}\frac{1}{A} \qquad \text{2a (Holdich)}$$

$$\frac{\Delta P}{L} = \frac{180\mu}{\Phi_s^2 D_p^2}\frac{(1-\epsilon)^2}{\epsilon^3}v_s \qquad \text{2b (Mc Cabe et al)}$$

In which, ΔP the pressure drop, L is the total height of the bed, μ the viscosity of the fluid, k a constant related to bed porosity, V the volume, t the time, A the area, ϵ the bed porosity, S_v the specific surface area, Φ_s the sphericity of the particles, and D_p the diameter of a spherical particle.

Various parameters used in the equations are highly correlated, e.g. porosity of the filter bed, is correlated to constant k but not necessarily linearly as illustrated in Figure 1a (Michaels and Lin), and also predicting the k value is far from trivial (Figure 1b; Chapuis and Aubertin). In the work of the latter authors, a lot of attention is put into bringing information available in different sources together, and they seem to have a reasonable agreement of fit for sand and clay filter beds, which are non-compressible particles. They stress that the measuring method is of great importance for getting correct k-values, therewith also indicating that the way that particle pack in a cake greatly influence the actual resistance against liquid flow.

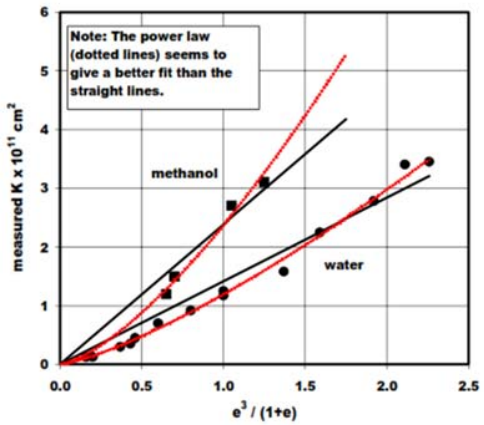

Figure 1a. Illustration of relationship between k and porosity (Michaels and Lin).

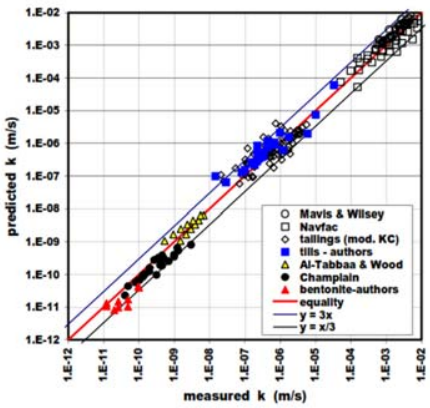

Figure 1b. Predicted versus measured k-values (Chapuis and Aubertin).

Besides, in literature various extensions have been suggested to capture e.g. flow conditions (see figure 2), using different relations depending on the Reynolds number. Furthermore, extensions for viscosity changes, and many other effects have been suggested as add-ons to the previously mentioned equestions. This does leads to better design of cake filtration processes; however, the applicability of the equations is very case specific.

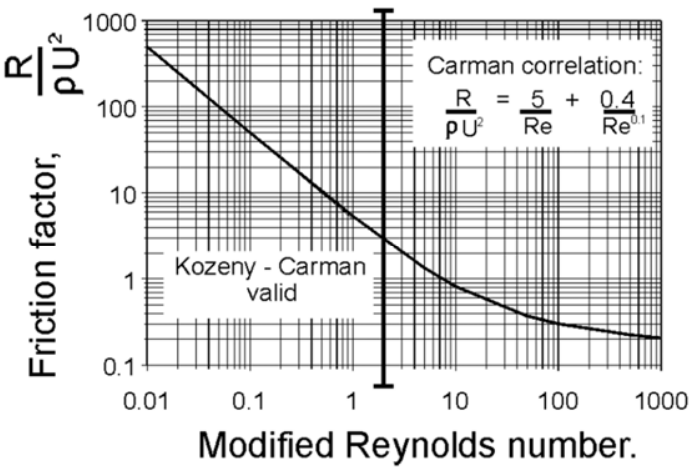

Figure 2. Friction factor in porous media as function of fluid flow conditions (Holdich).

Identification of missing links

When starting from a steady-state situation in the bed, as done in the equations mentioned earlier, obviously the dynamics taking place during filtration are not be covered. Just to name a few, locally particles can be displaced and settle in a different position leading to added resistance, or be removed to reduce the overall resistance. Also compaction of the bed may take place, again leading to increased flow resistance. Besides, the flow of the liquid through the bed will depend strongly on local resistance, and may go through preferred paths in which the actual flow may exceed the average flow considerably, and may also depend on shear thinning/thickening of the liquid. These aspects can also not be assessed when using large scale data that revolve around pressure, flux and bed height since the various effects are intertwined.

In order to distinguish between effects taking place in the liquid and in the particle bed, we propose to use microfluidic (microstructured) tools. We have worked with microfluidic devices that were

purposely designed for various projects since the early 2000, and have ample experience in using them to elucidate underlying mechanisms related to e.g. particle migration in flow, membrane separation, emulsification, ultrasound contrast agents, controlled release capsules etc.

Proposed tools and approach

As mentioned, we think that both liquid flow, and bed/particle properties need to be investigated in order to reach the level of mechanistic understanding needed to for elucidation of the importance of various effects taking place during cake filtration. In work that was carried out together with the soft matter and physical chemistry group of Wageningen university (dr. Joris Sprakel, and Ties van de Laar MSc), various devices have been developed that are also of interest for the current project; two are next described in detail.

In earlier work we have investigated liquid displacement in a labyrinth of idealised pores (see Figure 3a), and this can also be used for the current project to distinguish how liquid flows through the particle bed, and whether preferential flow takes place as function of pressure. The labyrinth in Figure 3a, consists of equally wide channels, but we found that the liquid does have preferred paths (unpublished results). The microfluidic technology that we use allows us to design any labyrinth, and that also allows us to investigate a wide range of bed properties. Those labyrinths that are of specific interest for the industrial partners can also be used in combination with various liquids, including viscosity, shear thickening and thinning effects (beginning versus end of the filtration, and presence of impurities).

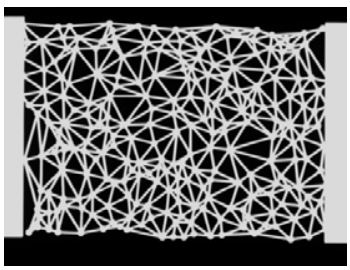

Figure 3a. Example of a flow labyrinth to elucidate preferential pathways.

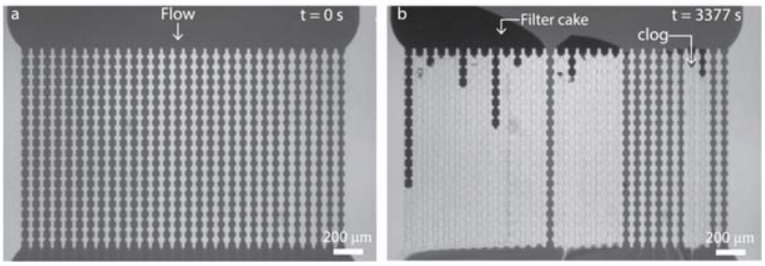

Figure 3b. Example of an idealised porous structure with pores with different geometries. In the image on the right, blocking behaviour is illustrated; the channels are then white in colour (van de Laar et al, 2016a).

Particle behaviour needs to be charted too in order to understand bed formation, and changes in bed morphology. For this devices similar to the one shown in Figure 3b, can be considered. This specific device was developed to investigate pore clogging in a membrane (both on top and internally). You see the device before use in the left image, with the open channels in dark grey, and the result after exposure to a particle dispersion with particles much smaller than the pore size on the right, with the clogged pores in white. Since the model membrane in Figure 3b is a porous structure, the analogy with a filter cake is very close (for that cross-connections would be needed). Besides, in the top of the image, the onset of cake formation that is taking place on top of the pores is visible, and that is also relevant for the current project. In the work of van de Laar (2015, 2016b), we showed that in very concentrated cake layers migration takes place, which is expected to influence permeability.

In these devices, various flow conditions can be applied, which will help in charting windows of operation for minimal flux decline during particle (cake) filtration. For this also the particle to channel

ratio needs to be investigated, the effect of particle polydispersity, and particle interactions. These aspects can easily be covered through channels of different widths, and preparation of particles of different sizes, and with different attraction strengths (a specialty of dr. Sprakel's group). This will lead to the first scaling relations that link liquid flow to reduced permeability and/or probability of blocking.

Using the microfluidic tools, also various process options can be tested that facilitate operation, such as backpulsing to loosen up the cake, addiational rinsing with liquids, building a sacrificial layer onto which the actual cake will form, specifically designed surfaces that minimise flux loss, and support sieve design. Given the flexiblity of design that microfluidics offer, these options can surely be mimiked, and we are open for suggestions by the industrial partners.

Besides microfluidic devices, cake filtration will be carried out at relatively small scale using sieves with uniform pores (Stork Veco) placed in a filtration column with which the first step can be made toward the more practical applications of the partners. The data that are obtained will be tested against the scaling relations derived from microfluidic investigations, and similarly, particle suspensions from the partners can be used to verify their behaviour. Furthermore, the various scaling relations that are available with the partners could be compared for common denomenators, using the description of flow and bed behaviour obtained from microfluidics and sieve experiments as a base.

Time plan

Year 1:

- Identification of industrially relevant conditions for cake filtration (including particle size (distribution), and flow conditions)
- Development of appropriate microfluidic tools for flow investigation (variation in channel width, length, open areas etc)
- Image analysis script development
- Analysis of flow of simple liquids through complex labyrinths, and first scaling relation
- First designs for filtration of small particle through a labyrinth of channels

Year 2:

- Analysis of flow of complex fluids through complex labyrinths
- Scaling relation linking fluid properties to flow distribution
- Analysis of blocking propensity of the channels by small particles
- Variation of channel and pore size, and design equation
- Particle interaction variation

Year 3:

- Development of the column system to investigate ideal particles, and industrially relevant sytems.
- Design of chips that allow investigation of process options to maximise cake dewatering (e.g. back pulse, washing steps, sieve design etc).
- Evaluation of these options, and recommendations for the partners
- Development of a toolbox for the industrial partners given their specific needs
- Comparison of existing scaling relations

Embedding, and fall back options

The described project is very complementary to the work that is done within the food microtechnology group. We have projects on filtration and emulsification for which we use microfluidic devices to elucidate the underlying mechanisms. The current project will become part of a long standing research collaboration with the soft matter and physical chemistry group of Wageningen University, with whom we have successfully worked within various PhD and other projects. This group has unique equipment to visualise particles while in flow, and present at very high concentration, while we have high speed imaging tools that we standardly use for our microfluidic investigations.

The design of the microfluidic devices will be achieved in house, the only limit is the resolution of the chips. At the moment of writing, I don't expect this to become an issue for the soft litography techniques that we use. If needed we can design the devices in glass, but that would be at an extra expense, since we would need to outsource this to a third party. The particles can also be made in house, as this is the core expertise of the Sprakel group, and also with Stork Veco, the manufacturers of the metal sieves, we have a long standing collaboration, and I am sure that they will be happy to help with the design of the metal sieves for the larger scale investigations.

What is obviously not known at the moment of writing is how the overall behaviour during cake filtration will be, but since we have split the project up into flow behaviour and bed behaviour, I think that changes for success are maximised in this way. The microfluidic designs will also be made keeping industrial needs closely in mind, and depending on the first outcomes, the research can be adjusted such that the relevant parameters are optimally covered.

As a last point, I would like to share that we are investigation options to start a microtechnology centre in Wageningen. Various parties have already reacted enthusiastically, and if the centre becomes a reality, that would also boost the current project.

Industrial support / contributions

As mentioned earlier, we would like to design the microfluidic devices in such a way that they are most relevant for the industrial partners, and for this we would like to carry out an inventory, to which I hope the partners are willing to contribute. In a later stage, when we are carrying out the larger scale experiments, I also hope that we can receive dispersions that are interesting for the industrial partners, including any existing scaling relations that may be available.

During the entire project, we will keep all partners updated, since the outcomes can be of immediate relevance. I suggest to do this via Skype every 3-4 months, and ideally we have yearly meetings in person with the entire team.

Referenced literature

- Chapuis, RP; and Aubertin, M (2003) Predicting the coefficient of permeability of soils using the Kozeny-Carman equation, Report EPM–RT–2003-03, Département des génies civil, géologique et des mines; École Polytechnique de Montréal, January 2003 http://www.polymtl.ca/biblio/epmrt/rapports/rt2003-03.pdf (accessed 2016-12-15)
- Goldich, RH (2002) Fundamentals of Particle Technology, Midland Information Technology and Publishing, Shepshed, UK.

- McCabe, WL; Smith, JC; Harriot, P (2005) Unit Operations of Chemical Engineering (seventh ed.), New York: McGraw-Hill, pp. 188–189, ISBN 0-07-284823-5
- Michaels, AS and Lin, CS (1954). The permeability of kaolinite. Industrial and Engineering Chemistry, 46(6):1239-1246.
- Van de Laar, T; Ten Klooster, S; Schroën, K; and Sprakel, J (2016a) Transition-state theory predicts clogging at the microscale, Scientific Reports 6, Article number: 28450.
- Van de Laar, T; Schroën, CGPH; and Sprakel, JHB (2015) Cooperativity and segregation in confined flows of soft binary glasses. Physical Review. E, Statistical nonlinear, and soft matter physics 92 (2). - 8 p.
- Van de Laar, T; Higler, R; Schroën, K; and Sprakel, J (2016b) Discontinuous nature of the repulsive-to-attractive colloidal glass transition, Scientific Reports 6, Article number: 22725.

Rebuttal section

This section contains the original message received from James Michaels in italic print, and my reaction to the points made in regular script.

I'm happy to report that your proposal received generally positive comments at our winter meeting in Amsterdam. There were a few questions about how you plan to represent pore structure - in particular, a concern was voiced about how the corrugated pore model can account for flow in the transverse direction as well as pore connectivity. Also, there was a request to provide more detail about the systems you plan to study in the project.

That is great to hear, and I am happy to explain how we would like to further shape the project, and the microfluidic tools that we would like to use.

I can imagine that the link of the tool shown in figure 3b to cake filtration may seem a bit farfetched, since interconnectivity is not present, but that has to do with the original goal for which it was designed; to investigate the propensity of pore blocking as function of a pore geometry. In cake filtration this may seem less relevant, but still propensity of blocking is an important factor, since it leads to re-routing of liquid to pores that are still available, which in turn leads to pressure build-up, and ultimately termination of the filtration process.

In order to understand the overall process, we need to link processes happening at pore level, to re-routing, and for that we propose to use tools, such as the ones depicted in figure 3a and b, but now specifically designed to tackle the processes occurring in cakes. We have great freedom in designing pores according to typical particle sizes present in a filter cake. For example, in figure 3a we worked with random placing of the circles that were connected by equally wide pores, and visualized liquid flow (that is far from uniform). We now propose to work with a particle size distribution (the black triangles in figure 3a), while allowing for variation in channel width at specific overall porosities. We will compare the lay-outs in terms of flow through the channels, and later after introduction of particles to the device also to likelihood to block / build up pressure fast. From the flow pattern and blocking behavior, flow paths will be identified that will be investigated in more detail on their propensity to blocking in absence of connectivity in devices that resemble the ones in figure 3b. The basic question we are answering in this way is over which distance re-routing can still efficiently mediate blocking effects, and this gives clues on which particle size distribution and process conditions lead to better filterability.

We also have the ambition to extend our investigations to *in situ* formation of a cake on a support, and again we will follow the flow patterns, and how they change in time. Besides this, these experiments can be used to evaluate the effect of the support on cake build-up. In the figure below you see two idealized membranes that we originally designed to investigate emulsification; the ones that we propose for the current project will start with one layer of obstacles, and become progressively more complex, ideally resembling the material used on large scale, therewith allowing for an educated choice of support material. To be complete, these tools can also be used to evaluate e.g. the effect of back pulsing.

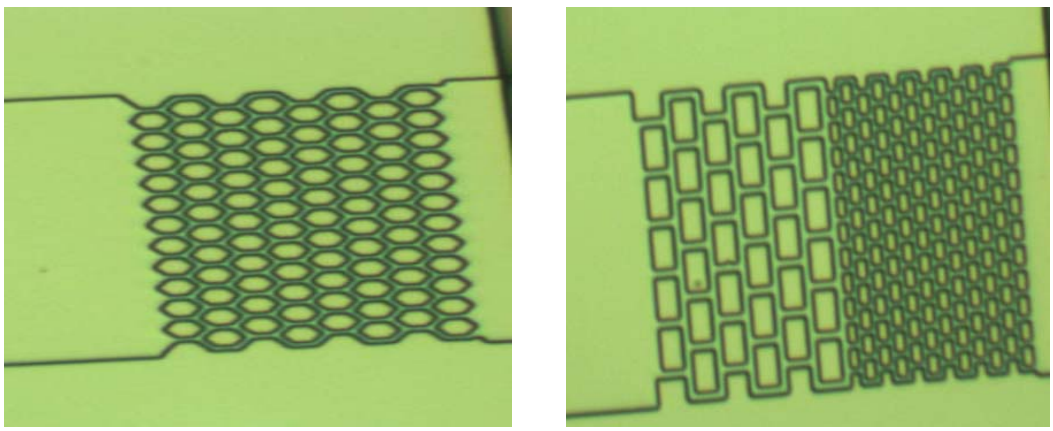

Examples of idealized filters onto which the cake can form in-situ.

I hope that I have given you more clarity over the devices that we intend to develop and use during the investigations. I am very enthusiastic about this project that has very clear industrial relevance, and to which I contribute by elucidating the underlying mechanisms that will help design even better processes! If you need more information, please let me know.

IFPRI Research Project Brief

Mixing Rules for Powder Blending

The International Fine Particle Research Institute (IFPRI) wishes to fund a research project to develop scaling rules for industrial powder blending processes based on first principles. Specifically, how can one predict how mixing mechanisms (e.g. shear, convection, percolation) change from bench- to production scale and thus develop quantitative tools to predict full-scale blending performance from small-scale experiment? We expect that the project will develop fundamental scaling rules for different mixing mechanism, determine the relative importance of each mixing mechanism in mixers of different type and scale, and determine how material properties affect both of these. Since IFPRI's members span a very broad range of particle technologies, understanding the role of particle morphology, mechanical properties, and cohesion are critical to a successful project.

In order to make the project as general as possible, the research should focus on generic and not proprietary mixer designs. We expect that the work will combine theory, simulation, and experiment: a fully theoretical and/or computational project is not sufficient. Finally, while we acknowledge the link between mixing and segregation, the project should focus on mixing. IFPRI is currently funding a project on segregation prediction (Prof. Joseph McCarthy at the University of Pittsburgh), thus an opportunity exists to link the two projects should it make sense to do so.

Mixing Rules for Powder Blending

Proposal Re-submitted to IFPRI

By: Benjamin J. Glasser, Department of Chemical and Biochemical Engineering, Rutgers University, 98 Brett Road Piscataway, NJ 08854, USA, bglasser@scarletmail.rutgers.edu

Summary

Particulate mixing operations are often poorly understood compared to their fluid counterparts. Traditionally, heuristic rules-of-thumb have been used to predict full scale blending performance from small scale experiments. A more desirable approach would be to predict scale up for industrial powder blending processes based on first principles. In this proposed project we will examine how mixing mechanisms change during scale up and thus develop quantitative mixing rules for powder blending. Fundamentally, mixing stems from variations in velocity between adjacent regions of a system. In this project we will numerically and experimentally study flow and mixing of granular material and powders in rotating shell blenders; this work can be expanded to consider horizontal axis agitated mixers. These mixers are representative of powder mixing equipment in industry. Experimental flows will be examined using Particle Image Velocimetry (PIV), MRI, blender sampling, and image analysis techniques. Particle dynamic simulation techniques will be used to compute flow properties that are not easily measured experimentally. Computational and physical experiments will be used to characterize mixing and we will explore the use of relevant dimensionless groups. Mixing will be characterized using the Relative Standard Deviation (RSD) of species concentration as well as other relevant mixing metrics. Mechanisms of particle mixing will be characterized for quasi-static flow regimes typical of mixing operations. A parametric sensitivity analysis will be performed to quantify the role of particle size distribution, particle density variations, surface properties and inter-particle cohesion. Initial work will consider non-cohesive particles with subsequent work allowing for cohesive particles. Inter-particle cohesion will be introduced through: a) adding liquid to the flows or b) reducing the particle size such that cohesion plays a role. Non-spherical particles predominate in industry, and particle shape strongly influences maximum packing density, angle of repose, and flow anisotropies. We will therefore examine the effect of particle morphology on flow and mixing. Scale-up will be examined in order to develop an understanding of how flow behavior and mixing changes with system scale and we will thus elucidate scale-up rules. Note: a response to the feedback from IFPRI on the original proposal is given in an Appendix.

1. Objectives and Significance

As discussed by Bridgwater[1] in a recent review article, there are two main classes of powder mixing equipment. In the first class, the shell rotates and these are often called tumbling blenders or rotating shell blenders; examples include cylindrical drums, double-cone blenders, V-blenders and tote (or bin) blenders. In the second class of equipment, the shell is stationary and there are internal blades that move in order to achieve agitation of the powder; examples include ribbon mixers (horizontal axis agitated mixers), planetary mixers and centrifugal mixers with a vertical axis (vertically shafted mixers). In this work, we will initially focus on rotating shell blenders. This work can be expanded to consider horizontal axis agitated mixers. Rotating shell blenders are common in a variety of industrial processes for mixing both wet and dry powders or granular materials. While in many cases these are used to homogenize a blend of dry solid particles, they also serve to enhance heat and mass transfer in wet flows (e.g. agitated dryers). While simple in form – basically a bucket that rotates about an axis– the effect of particle and process parameters on flow and mixing is still not well understood. In addition, it is hoped that information from rotating shell blenders will be able to be applied to more complex mixers like horizontal axis agitated mixers.

In year 1, we will carry out experiments and particle dynamic simulations of cohesionless spherical particles with the aim of developing scaling rules for blending based on first principles. We will examine how material properties affect mixing mechanisms by varying particle sizes, masses, densities, coefficient of restitution and frictional characteristics. We will initially start with monodisperse spherical particles and subsequently allow for distributions of cohesionless spherical particles.

In year 2, we will introduce inter-particle cohesion through adding liquid to our flows. In addition, we will also reduce the particle size for dry materials such that cohesion plays a role. For wet flows, we will control cohesion by varying the type of liquid added (allowing for variations in viscosity and surface tension), and the amount of added liquid to allow for a range of flow conditions from weakly cohesive flows to strongly cohesive flows as characterized by the Bond number. For dry flows, we will reduce the particle size to less than 100 microns such that van der Waals' cohesion becomes important. We will compare the cohesion due to liquid bridges with cohesion due to van der Waals' forces. We will investigate the effect that cohesion plays on scaling rules for mixing.

In year 3, we will investigate the effect of particle shape on scaling rules for powder blending. Methods to incorporate particle shape into particle dynamic simulations have been developed using various contact-detection algorithms for superquadrics and hyperquadrics, polygons, and arbitrarily shaped virtual particles. However, to maintain the computational speed afforded by the simulation of spherical particles, composite, non-spherical particles will be constructed by gluing a series of identical spheres together [2]. In this work, both physical and computational experiments of non-spherical particles will be carried out.

Critical unknowns that may influence the direction/outcome of the project include:

1) Scale up by its very nature requires doing simulations and experiments at a range of scales. We anticipate that experiments and simulations at Rutgers can be carried out for a number of systems ranging from the bench scale to the pilot scale. While it is possible that we may be able to carry out a small number of simulations at the manufacturing scale, we will need IFPRI members to carry out experiments at the manufacturing scale to test the scaling rules. This represents a critical unknown i.e. will IFPRI members partner with us to carry out experiments at the manufacturing scale?

2) The proposed project will introduce complexity in the material properties as we progress in time. The project will start by examining cohesionless spheres, and then proceed to examine cohesive spheres and eventually examine non spherical particles. An assumption that is being made is that scaling rules developed for the cohesionless spheres will give us information about scaling rules for cohesive spheres and non-spherical particles. If this is not the case, this will influence the direction and outcome of the project as the project will take longer than anticipated.

This project will leverage a number of existing activities in which my research team is engaged. We have been working on granular and powder flow for over 20 years. This effort has been funded by the Federal Government and pharmaceutical and chemical industry. I currently have a PhD student funded by the Federal Government of Thailand working on vertical axis paddle mixers with a focus on agitated drying. IFPRI funding would leverage our existing efforts on the vertical axis paddle mixer[3-11]. My research team is also involved in a number of research projects on powder processing through the Rutgers Catalyst Manufacturing Consortium (http://cbe.rutgers.edu/catalyst) including projects on particle drying, calcination in rotary drums, and powder handling and characterization. In addition, my research team is also involved in a number of projects on powder processing through the Engineering Research Center for Structured Organic Particulate Systems (ERC-SOPS: http://ercforsops.org) including continuous manufacturing of pharmaceuticals and characterization of powders with the goal of correlating powder properties to process performance. Along with these research efforts, we have millions of dollars of powder characterization equipment at Rutgers. We also have excellent computational facilities and access to particle dynamics simulation codes. IFPRI funding would leverage my current research efforts on powder flow, processing and characterization.

IFPRI members could support the research program through provision of model test materials, helping to decide research directions, and partnering on the research to provide industrial expertise. In addition, it is anticipated that work at Rutgers can be carried out on the bench and pilot scale, but cannot be carried out on the manufacturing scale. Thus, we will require IFPRI members to test scaling rules at the manufacturing scale.

2. Proposed Research

Powder mixing can be attributed to three mixing mechanisms: convection, diffusion and shear[1]. In rotating shell mixers we expect convection to dominate but diffusion and shear will still be important[12-15]. The need to improve fundamental understanding of mixing of particles in rotating shell mixers will be accomplished through numerical modeling and experiments. Particle dynamics simulations of compositions will be compared with blender sampling, PIV, MRI and image analysis in the laboratory.

2.1 Experimental Investigations

Our existing rotating shell mixer geometries are shown in Fig 1. Initial work will examine a cylindrical mixer (Fig 1a) with subsequent work examining the double-cone (Fig 1b). If there is interest from IFPRI members, we can also examine a V-blender (Fig 1c) and tote (bin) blender (Fig 1d). We have equipment at Rutgers as part of our powder processing labs, capable of working with shells ranging from tens of centimeters to around a meter in diameter (see Figs 1e-g) corresponding to blending of hundreds of grams to ~50 kilograms of powders. We have existing cylindrical, double-cone, V-blender and tote shells at a variety of different sizes. In addition, additional size shells can easily be fabricated or purchased in order to systematically examine mixing at different scales. We will start with the cylindrical mixer and examine mixing as a function of fill volume building on previous work[16, 17]. We will then examine cylindrical mixers of different sizes and then, based on IFPRI input, look at shells of different geometry (Figs 1b-d).

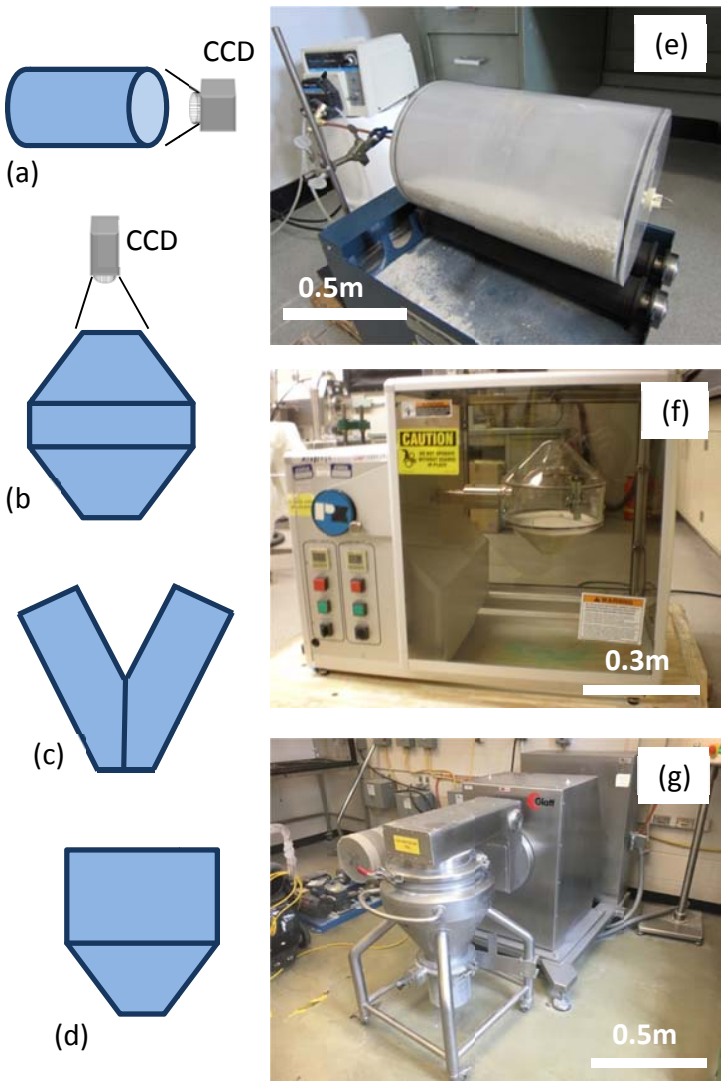

Figure 1: Rotating shell blenders to be studied. (a) Cylindrical, (b) double-cone, (c) V-blender and (d) tote blender. Available equipment at Rutgers: (e) rotating cylindrical blender, (f) Patterson Kelley Blend Master with double-cone shell, and (g) Glatt Twin Axle TAM 40 blender with tote shell.

In our experiments, a CCD camera with a spatial resolution of 150 microns/pixel will be placed directly above the flowing particles and used to record images of the free-surface at 500 frames per second. A second

camera location enables images to be obtained of flow visible through transparent sidewalls. Particle velocities are quantified with our existing PIV apparatus (Dantec Industries, NJ) which permits quantification of particle motion in either free-surface flows, or flows visible through transparent walls (see Fig 2a, b). Trajectories of individual particles are calculated by cross-correlation of sequential image frames, obtained from our high speed CCD camera and image capture software (Redlake Imaging, CA). Subsequent processing provides velocity fields and statistics that can be compared to particle dynamic simulations that will be carried out in an identical geometry.

An example of our PIV capabilities is shown in Fig 2a,b for flow of art sand down an inclined plane. A representative PIV image is shown in Fig 2b where regions of vorticity are evident. The instantaneous data provided by PIV can be used to characterize transient surface features of the rotating shell blenders. In order to characterize flow patterns and mixing within the powder bed we will make use of bed freezing via glue and solvent infiltration and setting that has been successfully implemented[14]. The subsequent solid mass can be sliced showing internal features of the powder flow. In Fig 2c,d we show images from previous work[14] demonstrating this bed freezing technique. Particles were placed in a cylindrical drum with green particles on the left and red particles on the right (see Fig 2c). After 0.75 revolutions of the blender, it is clear that significant mixing has already taken place (see Fig 2d). This bed freezing technique has been used for fine powders (with a d_{10} = 30μm) with the only limitation being that a low viscosity glue-solvent mixture is able to infiltrate the powder bed[18]. This bed freezing technique can readily be used for bench scale blenders. For pilot scale blenders we will make use of sampling in order to characterize mixing. A number of sampling devices are available at Rutgers including powder thief sampling tools of a variety of lengths and sizes. We will also make use of an MRI available at Rutgers to characterize flow and mixing. In Fig 2e we show a representative image from the MRI at the Rutgers Molecular Imaging Center showing 1mm particles in a tube. The Rutgers MRI has a resolution of 50μm and can readily image bench scale blenders with tracer particles that are impregnated with oil or water.

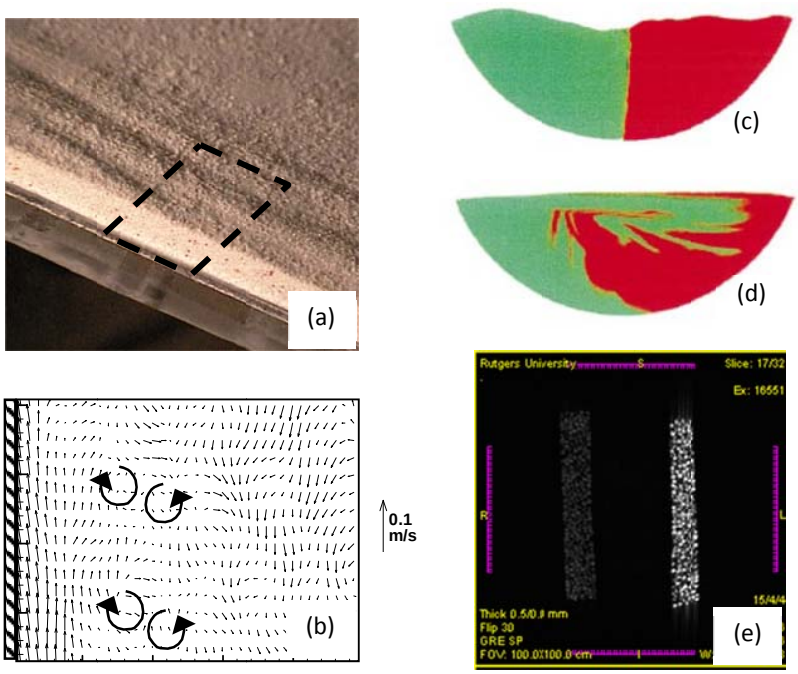

Figure 2: Experimental characterization of powder flow and mixing. (a) Flow of art sand down an inclined plane. Dashed lines indicate area of PIV analysis in panel b. (b) Instantaneous PIV vector plot with mean velocity subtracted. (c,d) Bed of frozen particles with sizes of 63μm to 180μm; images are from ref [14]. Initial condition is shown in c. Image after 0.75 revolution of the cylindrical tumbling mixer is shown in d. (e) MRI of particles in a tube, carried out at the Rutgers Molecular Imaging Center; image credit – N. Shapley.

2.2 Particle Dynamics Simulations

We will make use of soft-sphere particle dynamics simulation, referred to as DEM simulations, to examine granular/powder flow and mixing in rotating shell blenders (see Fig 3). With this technique,

information can be obtained on local flow and stresses that are difficult if not currently impossible to obtain experimentally. In addition, our experiments are limited in their ability to characterize all features of the flow so the simulations will be invaluable to measure particle behavior inside the bed. An important part of our work will be validation of the DEM simulations. In addition to accurately simulating particle velocities, we will want the DEM simulations to also reproduce the mixing kinetics observed in the experiments. We anticipate that the scale-up rules will be driven by simulations and confirmed experimentally.

Understanding the role of mixer parameters and operating conditions in rotating shell blenders is critical for designing and engineering reliable processes. Fig 4 shows our strategy for developing scale-up rules for powder blending. Three different size double-cone blenders have been simulated (see Fig 4a) making use of three different initial loading[19] conditions (see Fig 4b). Based on previous work[16] the three blenders of different size have been operated at the same Froude number. In Fig 4c, we show results for three different blender sizes (1.25 quarts, 4.2 quarts and 10 quarts) for mixing of cohesionless monodisperse particles. The relative standard deviation (RSD) of the concentration of the one species has been plotted as a function of number of revolutions and it can be seen that a scaling based on Froude number leads to similar mixing performance for all 3 system sizes. More complicated scale-up is expected for cohesive materials. An important part of our work will be validation of the DEM simulations. In addition to accurately simulating particle velocities, we will want the DEM simulations to also reproduce the mixing kinetics observed in the experiments.

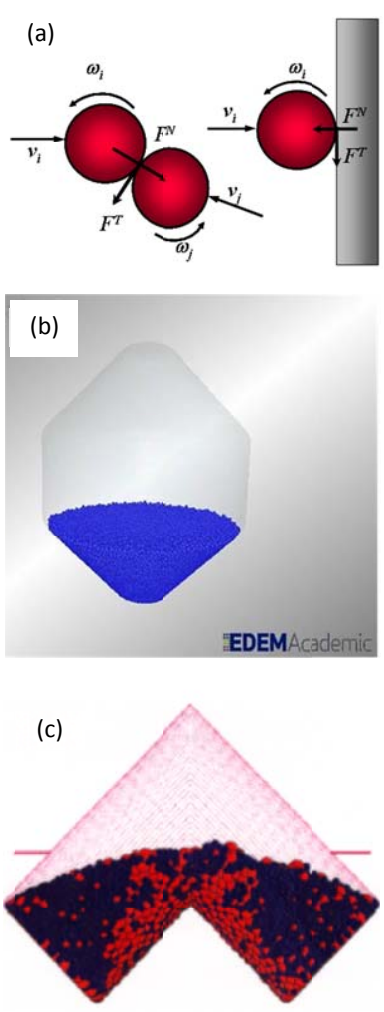

Figure 3: DEM simulations. (a) Particle-particle and particle-wall interactions. (b) DEM simulation of a double-cone blender; image credit- Y.Shen, Rutgers. (c) DEM simulation of a V-blender; image credit- A.Alexander, Rutgers.

2.3 Research Schedule Outline

The proposed work will be completed over a period of three years. Our focus in year 1 will be mixing of spherical non-cohesive dry granular materials. Glass beads of relatively large diameter (500 μm to 5 mm) will be used, to permit accurate representation by particle dynamics. We will start with monodisperse spherical particles and subsequently allow distributions of cohesionless spherical particles. The mixing of these particles will be fully characterized in year 1 using PIV, MRI, blender sampling, image analysis and freezing of the bed. Careful control of the parameters affecting mixing will allow an in-depth study. These parameters include system dimensions, operation conditions and material properties. Polymeric, metallic and glass particles will allow the coefficient of restitution, e_p to be varied from ~0.6 to 0.95, and a coating procedure[6] will allow frictional parameters to be varied to simulate relatively smooth and rough particles. Work in year 1 will extend investigations to distributions of particle size and mass. Particle dynamic simulations will mirror the progress in the experimental studies. The sensitivity of the particle dynamic simulations to parameter choices like spring constant, time step etc. will be investigated. Mechanisms of particle mixing (convection, diffusion, shear) will be characterized for quasi-static and intermediate flow regimes typical of mixing operations. Mixing will be characterized using the Relative Standard Deviation (RSD) of species concentration as well as other relevant

mixing metrics[10]. An important part of characterizing mixing will be recognition that the mixing metric will depend on the size of the sample or scale of scrutiny[1]. In order to characterize mixing we will either dye the particles or purchase particles of different colors. We will test that the particles of different colors that we purchase or dye have the same flow properties. We plan to focus on mixing of materials that are identical except for their color. This will ensure that the project will focus on mixing as opposed to segregation. If there is interest from IFPRI members to examine mixing of different (e.g. size, density) species, then this can be incorporated into the project. Work on rotating shell blenders will first be carried out on bench scale equipment and scale-up studies will subsequently be carried out in larger geometries. We anticipate carrying out experiments and simulations from the bench scale to the pilot scale.

In spite of the fact that cohesive particles prevail in industry, cohesion has rarely been considered in flow studies in cylindrical mixers. In industry, cohesion arises due to the fact that liquid is often present and/or particle sizes are sufficiently small for inter-particle cohesive forces to be important. In year 2, wet cohesive flows will be considered experimentally by adding liquid to our glass beads. We will build upon previous work[9] by considering the effect of cohesion on monodisperse systems and extend this to polydisperse systems in subsequent work. We will control cohesion by varying the amount of added liquid, and liquid surface tension and viscosity to allow for a range of flow conditions from weakly cohesive flows to strongly cohesive flows as characterized by the Bond number. Initial work will focus on water and glycerine mixtures with oils being used in later work. Care will be taken to evenly distribute the added liquid by thoroughly mixing the particles in our high shear agitated mixer. In year 2, we will also experimentally and computationally examine dry moderately cohesive flows by decreasing the size of the spherical particles we examine to 10μm and possibly smaller, based on input by IFPRI members. In year 2, cohesion will also be implemented in our particle dynamics simulations by assuming cohesive forces act only pair wise[20], such that multiple particle interactions can still be modeled as the sum of many two-body interactions.

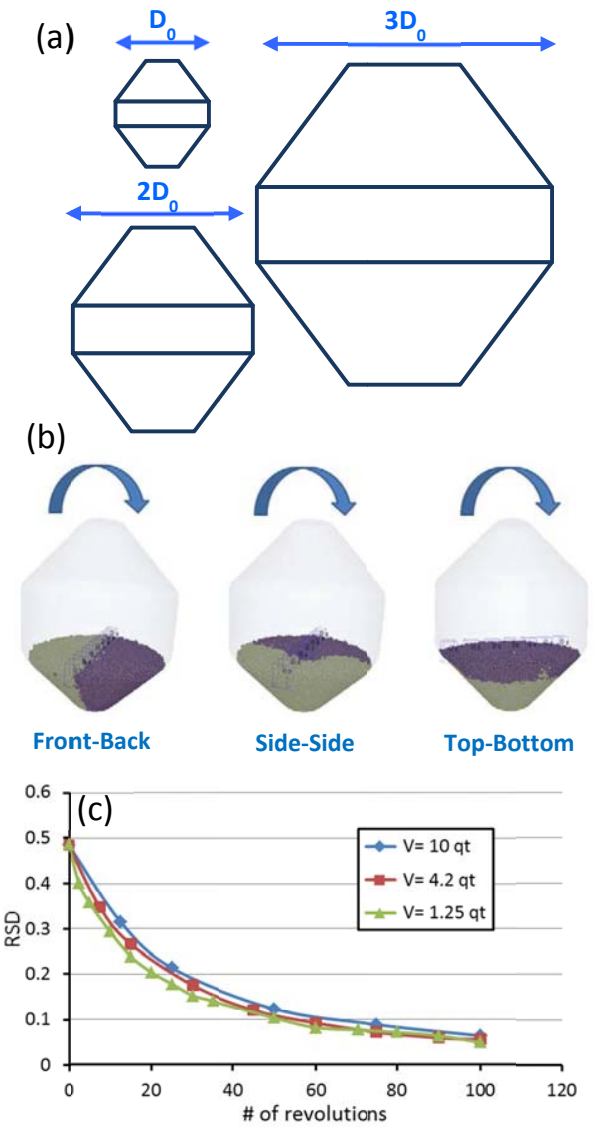

Figure 4: Scale-up of powder blending. (a) Three double-cone blenders that have been linearly scaled-up. (b) Three different initial loading conditions; image is from ref[19]. (c) Relative standard deviation as a function of number of revolutions; image credit- Y.Shen and S.Tomassone, Rutgers.

Work in year 3 will examine non-spherical particles. In particular, acicular needle-like morphologies are common in pharmaceutical crystals and these will be studied experimentally and modeled in the simulations. As

the major computational resources for simulating non-spherical particles are used to detect contacts, maintaining spherical particle contacts maintains reasonable processing times. Thus, non-spherical particle morphologies will be modeled by creation of *composite* particles of rigidly bonded spheres and adjusting the collision model accordingly. Experimentally, we will examine ideal needles by using cylinders with latter work examining needle-like crystals (e.g. L-Threonine). The cylinders will be characterized by their length to diameter ratio (L/D) and equivalent sphere diameter. We will characterize which behaviors can be explained by the increased equivalent particle sphere diameter. We expect that for L/D close to 1 the needles will behave like spheres with an increased particle diameter and only at higher L/D will deviations from spheres be observed, including formation of nematic phases and interlocking of particles. If additional IFPRI funding is available to fund the project beyond the initial 3 years, then other particle shapes will be considered as suggested by IFPRI members.

References

1. Bridgwater, J. Mixing of powders and granular materials by mechanical means—A perspective. *Particuology* **10**, 397-427 (2012).
2. Nolan, G.T. & Kavanaugh, P.E. Random Packing of non-spherical particles. *Powder Tech.* **84**, 199-205 (1995).
3. Boonkanokwong, V., Remy, B., Khinast, J.G. & Glasser, B.J. The effect of the number of impeller blades on granular flow in a bladed mixer. *Powder Technology* **302**, 333-349 (2016).
4. Conway, S.L., Lekhal, A., Khinast, J.G. & Glasser, B.J. Granular flow and segregation in a four-bladed mixer. *Chemical Engineering Science* **60**, 7091-7107 (2005).
5. Lekhal, A., Conway, S.L., Glasser, B.J. & Khinast, J.G. Characterization of granular flow of wet solids in a bladed mixer. *AIChE Journal* **52**, 2757-2766 (2006).
6. Remy, B., Canty, T.M., Khinast, J.G. & Glasser, B.J. Experiments and simulations of cohesionless particles with varying roughness in a bladed mixer. *Chemical Engineering Science* **65**, 4557-4571 (2010).
7. Remy, B., Khinast, J.G. & Glasser, B.J. The effect of mixer properties and fill level on granular flow in a bladed mixer,. *AIChE Journal* **56**, 336-353 (2010).
8. Remy, B., Khinast, J.G. & Glasser, B.J. Discrete element simulation of free flowing grains in a four-bladed mixer. *AIChE Journal* **55**, 2035-2048 (2009).
9. Remy, B., Khinast, J.G. & Glasser, B.J. Wet Granular Flows in a Bladed Mixer: Experiments And Simulations of Monodisperse Spheres. *AIChE Journal* **in press** (2013).
10. Remy, B., Khinast, J.G. & Glasser, B.J. Polydisperse Granular Flows in a Bladed Mixer: Experiments and Simulations of Cohesionless Spheres. *Chem. Eng. Sci.* **66**, 1811-1824 (2011).
11. Remy, B., Kightlinger, W., Saurer, E.M., Domagalski, N. & Glasser, B.J. Scale-up of agitated drying: Effect of shear stress and hydrostatic pressure on active pharmaceutical ingredient powder properties. *AIChE Journal* **61**, 407-418 (2015).
12. Ottino, J.M. & Khakhar, D.V. Scaling of granular flow processes: from surface flows to design rules. *AIChE J.* **48**, 2157-2166 (2002).
13. Ottino, J.M. & Khakhar, D.V. Mixing and Segregation of Granular materials. *Ann. Rev. Fluid Mech.* **32**, 55-91 (2000).
14. Shinbrot, T., Alexander, A. & Muzzio, F.J. Spontaneous chaotic granular mixing. *Nature* **397**, 675-678 (1999).
15. Li, H. & McCarthy, J.J. Cohesive Effects on Particle Mixing and Segregation. *Physical Review E* **71**, 021305 (2005).
16. Muzzio, F.J. & Alexander, A.W. Scale Up of Powder-Blending Operations. *Pharmaceutical Technology* **26**, 34-41 (2005).

17. Paul, E.L., Atiemo-Obeng, V.A. & Kresta, S.M. Handbook of Industrial Mixing: Science and Practice. (2004).
18. Brone, D. et al. Using flow perturbations to enhance mixing of dry powders in V-blenders. *Powder Technology* **91**, 165-172 (1997).
19. Romanski, F.S., Dubey, A., Chester, A.W. & Tomassone, M.S. Dry catalyst impregnation in a double cone blender: A computational and experimental analysis. *Powder Technology* **221**, 57-69 (2012).
20. Hsiau, S.-S. & Yang, S.-C. Numerical simulation of self-diffusion and mixing in a vibrated granular bed with the cohesive effect of liquid bridges. *Chem. Eng. Sci.* **58**, 339-351 (2003).

Appendix

Response to Feedback on the Original Proposal

1. Choice of mixer: a large number of members felt that the vertical axis paddle mixer was not representative of mixers used by industry for powder blending. Most everyone asked if you are able to study other mixer types, e.g. rotating shell blenders or horizontal axis agitated mixers

Response: I am able to study other mixers. I have revised the proposal to initially study rotating shell blenders and I can expand this to horizontal axis agitated mixers based on feedback from IFPRI members.

2. Characterization of flow in blender: there was a lot of discussion on this subject. The primary concern seems to be that you are constrained to measuring surface flows and are unable to probe internal flows in the powder directly.

Response: Based on this feedback, we have expanded our experimental characterization to include: a) freezing of the powder bed via glue and solvent infiltration, and b) MRI.

3. How are you going to discriminate between convective and diffusive flows?

Response: This will be examined in DEM simulations by measuring a diffusion coefficient in the blender. For granular or powder flows the diffusion coefficient is a tensor and can vary spatially. We have computed the diffusion coefficient from DEM simulations in previous work; see ref[7]. The relative contribution of convection and diffusion will be determined by computing a Peclet number. We have computed a Peclet number in previous work; see ref[7], and used it to determine whether convection or diffusion dominates the transport process.

4. What mixing scales will you probe, i.e. what is your scale of scrutiny for mixing?

Response: In DEM, the scale of scrutiny for mixing will be as small as the size of a particle. Experimentally, the scale of scrutiny for mixing will depend on the characterization technique. Making use of freezing of the powder bed, we expect to be able to go down to the scale of a few particle diameters. However, for sampling of the bed, the scale of scrutiny will be the size of the sample. In general, the size of the sample will be much larger than the size of a particle.

5. What flow regimes are you planning to investigate?

Response: We plan to initially investigate quasi-static flows. If there is interest in looking at other flow regimes, then I am open to adding this to the scope of work.

6. There was also a specific concern that you'll be constrained to investigating large particles by the resolution of both your camera and by DEM.

Response: We do not believe that we will be constrained to investigating large particles due to the resolution of our camera. Our camera has a resolution of 150 microns/pixel. In principle, we can work with particles as small as we want, but at some point we will not be able to follow the motion of individual particles. For example if we work with 10 micron particles we will not be able to follow the motion of a single particle but with such small particles we expect highly cohesive flows with particle

flowing as weak agglomerates. If it is of interest to IFPRI members to examine flow at a resolution smaller than 150 microns, there are some high speed cameras available at Rutgers with smaller resolution than our camera. However, we believe that a resolution of 150 microns is adequate for the proposed work. DEM does have limitations in terms of simulating small particles for long times in large blenders. There will need to be a careful balance between the length of time of the simulation, size of the particle and size of the blender in order to obtain results in a reasonable amount of time.

7. There were a number of positive comments about your inclusion of cohesivity in the plan, although a few of us wondered if cohesion by liquid bridges is qualitatively similar to dry van der Waals cohesion. Related to this, one member asked if you can apply your approach to fine cohesive and compressible powders, e.g. <50 microns.

Response: I agree that cohesion from liquid bridges will not be the same as dry van der Waals cohesion, but some features of the two may be similar e.g. the formation of agglomerates that deform in the flow. The proposed work will consider fine cohesive and compressible powders that are <50 microns.

8. Finally, there was a consensus that if choices have to be made, cohesion is more important to study than shape.

Response: If the proposal is funded, we will prioritize cohesion over shape.

UNIVERSITY OF
KWAZULU-NATAL

30 April 2017

IFPRI Research Project Proposal

on

Mixing Rules for Powder Mixing

Proposal Prepared by
Indresan Govender

School of Engineering

Postal Address: Howard College Campus, Durban, 4041, South Africa

Telephone: +27 (0)31 260 3727 **Facsimile:** +27 (0)31 260 1118 **Email:** govenderi5@ukzn.ac.za **Website:** www.ptg.ukzn.ac.za

Founding Campuses: Edgewood Howard College Medical School Pietermaritzburg Westville

Introduction and Background

Mixing (and segregation) plays a vital role in several industrial processes. In the pharmaceutical industry, the effectiveness of the drug is directly related to the mixture of active ingredient and excipient. Central to the low efficiency (< 5%) reported in mineral grinding processes [1] is the inability to control the relative mix of grinding balls and small rocks in the high shear zones where most of the energy is dissipated [2]. The canonical rotating drum system encountered in the mineral processing, food and pharmaceutical industry is well known to exhibit axial and radial mixing; however, their interplay for optimal performance is not well understood [3]. A further limitation relates to the low Froude regimes explored by many investigators that ultimately lead to a restricted mechanistic interpretation. For example, the kinetic-stress models [4-6] argue that larger particles feel a relatively larger lithostatic pressure per unit volume than smaller particles and consequently the smaller particles fall through the interstitial spaces while the larger ones rise to the surface. However; in rotating drum flows operated in the cascading and cataracting Froude regimes, exactly the opposite is observed [7].

The lack of fundamental understanding of mixing is intimately coupled to the lack of a universally valid granular flow theory. A compounding factor relates to the rich coexistence of flow regimes encountered in typical industrial granular flows that simultaneously exhibit solid-, liquid- and gas-like behaviour; see figure (1), which is derived from [8], for more details. The problem in realising a universally valid granular flow theory is strongly related to the difficulty in measuring:

a) Solid volume fraction distributions, ϕ (as shown in figure 1),
b) Detailed velocity fields and the associated shear rate, and
c) Stress fields.

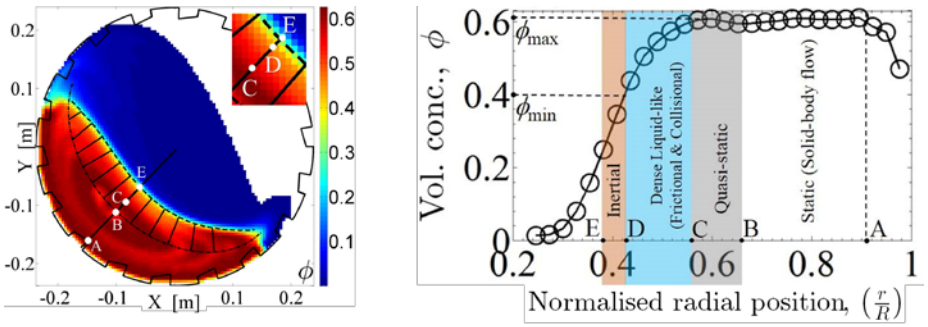

Figure 1: PEPT derived solid volume fraction along the radial line passing through the thickest region of a tumbling mill flow. The figure on the left shows the rich coexistence of flow regimes that have hitherto not been quantitatively delineated. Figure adapted from [8].

Unfortunately, most measurements of granular flows lack sufficient detail and coverage of the phase space to yield universally valid results—see [9] for a detailed review of measurement schemes employed to study granular flows. Positron Emission Particle Tracking (PEPT) is arguably the most accurate and detailed measurement tool for determining (a) and (b). To determine the stresses requires a constitutive choice in the absence of direct stress measurements. Robust scaling laws bound the theoretical development of these constitutive choices to a narrow slice of reality—the physics, if you will. Pragmatically, this is the most expedient route to realising a robust theory of granular flow and mixing.

Computational modelling also offers complimentary "measurements" that are not possible with traditional in-situ measurement schemes. In this regard, outputs (force, velocity, energy dissipation) from Discrete Element Method (DEM) simulations can be up-scaled into a continuum framework to yield the full stress tensor which can be used as cross validation of the constitutive choices. Taken together with PEPT measurements, these three ingredients—as listed above—can be used to formulate a coherent theory of granular flow, and indeed the resulting scaling rules that drive mixing.

We thus hypothesise that detailed in-situ measurements coupled with continuum up-scaling of equivalent DEM simulations will provide the key ingredients to accurately characterise the constitutive laws governing granular flow. Robust scaling rules can then be derived from the experimental and numerical measurements, and safely extrapolated to production scale operations.

The Particle Technology Group (PTG)

The Particle Technology Group is a multidisciplinary research group comprising of physicists, chemical engineers, computer scientists, applied mathematicians and nuclear chemists. The group straddles two Universities—University of Cape Town (UCT) and University of Kwazulu Natal (UKZN). The collective resources include:

1) Positron Emission Particle Tracking (PEPT) capabilities
    a. The ring scanner (see figure 2a) is the highest resolution scanner on the planet and offers the ability to produce high resolution, in-situ trajectories of small grains in dense, complexly flowing systems.
    b. New and improved tracking algorithms for PEPT now allow for the tracking of multiple particles—see [14] for more details.
    c. Experience in extracting scaling laws from fundamental measurements; see [12] for more details.
    d. Extensive experience over more than a decade in PEPT experimentation, analysis of PEPT data and nuclear chemistry to produce suitable PEPT tracers down to 20 microns in size.
2) Expertise in DEM and Computational Fluid Dynamics (CFD)—see [11] for more details. We also have experience with computing clusters via the Centre for High Performance Computing (CHPC) located in South Africa.
3) Expertise in granular flow modelling and the formulation of scaling laws from in-situ, fundamental measurements—see [8, 12, 13] for more details.

Positron Emission Particle Tracking (PEPT)

PEPT, an adaptation of Positron Emission Tomography (PET), is a technique for tracking a single particle that has been labelled with a radionuclide that decays by β+ emission. The emitted positron quickly annihilates with an electron producing a pair of 511 keV back-to-back gamma rays that define a line of response (LOR) passing close to the tracer. An accurate location of the tracer can be obtained by the triangulation of a few such LOR's passing in the field of view of the tuned detectors.

While the parallel plate configuration, figure 2(b), is useful for specific geometries, the ring configuration, figure (2a) is generally preferred in the presence of highly attenuating environments like dense slurries. In particular, it is optimised for studying horizontal axis mixers.

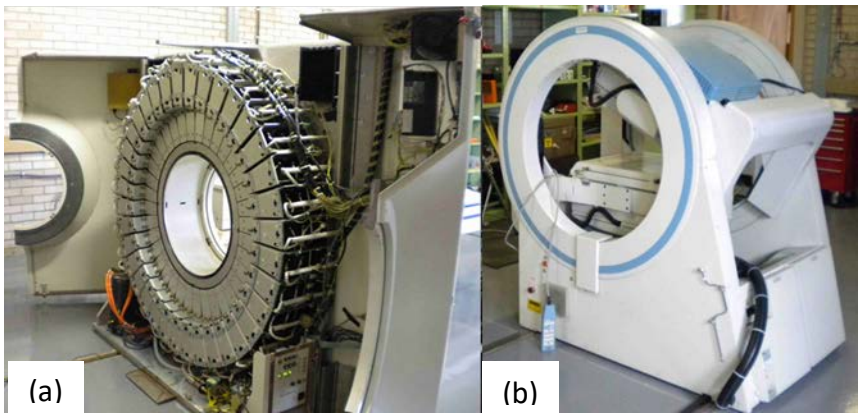

Figure 2: The (a) ring and (b) parallel plate detector configurations of the two positron cameras at iThemba LABS, Cape Town.

The ring configuration consists of a 450-mm diameter ring of detectors with an active length of 230 mm: these dimensions define the maximum field of view (FoV) for tracking. The speed and accuracy of tracking depend on the activity of the tracer and the amount of material through which the gamma-rays must traverse to reach the detectors. As well as reducing the detected event rate, interactions with the intervening material generate a background of scattered gammas. This background is removed by an iterative algorithm whereby an initial estimate of location is calculated from a sample of detected events. Consequently, the events lying furthest from this location are discarded and the estimate is recalculated. Typically, 200 to 800 events are used in the

initial triangulation sample, of which anywhere between 20% and 90% are then discarded, giving a final location which is accurate to ~1 mm (in 3D) provided the tracer does not move too far during the location interval. Figure 3 illustrates the triangulation of a single space-time point (in 3D) determined over a few milliseconds.

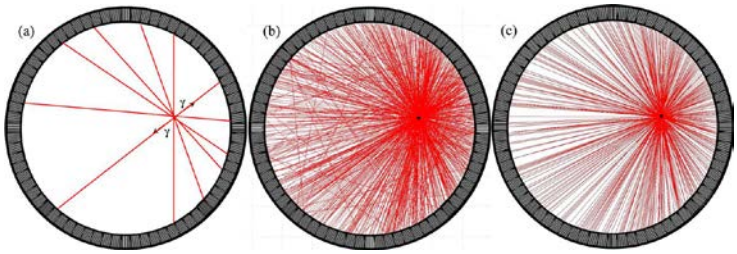

Figure 3. (a) Illustration of a selection of lines of response (LoRs) emanating from the tracer particle and terminating on the ring of detector elements. (b) A typical set of LoRs sampled over a few milliseconds. (c) The remaining LoRs after the spurious LoRs have been iteratively removed.

Radioactive labelling of tracer particles

PEPT Cape Town offers two methods for radioactively labelling particles for PEPT tracking. For large, non-brittle particles a hole is carefully drilled to the centre of the particle and a drop of radioisotope (^{68}Ga or ^{22}Na) inserted. The hole is then filled with a material identical to the particle and sealed with an inert glue. Using this method, activities of up to 1.3 mCi are possible.

For very small particles (< 1mm in size) a resin bead with specific gravity of 1.08 is used to construct the tracer. ^{68}Ga is adsorbed onto the resin after which metal ions are attached to the resin to bring its density up to that of the particle densities being studied. The attachment of metal ions is achieved via cation exchange chromatography. Finally, an inert glue is used to ensure that the metal ions do not "leak" out of the resin, especially in wet systems under study. The smallest tracer currently produced using this method is ~ 20 μm. For more details of the process, the reader is referred to [10].

Analysis of PEPT data

The resulting trajectory [*x*, *y*, *z*, *t*] of the tracer particle is then recorded. Figure (4) shows typical trajectories followed by glass beads (figure 4a) and slurry (figure 4b) tracers rotated in a 300-mm diameter drum that was operated in the cataracting Froude Regime.

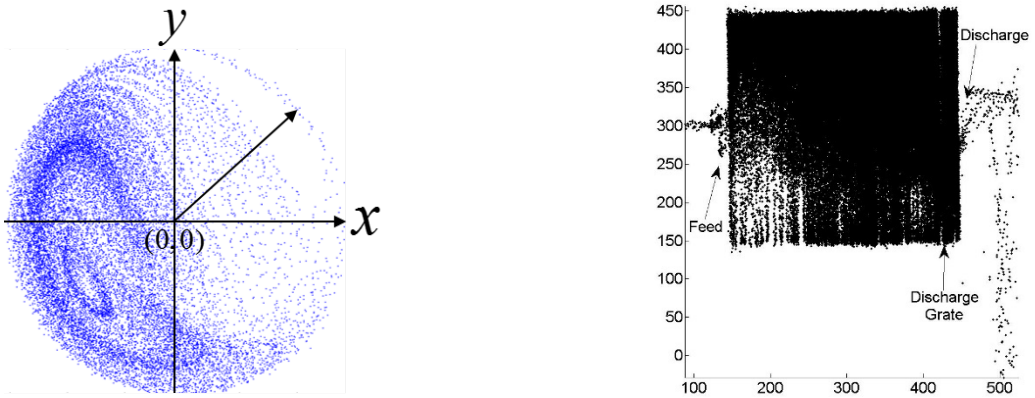

(a) Front View (b) Side view

Figure (4): Typical trajectories followed by glass beads (figure 4a) and slurry (figure 4b) tracers rotated in a 300-mm diameter drum that was operated in the cataracting Froude Regime. In the slurry tests, the slurry tracer (~ 0.5 mm) was recirculated through the drum along with the rest of the slurry.

The trajectories are then converted into space-time averages per unit volume using a binning procedure called *Residence time binning*: Consider the illustrative trajectory shown in figure (5). It consists of a series of sample points along a path in 2D space, shown here as a dashed line. This sample trajectory is approximated by fitting a series of interpolating polynomials, as a function of time, to the sample points. Separate polynomials are

fitted for each dimension– *x*, *y* and *z*– for a moving window of three tracer particle locations, corresponding to the span of a second order Lagrange polynomial. Thus, a trajectory consisting of *N* tracer locations will be approximated by $3(N-2)$ polynomials of the form $s_j(t) = p_j t^2 - q_j t + r_j$, where *s* is the generalised spatial coordinate, *t* is time, and the coefficient subscript *j* refers to the moving time interval for which the polynomial is defined. These piecewise approximations to the sample trajectory thus provide not only a means of estimating the tracer particle's position, but also–by taking their time derivative–its instantaneous kinematics, at any given time. The first step in recasting this now-continuous trajectory as a Eulerian flow field is to discretise the space into sample volumes (or voxels), as shown schematically in figure 4b. For clarity, the binning procedure is illustrated in 2D but, in practice, it is performed in 3D. These voxels represent the resolution of the flow field that will result from the binning procedure, and their minimum size is determined with reference to both the resolution of the imaging technique, and the chosen ergodic criterion.

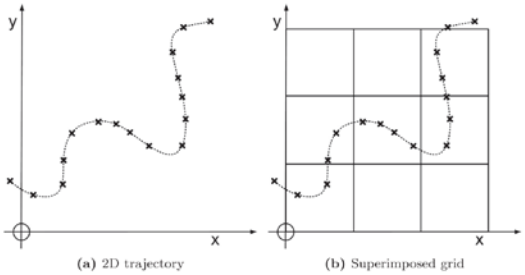

Figure 5: An illustrative trajectory in 2D space without (left) and with (right) a binning grid or voxel superimposed. (a) 2D trajectory. (b) Superimposed grid.

The first Eulerian field of interest is the probability density, the likelihood that a particle of the sort represented by the tracer particle will be at any given location at any given time. By the ergodic assumption, this is the same as the residence time distribution (RTD). That is, the length of time spent by the tracer particle in each voxel is proportional to the likelihood of such a particle being in that voxel at any instant. The RTD of a tracer particle is obtained from its Lagrangian trajectory as follows. Once the grid has been assigned, the sample points are replaced by the sample trajectory, defined in terms of the piecewise interpolating polynomials above. These interpolating polynomials can be inverted and solved for the boundaries of the voxels to determine the times at which the tracer particle entered and left each voxel, as illustrated in figure 6a.

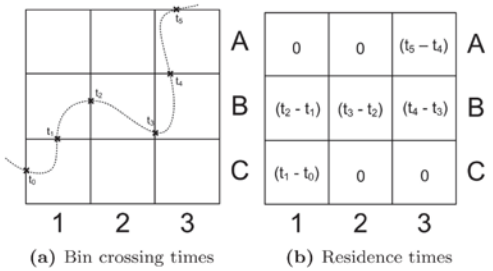

Figure 6: The residence time binning procedure: calculating bin boundary crossing times (left) and thus bin residence times (right). (a) Bin crossing times. (b) Residence times.

These times bound the time interval spent by the tracer in each voxel, as illustrated in figure 6b. Of course, the trajectory may pass through the same voxel many times, and so each voxel will contain a sum of all of the intervals that the tracer spent inside it. The more likely that the tracer will be in a given voxel at any time, the more times it will pass through that voxel, and the longer it will spend in that voxel, as per the ergodic assumption. Hence the raw RTD is proportional to the probability density. Finally, to obtain the average fraction of time (τ) spent by the tracer in a given voxel, the raw RTD is normalised to the total time that the tracer was tracked for. We note that under the ergodic assumption $\tau_i \propto \phi_i$, where ϕ_i is the packing fraction in the i^{th} voxel. In terms of mixing, the relative fractional concentration (η_i) is relevant to characterising mixing efficiency. Thus, for a multicomponent system comprising *M* species (say by size), the relative fractional concentration (η_i) of the i^{th} species in the n^{th} voxel is given by:

$$\eta_i = \frac{\tau_i^n}{\sum_{j=1}^{M} \tau_j^n}. \tag{1}$$

The procedure for obtaining τ also facilitates that for obtaining the kinematics of the system. In particular, once the times that the tracer entered (t_i) and left (t_f) a voxel on a transit *j* have been obtained, the average *s*-velocity of the tracer on that transit can be written as:

$$\bar{v}_{s,j} = \frac{\int_{t_i}^{t_f} v_s(t)dt}{\int_{t_i}^{t_f} dt} = \frac{s(t_f)-s(t_i)}{\Delta t_j}, \quad (2)$$

where *s*(*t*) is the relevant piecewise polynomial as defined above. A single, representative value of each kinematic quantity is assigned to each voxel based on a time-weighted average of the values determined for each transit by Eq. (2). This corrects for the variation in transit length due to different tracer trajectories through the voxel, and for outlier values. The time-weighted average s-velocity of the *N* transits of the tracer through a given voxel is:

$$\bar{v}_s = \frac{\sum_{j=1}^{N}\{s_j(t_f)-s_j(t_i)\}}{T}, \quad (3)$$

where $T = \sum_{j=1}^{N} \Delta t_j$ is the total time spent by the tracer particle in the voxel over all of its transits. This procedure can be performed in all three dimensions. A typical velocity field map derived from this procedure is shown in figure (7).

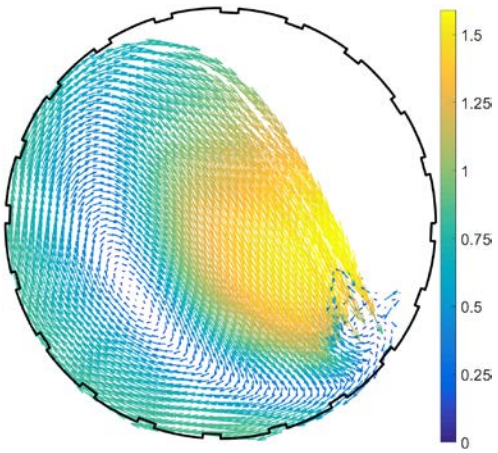

Figure 7: Time and volume averaged velocity field map in [m/s].

Granular Mixing Quantities

The relative fractional concentration distribution and corresponding velocity field data are key ingredients for characterising mixing efficiency, and for testing mixing mechanisms and their relative importance. As described in the previous section, PEPT is very well suited to quantifying the detailed distribution of these quantities. It should be noted that voxel size is a critical choice in the PEPT analysis.

Mixing Efficiency (I_m)

A measure of mixing (or segregation) can be obtained on a per voxel basis from PEPT data using the mixing efficiency (I_m):

$$I_m = 1 - \frac{1}{I_m^{\max}}\left[\frac{\sum_{n=1}^{n=N}(\eta_i^n-\eta_i^m)^2}{N_c}\right]^{1/2}, \quad (4)$$

where *N* is the total number of voxels, η_i^n the relative fractional concentration of the i^{th} species in the n^{th} voxel and η_i^m the mean concentration of the i^{th} species for the system as a whole. $I_m^{\max}$ is a normalization factor and is equal to the maximum of $\left[\frac{\sum_{n=1}^{n=N_c}(\eta_i^n-\eta_i^m)^2}{N_c}\right]^{1/2}$ thus ensuring that a value of $I_m = 1$ denotes a perfectly mixed voxel while $I_m = 0$ denotes a completely segregated voxel.

Convection versus Diffusion

The relative importance of convection versus diffusion is best described by the Peclet number (P_e):

$$P_e = \frac{Lv_x}{D}, \tag{5}$$

where L is a characteristic length, v_x is the velocity in the stream-wise direction and D denotes the diffusion or dispersion coefficient. Following [17], we define the diffusion coefficient (D) as:

$$D = f(\emptyset)d^2\left(\frac{dv_x}{dy}\right) \tag{6}$$

where d is the particle diameter, $\frac{dv_x}{dy}$ is the velocity gradient in the region of interest (typically in a voxel) and $f(\emptyset)$ is a function of solids volume fraction ($\emptyset$) that must be scaled to fit experimental data. [15] suggest that $f(\emptyset)\sim 10^{-2}$. Incorporating the diffusion coefficient into the Peclet number (equation 5) we get:

$$P_e = \frac{h\langle v\rangle}{f(\emptyset)d^2\left(\frac{dv_x}{dy}\right)}, \tag{7}$$

Where h is typically the size of the voxel (or region of interest) and $\langle v\rangle$ is the average velocity within the voxel. All the terms contained in P_e can be obtained directly from PEPT, including $f(\emptyset) = \frac{\emptyset_m}{10}$, where $\emptyset_m$ is the measured solids volume fraction which has been scaled according to [15] to yield $f(\emptyset)$.

Kinetic-stress model proxies for mixing

For a sufficiently dense particle assembly, [4, 5] suggest that larger particles feel a relatively larger lithostatic pressure per unit volume than smaller ones and consequently the smaller particles fall through the interstitial spaces while the larger ones rise to the surface. In terms of the stresses, this implies that larger particles bear a greater proportion of the contact stress (p_c) than they do the kinetic stress (p_k), with the inverse being true for smaller particles. Consequently, smaller particles should have more fluctuation energy ($\widetilde{\mathrm{E}}$) than larger particles within a given volume and are thus more efficiently expelled from the volume than larger ones. The movement of smaller particles through the porous network is referred to as "squeeze expulsion". This implies a net flux of smaller (respectively, larger) particles towards a lower-$\widetilde{\mathrm{E}}$ (respectively, higher-$\widetilde{\mathrm{E}}$). Interestingly, the converse is true for a sufficiently dilute bed. The fluctuation energy vector for a given region of the bed is given as:

$$\tilde{E}_i = \frac{\sum_{n=1}^{N}\left(\langle v_i\rangle - \langle v_i^n\rangle\right)^2}{N} \qquad (i = x, y, z), \tag{8}$$

Where $\langle v_i\rangle$ is the mean velocity in the i-direction within the voxel and $\langle v_i^n\rangle$ is the i-velocity for the n^{th} particle of the total (N) particles contained in the region of interest (i.e. the voxel). Combining the fluctuation energy map with the corresponding map of the local species concentration, it is possible to explain via the "squeeze expulsion" hypothesis the net species flux that ultimately influences mixing.

NB: This calculation can be done component-wise and for the total fluctuation energy vector. Again, PEPT data is ideally suited for such computations. Going beyond the energy argument, a more direct approach of testing "squeeze expulsion" probabilities is to calculate the contact and kinetic stresses. In this regard, recent work [2] within the PTG has resulted in models for these stresses which are functions of PEPT outputs.

Cohesion

Cohesion forces are attractive and usually caused by viscous suspending fluids. If the Stokes number $St = \frac{\rho\left(\frac{dv}{dx}\right)d^2}{\mu} < 1$ then lubrication forces are relevant; with $\left(\frac{dv}{dx}\right)$ the shear rate and μ the fluid viscosity. In this case granular bond number (B_o) is used to quantify the intensity of cohesion:

$$B_o = \frac{F^c}{mg}, \tag{9}$$

where F^c is the maximum attractive force. A variation of this is:

$$\tilde{B}_o = \frac{F^c}{Pd}, \tag{10}$$

where P is the total pressure, m the particle mass and d its diameter. Again, recent work [2, 8] within the PTG has resulted in models for the pressure which is a function of PEPT outputs.

Computational modelling

Computational modelling of granular suspensions can be achieved by coupling DEM with Computational Fluid Dynamics (CFD). Unfortunately, a fully coupled DEM-CFD simulation of a realistic system is computationally very expensive. In addition, the coupling poses significant numerical problems along free surfaces with the CFD part being highly susceptible to divergent solutions. The PTG has performed fully, two-way coupled DEM-CFD simulations of tumbling mills comprising rocks and slurry [11].

For the current IFPRI project, we propose to use a DEM framework that has been modified to explicitly incorporate a lubrication force [18]. The lubrication force is modelled as $F^{\ell} \propto \mu(v_i - v_j)$, where $(v_i - v_j)$ is the relative velocity of the interacting particles. In terms of mixing, the main purpose of numerical modelling is to determine the lubrication force which is otherwise difficult (near impossible) to measure in-situ in typical granular suspension flows. Once determined, mixing quantities like the Bond number can be directly determined. To ensure that the simulation outputs are realistic, PEPT will be used to measure the flow field of the granules and suspending fluid. The DEM simulation is then performed and validated against the outputs from PEPT. With validated confidence in the DEM model, we then extract the corresponding pressure and lubrication forces on a per voxel basis. These quantities serve a dual purpose:

(a) They are incorporated directly into quantities like the Bond number.
(b) They can be used to validate the constitutive choices made by the PTG in [2, 8].

Scale up rules

The development of scale up rules necessarily requires insights into the key fundamental quantities governing the system flow. In this regard, dynamical quantities like the stress distribution are key to quantifying scalable mixing quantities. As an example, consider the "squeeze expulsion" phenomena described by [4, 5]. While the fluctuation energy vector maps provide a quantitative analysis of the net species flux from a given voxel, it does not contain the necessary information for scale up. To achieve this, requires insights into the relative contributions of contact and kinetic stresses. Consider the following stress scaling relation:

$$A = f\left(\frac{p_c}{p_c + p_k}\right), \tag{11}$$

where p_c and p_k are respectively, the contact (frictional) and collisional pressures[1] with the final functional form of equation (11) yet to be determined. Using suitable constitutive choices for the stresses within a granular flow modelling framework (see [2, 8] for details) it is possible to write the pressure terms with respect to:

1) Material density (ρ_m),
2) Shear rate $\left(\frac{dv}{dx}\right)$,
3) Particle size (d),
4) Solids volume fraction (ϕ), and
5) A shape factor (α).

[1] Other stress terms, like turbulence, may be relevant in the system and can be included in the scaling rule.

System size can be incorporated indirectly into the formulation via empirical correlations of the PEPT measured shear rate (via PEPT) with system flow rate (depends on measurement access). With these in place, equation (11) provides the scaling rule that facilitates safe scale up from bench to larger scales.

Similar schemes can be developed for maintaining a relative combination of mixing mechanisms per region of interest depending on the requirements at the larger scale.

Finally, we note that the above discussion is simply an illustrative example of a possible scale up strategy. In practice, it is difficult to know *apriori* what the exact form of the scale up will be prior to making measurements.

Proposed scope of work

Preamble

The PEPT system is optimised for studying horizontal axis mixers. Accordingly, the PTG can study any mixer configuration. Based on the costing of these experiments, the PTG will only be able to study one configuration against the IFPRI funding. Notwithstanding—and as previously done with projects funded by IFPRI partners (like Johnson Matthey)—the PTG will make every effort to include experimental data from other funded projects; however, this is not always possible and cannot be guaranteed. The proposed work described below will (optimistically) assume that more than one tumbler geometry per annum is studied. To ensure tractable numerical simulations, particles studied will be greater than 1mm in size and made up of glass and plastic beads. In the experiments involving a suspending fluid, tracers of approximately 500 μm in diameter will be used to measure the flow of the suspension. In the wet experiments, cohesion will become relevant for small particle sizes and/or highly viscous suspensions. Given the above choices, the scale of scrutiny will be mesoscopic to macroscopic.

The proposed work will evaluate mixing rules in different tumbler geometries and mixers with blades using:

I. in-situ measurements via PEPT
II. numerical simulation via DEM with the granular suspension modelled via explicit integration of a lubrication force into the DEM framework exists.
III. theoretical continuum modelling with PEPT and DEM data as inputs to the continuum equations.

The work will be conducted in three phases, with each phase taking approximately one year. Phases may overlap wherever this makes sense; see table 1 for the nominal timelines, descriptions, and expected technical outputs.

<u>Phase 1</u>: In-situ measurements using PEPT

1) For each of the tumbler and mixer geometries, batch experiments will be performed using combinations of particle size, density, and shape.
2) Using previously developed methodologies [13, 14] we extract the:
    - Kinematic fields (velocity, acceleration, shear rate, granular temperature, etc).
    - Bulk properties (solids concentration).
3) Extract mixing quantities as described in the section on Granular Mixing Quantities.
4) Incorporate continuum stress models into mixing quantities for the purpose of developing scale up rules.

<u>Phase 2</u>: Computational modelling

1) For each of the tumbler and mixer geometries, DEM simulations will be performed using combinations of particle size, density, and shape.
2) Using the continuum upscaling methodologies, we extract the bulk properties (stress, strain, solids concentration)
3) Cross validate the constitutive choices made in Phase 1 with the total stress derived from DEM
4) Extract dynamical quantities, like lubrication force distribution, for incorporation into mixing dimensionless numbers.
5) Extract mixing quantities as described in the section on Granular Mixing Quantities.

Phase 3: Determination of scaling rules:

The development of scale rules is the final stage of the project and includes the following modelling ingredients:

1) Optimised DEM simulation data.
2) Processed PEPT outputs.
3) Validated constitutive models for the stress constituents.

Table 1: Breakdown of phases with nominal timelines

Phase	Time Line	Description of work	Technical Outputs	Unknowns & potential resolutions
Phase 1: PEPT experiments on tumbler and mixer geometries	1st two years from commencement of project	(1) Design and manufacture of tumblers and mixers (2) Preparation of PEPT tracers (3) Running of PEPT experiments (4) Analysis of data	(1) Kinematic and bulk properties (2) Delineation of flow regimes (3) Scaling laws governing flow regimes (4) Constitutive models of stresses matched to flow regimes (5) Extraction of mixing quantities from PEPT data (6) Methodologies for specific tracer production (7) Journal publication(s) (8) Reports to IFPRI	(1) Tracer quality can vary. (2) Downtime of PEPT scanner --- Additional PEPT days will be allocated to offset these potential issues that usually require extra time to repair scanner or repeat tracer production
Phase 2: Numerical modelling via DEM	1st two years from commencement of project	(1) DEM model setup (2) Continuum upscaling to extract bulk properties (3) Validation of constitutive choices with DEM-derived stress tensor	(1) DEM simulation framework (2) Continuum outputs (stress, kinematics, volume concentration) (2) Validation study (3) Extraction of mixing quantities (4) Journal publication (5) Reports to IFPRI	(1) Access to CHPC, i.e. booking schedule of National facility. --- Smaller clusters exist at UCT & UKZN. We will also book time on these clusters to offset delays in accessing CHPC
Phase 3: Scaling Rules	2nd and 3rd year	(1) Characterisation of dimensionless numbers (2) Characterisation of mixing quantities (3) Determination of mixing rules (4) Development of scale up rules	(1) Mixing quantities and scale rules (2) Journal publication (3) Reports to IFPRI	Validity of mixing indices --- The expected quality of PEPT data and related dimensionless numbers should allow for the derivation of new mixing indices

Leverage into existing programs

The Particle Technology Group is currently undertaking research for a host of industrial partners and research providers. The latter is mainly linked to government funding agencies. In this regard, agreements are in place with certain government funding agencies to link the research activities with industrial partners. One of the funding agencies that strongly encourages such links is the South African Minerals to Metals Research Institute (SAMMRI). If we are successful with IFPRI, we will certainly leverage any learning and resources from SAMMRI for the IFPRI project.

Regarding industrial partners, De Beers Marine have approved mutual leveraging of non-sensitive data and modelling between projects whenever it makes sense.

IFPRI member support

The PTG has a longstanding research relationship with Johnson Matthey. We are confident that their vast industrial experience will facilitate our material selection and operating conditions employed in the PEPT experiments. And where it makes sense, we will seek access to their material testing facilities in South Africa. In general, our PEPT capabilities can be applied to most industrial materials down to ~20 microns in size. We are keen to explore specific materials in our PEPT work that may be of specific interest to the various IFPRI members.

Risk and contingency plans

1. The PEPT laboratory is located at the National Accelerator Centre (iThemba LABS) and thus comes with all the necessary safety protocols and measures for performing the PEPT measurements.
2. While we will endeavour to perform much of numerical work using in-house computing tools, we also have direct access to the high-performance clusters located at UKZN, UCT and the CHPC.
3. The PTG has permanent staff employed to run PEPT and computational modelling. In the first instance, the staff will facilitate the training of new MSc and PhD students; however, if we are unsuccessful in finding good students to perform the research, the current staff are more than competent to do the work.
4. Thus far, the PTG has had good success in finding competent students. Our PG student body represent a wide cross-section of nationalities and disciplines. Our current cohort of students includes physicists, chemical engineers, computer scientists, applied mathematicians and nuclear chemists. This is a rich and unique mix of skills that has proven very effective in the cross pollination of ideas and the solution of complex problems.

References

1. B. A. Wills and T. J. Napier-Munn (2006). Mineral Processing Technology: An Introduction to the Practical Aspects of Ore Treatment and Mineral Recovery. *Elsevier Science & Technology Books*
2. T. Pathmathas (2015). Granular flow modelling of rotating drum flows using Positron Emission Particle Tracking. *PhD thesis*, University of Cape Town, South Africa.
3. C. R. K. Windows-Yule, B. J. Scheper, A. J. van der Horn, N. Hainsworth, J. Saunders, D. J. Parker and A. R. Thornton (2016). Understanding and exploiting competing segregation mechanisms in horizontally rotated granular media. *New J. Phys*., 18(2), 023013
4. J. M. N. T. Gray and A. R. Thornton (2005) A theory for particle size segregation in shallow granular free-surface flows. *Proc. Royal Soc. A* 461, 1447–1473.
5. Y. Fan and K. M. Hill (2011). Theory for shear-induced segregation of dense granular mixtures. *New J. Phys*. 13, 095009
6. Y. Fan and K. M. Hill (2011). Phase transitions in shear-induced segregation of granular materials. *Phys. Rev. Lett*. 106, 218301
7. L. S. Bbosa (2013). Probability based models for the power draw and energy spectra of a tumbling mill. *PhD Thesis*, University of Cape Town.
8. I. Govender, T. Pathmathas (2016). A Positron Emission Particle Tracking investigation of the flow regimes in tumbling mills. *J. Phys. D*. Accepted for publication on 1 Dec 2016.
9. I. Govender (2016). Granular flow in rotating drums: A rheological perspective. *Minerals Engineering*. 92, 168-175.
10. G. B. Tupper, I. Govender, D. N. De Klerk, M. C. Richter, A. N. Mainza (2016). Testing of a new dynamic Ergun equation for transport with Positron Emission Particle Tracking. *AIChE*, 62(3), 939-946
11. K. Mayank, M. Malahe, I. Govender, N. Mangadoddy (2015). Coupled DEM-CFD model to predict the tumbling mill dynamics. Procedia IUTAM. 15, 139-149.
12. I. Govender, M. C. Richter, A. N. Mainza, D. N. De Klerk (2016). A positron Emission Particle Tracking investigation of the scaling law governing free surface flows in tumbling mills. *AIChE*, DOI 10.1002/aic.15453

13. A. J. Morrison, I. Govender, A. N. Mainza, D. J. Parker (2016). The shape and behaviour of a granular bed in a rotating drum using Eulerian fields from PEPT. *Chemical Engineering Science*. 152, 186-198.
14. D. Blakemore (2016). Multiple particle tracking in PEPT using Voronoi tessellation. MSc thesis, University of Cape Town.
15. S. C. Yang (2006). Density effect on mixing and segregation processes in a vibrated binary granular mixture. *Powder Technology*. 164, 65-74.
16. D. V. Khakhar, J. J. McCarthy, J. M. Ottino (1997). Radial segregation of granular mixtures in rotating cylinders. *Phys. Fluids*. 9, 3600-3614.
17. S. B. Savage (1993). Disorder, diffusion and structure formation in granular flow. *Disorder and Granular Media*. 255-285
18. C. Ness, J. Sun (2015). Flow regime transitions in dense non-Brownian suspensions: Rheology, microstructural characterization, and constitutive modelling. *Phys. Rev. E*. 91, 012201.

3D PRINTED "PERFECT PARTICLES"

KAREN HAPGOOD, DEAKIN UNIVERSITY, AUSTRALIA

IFPRI PROJECT GRANT RENEWAL PROPOSAL DECEMBER 2016

PROGRAM OUTLINE:

BACKGROUND

One of the long term barriers to advanced and accurate modelling of particulates is the lack of a suitable set of test particles that can be used to validate particle models. Generally the approach has been to take a specific, simplified particle system, measure the relevant properties as accurately as possible, and input these parameters into a model and compare the predictions to experimental measurements. Despite the increase in computing power, we are yet to produce an accurate prediction of the full distribution of behaviour of a simple particle system, let alone the behaviour of far more complex industrial powders.

There are two key limitations with the existing approach. Firstly, we collapse our experimental data to an average particle shape (usually spherical or close to it), average roughness, etc. and eliminate the complexity of real particles. The final model becomes "an average of averages", and the important details are lost. Secondly, both agglomerate breakage and dissolution are destructive experimental tests, and so the experiment represents the date from a single individual agglomerate in a single test condition and the test can never be replicated with an *identical* particle under *identical* conditions. Ideally, what we want is the ability to create hundreds of identical agglomerates, and to test them repeatedly in the same orientation/condition multiple times, and then in many different orientations/conditions. To date, this has not been possible via experimental agglomeration production techniques.

In the first IFPRI project, we designed and printed multiple identical copies of agglomerates, and compared the breakage behaviour a DEM simulation. The agglomerates are printed on a "polyjet" printer which can print multiple materials simultaneously in a single print run, including rigid or rubber-like flexible materials with well defined mechanical properties. Agglomerates can be designed in CAD or DEM software, and exported to the printer and multiple replicates produced for experiments.

To date we have printed rigid particles with ductile cylindrical inter-particle bonds (representing "dried liquid bridges"). We can systematically vary the agglomerate structure and the strength of agglomerates (by changing the polymer used to print the bonds), and investigate strength and structure independently. DEM modelling using the TBBM model by Ooi [1] in EDEM has shown a better match between quasi-static compression and experimental data than has previously been achieved (see Figure 1). The method is in its early stages of development but shows promise for the future.

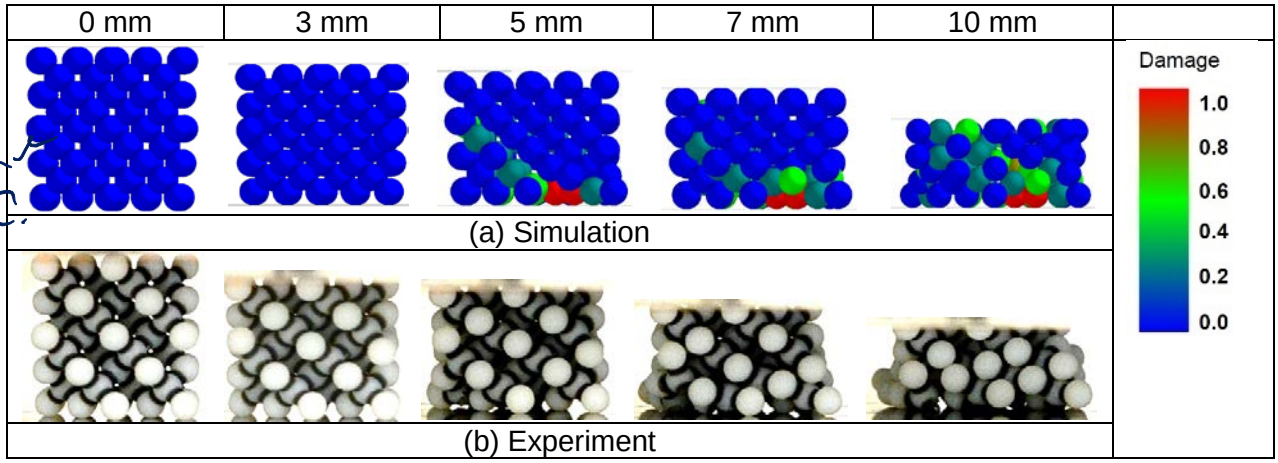

Figure 1. Simulated and experimental breakage results for a cube shaped agglomerate with ordered, tetrahedral internal structure as a function of the displacement (in mm) of the upper platen. (Ge, Ghadiri, Hapgood, unpublished data, work funded by IFPRI & ARC)

ADVANTAGES OF 3D PRINTING AGGLOMERATES:

- Mimic any real particle shape, size and surface topology, including any interparticle bridge geometry
- Produce an unlimited number of identical agglomerates, from simulations or XRT data.
- Multiple materials with well-defined mechanical properties spanning a range from rigid to ductile to "tune" the agglomerate properties.
- Systematic agglomerate design by varying the agglomerate geometry and the material properties of the particles *independently*.
- Manufacture convenient shapes for characterisation tests of surface properties, mechanical properties, and other measurements required for simulations.
- Utilize transparent and colour printing features, to view and identify individual sub-particles or sections within the agglomerate.

MAKING THE MOST OF DISRUPTIVE TECHNOLOGY

The work on the IFPRI project to date has focussed exclusively on granule breakage via quasi-static compression and higher strain-rate impact tests, and utilised what was (3 years ago) a state of the art polyjet 3D printer. The renewal project would focus on making the most of the advances in 3D printing since then, including colour printing, multi-material printing and improved support matrix polymers.

The Deakin School of Engineering[1] is housed within the CADET building which includes a 3D printing lab, which houses multiple 3D printers including the ability to print in various polymers, silicon and titanium, which will allow a broad range of experimentation. Of particular relevance to IFPRI is the Stratasys Object 500 Connex 3 which is the next model up from the printer used so far. This printer is able to produce models with the polymer range used to date, but in colour. Colour options are shown to the right. This means each particle in an agglomerate could be printed in a different colour, to allow individual particle tracking (based on colour) in experiments and simulations. This newer model also uses a new type of soluble support matrix which will vastly reduce the cleaning time of agglomerates with complex internal geometries from ~1 week to less than a day.

The new project would demonstrate the multiple different ways that 3D printing could be used to advance our understanding of the three broad areas of powder flow, agglomerate dissolution, as well as continuing the work on agglomerate breakage. Each topic listed below would be demonstrated and presented to IFPRI up to "proof of principle" stage, building as much as possible on current or previous IFPRI projects. The newly developed approach would then be published to enable the entire particle technology community to take up the ideas and implement them broadly. The matching CAD and 3D print design files would also be made publically available on a website and/or supplementary information section of the paper. Implementation for companies and researchers without specific additive manufacturing experience is now straightforward given the ability to outsource 3D printing to specialised vendors, who receive design files and deliver the finished agglomerates. Although it is helpful to have immediate local access to a 3D printer when developing a new method from scratch, it is not critical for implementing an already developed method. **The outcome will be a suite of designs for particles, agglomerates and substrates, including "tunable" properties, to validate and advance more realistic models of powder flow and segregation, agglomerate breakage and dissolution.**

[1] *Karen is relocating to the School of Engineering at Deakin University, starting in March 2017. Deakin is located in Geelong, which is a regional city outside of Melbourne. She will retain access to the printers at Monash Uni via the current PhD student Ruihuan Ge, who will remain based at Monash, and gain access to a much broader suite of printers at Deakin and a host of new collaborators who focus on additive manufacturing.*

In 2017, a postdoc will be hired for 2 years as part of the final stages of the existing ARC Discovery grant (Hapgood & Ghadiri) on tuneable particles for agglomerate breakage and the current IFPRI project. The postdoc will conduct more complex breakage experiments than have been previously attempted, using coloured and clear particles, as well as DEM modelling using EDEM and the TBBM model [1]. A new PhD student Anthony Antic has been recruited to start at Deakin University in 2017, looking at Pharmaceutical applications of 3D printing. The dissolution experiments outlined below should fit well as part of the 2nd and 3rd year of his PhD project. A second PhD student will be recruited in 2017-2018 using startup package and/or IFPRI funds and will focus on the powder flow and segregation aspects.

Agglomerate Breakage (Postdoc):

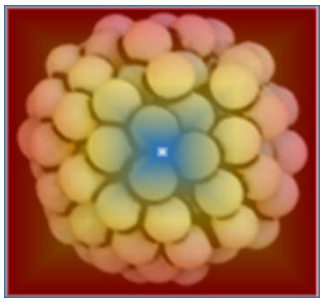

- **Coloured tuneable agglomerates:** Print a new set of randomly structured agglomerates where the particles are joined by liquid bridges, but with each particle or particles in each region (inner, middle, outer, see conceptual picture on right) printed in a unique colour. This will allow better tracking of individual particle positions, particularly after high strain rate impacts which lead to shattering of the agglomerate.
- **3D motion tracking during compression:** In the granule breakage experiments to date, we have used a single camera and 2D tracking from the front only as shown in Figure 1. A more sophisticated approach would be to print particles within an agglomerate using a clear polymer but with a coloured "dot" at each particle centre. Using two cameras at different angles we could track particle motion during compression in three dimensions [2].
- **Bi-refringent polymer agglomerates:** Given the expertise at Deakin in 3D printing, we could print adapt an existing printer to produce single material particles using bi-refringent polymers, in any shape and size distribution, to be able to visualise force chains in particle assemblies. This may intersect with Karen Daniel's IFPRI project which uses bi-refringent discs.

Agglomerate Disintegration and Dissolution (Anthony Antic, PhD Student):

- **Active distribution and dissolution profiles**. Stepanek [2] published a paper on dissolution of several idealised scenarios of active ingredients within a granule. We would print agglomerates using soluble support matrix embedded with individually coloured insoluble polymer particles, distributed similar to the six cases shown on the right [2], and conduct dissoltuion testing of multipe identical agglomerates and compare this to the existing simulations of active release profiles (assuming simple 1st order dissolution of the "active" once it is released into the dissolution medium). Data from a real pharmaceutical system representing several of the test cases is also available for comparison [2], and a fresh collaboration with Stepanek in this area is the proposed topic of a 2018 Australian Research Council grant application.

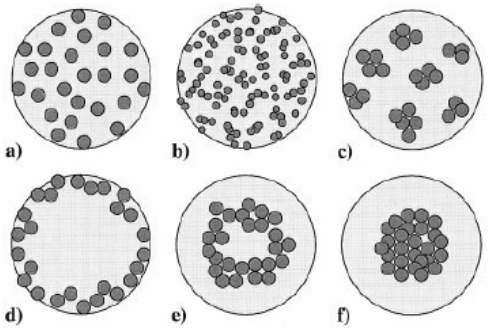

Figure 4. Possible distribution of an active ingredient within a granule.
Cases a-c show a random dispersion of normal, milled, and pre-agglomerated particles of the active. Cases d-f show the active located in the shell, in an intermediate layer, and in the core of the granule.

- **Liquid imbibition into a porous substrate.** Most models of liquid infiltration into an agglomerate rely on the Washburn equation, which assumes spherical capillaries with some tortuosity. We could be able to print porous channels building from simple to complex, and examine liquid infiltration as a function of geometries. Printing of sections of the channels with PLA would allow functionalisation of

[2] *This idea is credited to Norm Wagner after a discussion at the IFPRI AGM in June 2016*

the surfaces to create hydrophobic and hydrophillic regions, and thus systematically investigate the wetting behaviour of realistic complex channels. This could link with McCarthy's recent work on a new approach to granular filtration that avoids the Kozeny equation and looks at the size size and proportion of larger voids [4].

Powder flow and segregation (new PhD student, starts 2017-2018):

- **Flow of irregular shaped particles.** A common approach is to assume spheres, or a set of fused spheres to approximate the particle shape. Building on the work by Hare & Ghadiri [3] on corn seed flow, we would print the corn seeds approximated by 5-20 spheres (see right image from [2]), plus the full corn seed, and conduct flow experiments in a seed coater. A subset of tracer seeds would be printed in different colours (but otherwise identical) to track the flow pattern and confirm that the flow is accurately represented by the fused spheres.

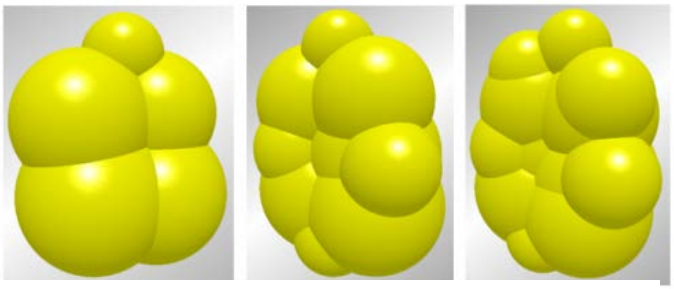

Corn seeds approximated by spheres [2]

- **Density Segregation:** we can print particles with the same size and shape but different density by varying the amount of solid "infill" inside a particle (see example below).

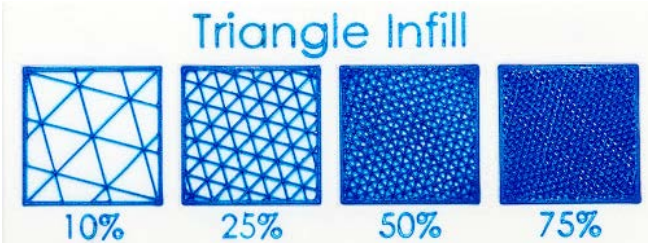

This will allow us to replicate experiments on segregation during powder flow, fluidisation, or minerals separation etc, and systematically vary the degree of density difference. Previously this kind of precise control of particle density was only possible within simulations. Potential collaboration with the SIMPAS group at Monash, led by Aibing Yu, to mimic a suitable simulation that we can experimentally match.

- **Matching boundary conditions in flow experiments.** It is common in DEM simulations of flow to simulate wall friction via an array of stationary particles fused to the walls of the simulation (see example on right). However, the experimental rig uses sandpaper.

this addresses a major complaint by modelers in the powder flow collab.

Using 3D printing, we would print an exact replica of the stationary layer shaped as a flat or curved surface, cylindrical pipe etc. The printed piece would be used directly in the experiments to replace the sandpaper, to ensure the boundary conditions of the simulation and experiment were identical. This experiment could be conducted in combination with coloured tracer particles, or varying shapes or densities etc.

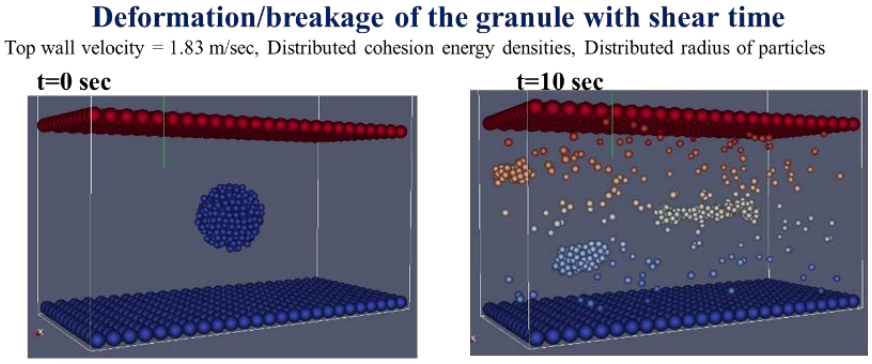

Fixed spheres on upper & lower surface of DEM simulation of breakage in shear flow, Akiti, Khakhar, Hapgood, unpublished).

OUTLINE OF ACCOMPLISHMENTS IN NEXT 3 YEARS

(2017: New PhD student A Antic commences PhD on pharmaceutical applications of 3D printing, and a postdoc is hired to work on DEM modelling and existing ARC grant for 2 years)

2018 Year 1:

- Postdoc designs and produces multi-coloured agglomerates and conduct impact tests.
- Postdoc sets up dual motion capture camera system to follow agglomerate compression (clear agglomerates with dots in centres), and conducts DEM simulations to match impact tests.
- Hire new PhD student #2 working on powder flow and segregation. Training on 3D printer and associated software at CADET at Deakin. Print fused sphere models of corn by Hare & Ghadiri [3].
- Anthony Antic designs and prints agglomerates with distributed API and conducts dissolution tests to model controlled case studies of active release.
- Prepare review of 3D printing technology in particle applications (food, pharma, catalysis, consumer products).
- Prepare review of the key research groups working on 3D printing internationally and their specific expertise.
- Produce IFPRI annual report
- All design files and printing files developed are made publically available for use.

2019 Year 2:

- Anthony Antic looks at liquid imbibition into porous channels. Collaboration with Frantisek Stepanek on modelling of the results. Writes up PhD thesis.
- PhD student #2 conducts flow experiments in the seed coater (either at Deakin or in the UK) for comparison with existing experimental data and DEM simulations, and conducts fluidisation experiments looking at segregation of different density particles.
- Produce IFPRI annual report
- All design files and printing files developed are made publically available for use.

2020 Year 3:

- PhD student #2 writes up PhD thesis
- Modify a polyjet printer to print bi-refringent polymer(s)
- All design files and printing files developed are made publically available for use in a public website or a repository
- Review of key groups worldwide and current directions in additive manufacturing relevant to IFPRI members is updated.
- Produce IFPRI final report

LEVERAGE EXISTING PROGRAMS

The proposal will dovetail with the 4th and final year of Australian Research Council Discovery grant on “perfect particles” for understanding Agglomerate breakage (Hapgood & Ghadiri).This renewal proposal will build in part on the ongoing IFPRI program with Jin Ooi, which looks at the TBBM bond model.

ADDITIONAL IFPRI SUPPORT

This proposal is a series of sub-projects, most of which involves a significant level of collaboration, mostly with other IFPRI researchers. Many of these visits can be combined with existing conference and AGM travel

plans, but some collaboration support grants may be useful in year 2 or 3 to facilitate travel on some of the sub-projects. We would prepare a separate proposal for consideration by IFPRI.

REFERENCES

1. Brown, N.J., J.-F. Chen, and J.Y. Ooi, *A bond model for DEM simulation of cementitious materials and deformable structures.* Granular matter, 2014. **16**(3): p. 299-311.
2. Ansari, M.A. and F. Štěpánek, *Design of granule structure: Computational methods and experimental realization.* AIChE Journal, 2006. **52**(11): p. 3762-3774.
3. Pasha, M., C. Hare, M. Ghadiri, A. Gunadi, and P.M. Piccione, *Effect of particle shape on flow in discrete element method simulation of a rotary batch seed coater.* Powder Technology, 2016. **296**: p. 29-36.
4. Zhang and McCarthy, *Validity of Kozeny-Carman Equation in Constant-Pressure Cake Filtration* http://d-scholarship.pitt.edu/26405/ presented at AICHE Nov 2016.

IFPRI Grant Proposal: Flowability Assessment of Weakly Consolidated Powders

Colin Hare[1] and Ali Hassanpour[2]

[1] Department of Chemical Engineering, University of Surrey, UK

[2] Institute of Particle Science and Engineering, University of Leeds, UK

Background

The inability of cohesive powders to flow easily is a major cause of process downtime and reduced efficiency. Shear cells are the most established method of powder flow measurement [1], with methods developed for hopper design based on the measurements made [2,3]. Many processes exhibit only low stresses on powders (<1 kPa), as such reliable measurement of powder flow under these process conditions is troublesome since in most instances shear cells are unable to generate a yield locus. In the last decade or so, a number of devices have been developed for measuring powder flow at low stresses, such as the Raining Bed method (RBM) [4], the Sevilla Powder Tester (SPT) [5], The Freeman FT4 Powder Rheometer (FT4) [6] the SSSPIN tester and ball indentation [7]. The RBM and SPT directly measure the tensile yield stress of powders at a given packing state by application of airflows. The RBM supports a powder bed column against gravity by an upward airflow, the velocity of which is reduced until the powder 'rains down'. The SPT uses a downward airflow to consolidate a powder column, followed by an upward airflow to temporarily lift the column from the base of the vessel. In comparison to shear cell measurements at moderate stresses, the SPT has been observed to be more reliable than the RBM [8], however the method is only suitable for slightly cohesive powders, as highly cohesive powders exhibit channelling behaviour which prevents the powder column from being lifted.

The SSSPIN tester is the only alternative powder flow measurement device applicable at low stresses which directly measures the unconfined yield strength. This device uses centrifugal forces both to consolidate and to fail the powder, with the yield point determined by powder flowing past a laser detector. The small bed volume used in this technique may result in the shear stress introduced by removal of the die wall prior to failure stress measurement being significant. Furthermore, there are no published results using this technique, so the reproducibility and accuracy of the measurement is yet to be established.

In the ball indentation method a powder bed is consolidated in a die to the desired packing state, prior to indentation of the powder bed with a spherical indenter. The force and penetration depth are measured and hardness,

$$H = \frac{F_{max}}{A} \qquad \text{(Eq. 1)}$$

where F_{max} is the maximum vertical force acting on the indenter during loading and A is the contact area, which is given by

$$A = \pi\left(D_I h - h^2\right) \qquad \text{(Eq. 2)}$$

where D_I is indenter diameter and h is maximum penetration depth. Pasha *et al.* [9] and Zafar *et al.* [10] found that hardness is stable for a dimensionless penetration depth, h_d, range of 0.2 – 0.9 and 0.4 – 0.9, respectively, where

$$h_d = h/R_I \qquad \text{(Eq. 3)}$$

and R_I is indenter radius.

Powder flowability measurements are usually carried out to determine the unconfined yield stress, σ_c. The ball indentation hardness measurement is related to the yield stress by the constraint factor,

$$C = H/\sigma_c \,, \qquad \text{(Eq. 4)}$$

The constraint factor represents the increased local yield strength due to the elastically deformed region surrounding the failure zone [11]. The most common method for establishing the unconfined yield strength is by shear cell measurement, however it could by measured by uniaxial compression. Uniaxial compression tests result in a lower value of σ_c than shear cell measurements [12], and hence the established value of constraint factor would depend on the method of unconfined yield stress measurement.

The ongoing IFPRI project determined for silanised glass beads that the constraint factor (comparing indentation hardness to shear cell measurements at identical major principal stress) is independent of particle size and particle size distribution (Figure 1). Zafar [13] investigated a wide range of powders by ball indentation and found constraint factor values ranging from 1.8 – 8, however this was determined using the value of σ_c arising from uniaxial compression measurements, which differed significantly from the measurements in a shear cell. Our analysis [14] using σ_c determined in a shear cell shows that C varies from 1.9 – 4.8 for the powders tested in the ongoing IFPRI project and by Zafar [13]. This reduced range of constraint factor values may be explained in part by the improved reliability of shear cell measurements over the uniaxial compression tests of Zafar [13]. It is important to note that while the uniaxial compression test underestimates σ_c, the consolidation step is identical to that used in the ball indentation method. In contrast, the shear cell shears the bed to achieve steady state failure prior to testing, and as such the packing fraction for a given major principal stress is typically greater than that in the ball indentation and uniaxial compression methods.

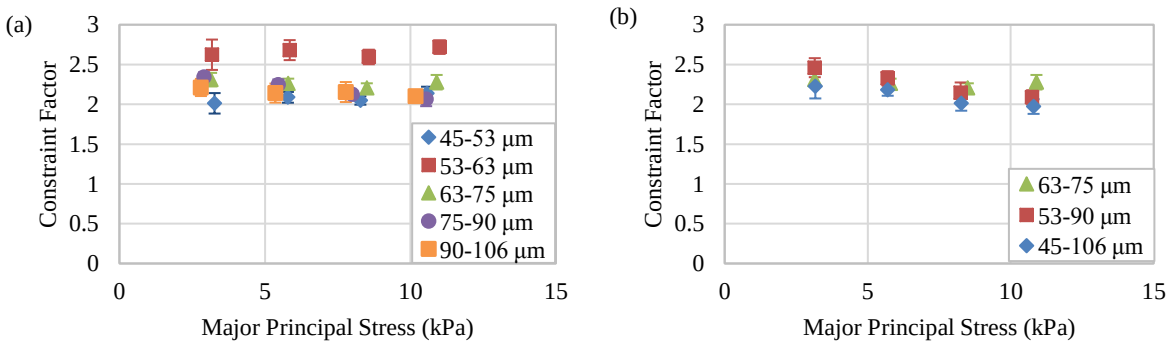

Figure 1. Constraint factor for silanised glass beads (a) single sieve-cuts (b) consecutive sieve cuts

There is no knowledge in the literature of how particle properties influence the value of constraint factor for indentation into a powder bed. The ongoing IFPRI project aims to establish the particle attributes that greatly influence constraint factor by strategically manipulating properties including, size, size distribution, surface energy, density and shape. With the relationship between these properties and constraint factor developed, then for a given powder the value of constraint factor can be estimated, thus allowing σ_c to be determined from ball indentation measurements. In order to determine the constraint factor the unconfined yield stress must be measured under the same consolidation conditions. It has been shown for a number of powders that C is approximately constant in the moderate stress range (> 1 kPa) [13,14], however due to the difficulty in measuring σ_c at low stresses [15] the constraint factor has not been reported below this range. In the ongoing IFPRI project, reproducible unconfined yield stress measurements have recently been made at remarkably low stresses for 45 – 53 µm silanised

glass beads using the FT4 shear cell. For these glass beads an almost linear yield locus is generated at stresses as low as 1 kPa, however below this stress the behaviour is erratic (Figure 2). Despite this, the reproducibility of the shear cell measurement is high (error bars of one standard deviation obscured by data points in Figure 3). In addition, the value of the measurement is similar to that inferred by ball indentation[1], thus suggesting that constraint factor is in fact constant in the stress range 0.1 – 10 kPa.

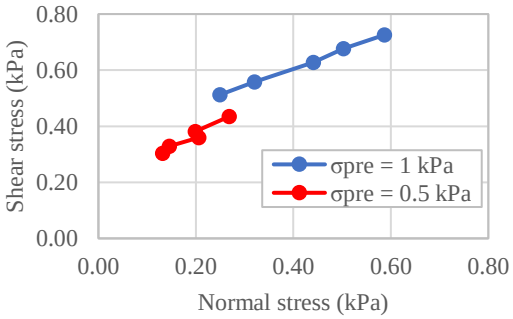

Figure 2. Unconfined yield stress for 45 – 53 µm silanised glass beads

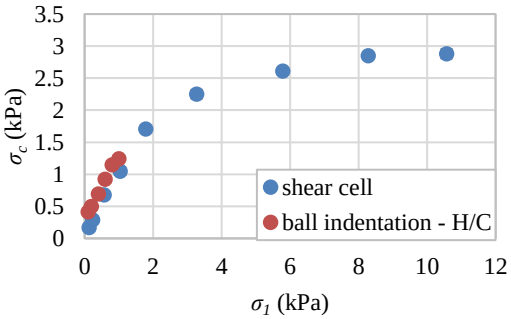

Figure 3. Low stress shear cell behaviour

For many powders it is not possible to reach steady state shear at such low stresses, hence the investigation into ball indentation as an alternative method to determine σ_c. The ongoing IFPRI project will utilise DEM to analyse constraint factor at lower stresses by assessing internal bed stresses, in order to determine whether the constraint factor is independent of consolidation stress. The proposed work for further IFPRI support will be an entirely experimental analysis of powder flow at low stresses.

Research hypothesis and objectives

Powder flowability at low stresses will be primarily examined using the ball indentation method. In order to develop this method it is critical to establish a robust method for predicting or measuring the constraint factor for a given powder. To determine the constraint factor for a given powder, hardness must be measured (by ball indentation) and unconfined yield strength must be measured (by a shear cell or uniaxial compression) under the same consolidation conditions. Uniaxial compression provides an identical consolidation method to ball indentation, but may underestimate unconfined yield strength, whereas a shear cell provides a greater packing fraction for the same consolidation stress. The following approaches for determining constraint factor will be explored:

1. Ball indentation carried out at identical major principal stress to uniaxial compression
2. Ball indentation carried out at identical major principal stress to shear cell tests
3. Ball indentation carried out at the same packing fraction as shear cell tests

The constraint factor is expected to depend on the physical, chemical and mechanical properties of the particles, therefore a wide range of powders will be tested and their properties measured. Statistical analysis will be used to relate the constraint factor to the particle properties.

The reliability of the measurement at lower stresses will be established for all three techniques. The lower stress limit in which a reliable measurement can be achieved is expected to be material dependent, with more cohesive powders expected to give reliable measurements at lower stress levels.

[1] By calculating σ_c from the measured hardness in Eq. 4, where C is determined by comparing indentation hardness to unconfined yield stress in the shear cell at pre-shear stresses of 2 – 8 kPa (Figure 1a).

The overall objectives of the research are as follows:

1. Establish the optimal method for determining constraint factor
2. Establish a relationship between constraint factor and particle properties
3. Determine the lower operational limit of the three techniques as a function of particle properties

Deliverables
D1: an optimised procedure for the shear cell pre-shear step at low stresses
D2: determine the lower operational limit of the shear cell as a function of particle properties
D3: determine the lower operational limit of the uniaxial compression as a function of particle properties
D4: establish the influence of particle properties on constraint factor

Description of project
A wide range of materials will be examined and the influence of their properties on constraint factor and the lower operational limit of the testers will be established. Flowability measurements will be carried out for all materials using ball indentation, the FT4 shear cell and the Freeman Technology Uniaxial Powder Tester.

Materials
The ongoing IFPRI project (funded until end of Feb 2018) examines particles of well-defined properties, including cohesive glass beads to analyse the effect of size, size distribution and surface energy, along with talc, alumina and copper powders to explore the effect of shape (for each material, size distribution is closely maintained). The proposed work will extend the investigation to a much broader class of (~20) cohesive powders, including various grades of specific materials (e.g. TiO_2), and will involve statistical analysis to ascertain the effect of individual particle properties; supported by the findings of the original IFPRI project.

Methods
It has been shown for 45-53 μm silanised glass beads that the inferred unconfined yield stress measurement from ball indentation is similar to that determined in the shear cell in the pre-shear stress range of 0.06 – 1 kPa. Although the reproducibility of the shear cell measurement is good in this range, the reliability in obtaining steady state flow is questionable, and as such additional measurements by uniaxial compression will enable a more detailed analysis of the limitations of powder flow testing at low stresses for very cohesive powders. Furthermore, determination of constraint factor by comparison of ball indentation to uniaxial compression, instead of the shear cell, may be a more robust approach due to the similarity in consolidation methods.

Ball indentation – the ball indentation method uses a 4 mm diameter spherical steel indenter attached to an Instron 1175 mechanical testing machine. The procedure is now well-established; the sieve-filling method of Zafar [13] will be used and the reliable penetration depth range determined for each material. The constraint factor will be determined by comparison with both shear cell and uniaxial compression measurements. The value of constraint factor is expected to vary for comparison to each of these methods, since the load application differs in the consolidation process.

Shear cell – flow measurement by shear cells can be applied by using a number of different pre-shear approaches. The Schulze shear cell applies a single pre-shear step, with pre-shear ending once a steady shear stress is obtained, before any reduction in shear stress occurs [12]. In contrast, the Peschl

approach is to record the peak stress during pre-shear and wait until steady state shear is maintained for at least one minute before ending the pre-shear step, following which additional pre-shear steps are carried out until the peak is no greater than that of the previous step [16]. The pre-shear method in the FT4 shear cell is a compromise between the two approaches. In the FT4 shear cell a pre-shear step is ended 20 seconds after the maximum shear stress is reached, with no subsequent increase in shear stress, following which successive pre-shear steps are carried out until the maximum shear stress between consecutive pre-shears is within 1% of each other. When operating at low stresses with the Schulze method the pre-shear step typically fails to complete, leading to no measurement being made, whereas with the other approaches consecutive pre-shears may be deemed sufficiently similar due to the reduced resolution at low stress, however the accuracy of the flow measurement is reduced.

The FT4 shear cell will be used in this work, in which the pre-shear method is modifiable; with the capability to precisely follow the method of Schulze or Peschl. The number of pre-shear steps applied, their end point and required agreement between consecutive pre-shear steps will be manipulated in this research. The reliability of the yield locus will be assessed to determine the minimum operating stress for a given powder and the influence of the pre-shear approach on this. On this basis a recommended pre-shear protocol will be established and applied to the remaining powders. For the remaining powders the minimum pre-shear stress that enables a reliable measurement will be determined. The influence of the pre-shear process will be reassessed for a number of these powders, to determine if this is influenced by the physical properties or flow properties of the material.

Uniaxial compression – the Uniaxial Powder Tester provides vertical consolidation stresses to the powder column from above and below. Following consolidation the sleeve surrounding the column is lifted and the unconfined yield stress is determined by compression with a piston from above the powder. In this research the powder bed will be prepared by sieve-filling in the same manner as for ball indentation. As with the other techniques, the reproducibility of the measurement will be assessed for all powders, and the minimum stress for which a reliable measurement can be achieved will be established.

Packing fraction – bulk measurements of packing fraction are achieved in all three flow measurement techniques, however for a given bulk density, the packing fraction may differ within the flowing zone across the three techniques. A more detailed analysis of the distribution of packing under the indentation zone and in the failure plane of the shear cell and uniaxial compression tests will be carried out for key materials of varying constraint factor using the X-Ray Tomography technique available at the University of Leeds.

Particle properties – the physical properties of all powders will be assessed using the QICPIC optical method in wet dispersion mode. In addition to size information, this technique provides the distribution of a number of shape descriptors, including aspect ratio and sphericity. The surface energy of all powders will be assessed using the drop test technique [17]. The mechanical properties of the powders will be determined using the Micromaterials NanoTest indenter at the University of Leeds. These measurements will allow the lower limit of reliable flow measurement in the shear cell and uniaxial compression tests to be related to powder properties. In addition the dependency of the constraint factor on particle properties will be established.

References

[1] J. Schwedes, Review on testers for measuring flow properties of bulk solids, Granul. Matter. 5 (2003) 1–43. doi:10.1007/s10035-002-0124-4.

[2] G. Enstad, On the theory of arching in mass flow hoppers, Chem. Eng. Sci. 30 (1975) 1273–1283. doi:10.1016/0009-2509(75)85051-2.

[3] J. Tang, R.P. Behringer, How granular materials jam in a hopper., Chaos. 21 (2011) 41107. doi:10.1063/1.3669495.

[4] A. Formisani, B., Bernado, P., Girimonte, R., Minnicelli, The bed support experiment in the analysis of the fluidization properties of fine solids, in: Proc. Conf. 4th World Congr. Part. Technol., Sydney, 2002: p. 373.

[5] a. Castellanos, J. Valverde, M. Quintanilla, The Sevilla powder tester: a tool for characterizing the physical properties of fine cohesive powders at very small consolidations, Kona. 22 (2004) 66–81. doi:10.14356/kona.2004011.

[6] R. Freeman, Measuring the flow properties of consolidated, conditioned and aerated powders — A comparative study using a powder rheometer and a rotational shear cell, Powder Technol. 174 (2007) 25–33. doi:10.1016/j.powtec.2006.10.016.

[7] A. Hassanpour, M. Ghadiri, Characterisation of flowability of loosely compacted cohesive powders by indentation, Part. Part. Syst. Charact. 24 (2007). doi:10.1002/ppsc.200601111.

[8] U. Zafar, C. Hare, G. Calvert, M. Ghadiri, R. Girimonte, B. Formisani, M.A.S. Quintanilla, J.M. Valverde, Comparison of cohesive powder flowability measured by Schulze Shear Cell, Raining Bed Method, Sevilla Powder Tester and new Ball Indentation Method, Powder Technol. 286 (2015) 807–816. doi:10.1016/j.powtec.2015.09.010.

[9] M. Pasha, C. Hare, A. Hassanpour, M. Ghadiri, Analysis of ball indentation on cohesive powder beds using distinct element modelling, Powder Technol. 233 (2013) 80–90.

[10] U. Zafar, C. Hare, A. Hassanpour, M. Ghadiri, Ball indentation on powder beds for assessing powder flowability: Analysis of operation window, Powder Technol. 310 (2017) 300–306. doi:10.1016/j.powtec.2017.01.047.

[11] G. V Kozlov, V.D. Serdyuk, V.A. Beloshenko, The plastic constraint factor and mechanical properties of a high-density polyethylene on impact loading, Mech. Compos. Mater. 30 (1995) 506–509.

[12] D. Schulze, Powders and bulk solids: Behaviour, Characterization, Storage and Flow, Springer, Berlin, 2007.

[13] U. Zafar, Assessing Flowability of Cohesive Powders by Ball Indentation, University of Leeds, 2013.

[14] C. Hare, A. Hassanpour, A. Stavrou, Flowability Assessment of Weakly Consolidated Powders, 2016.

[15] D. Schulze, A. Wittmaier, Flow Properties of Highly Dispersed Powders at Very Small Consolidation Stresses, Chem. Eng. Technol. 26 (2003) 133–137. doi:10.1002/ceat.200390019.

[16] Standard Test Method for Measuring Shear Stresses of Powders Using Peschl Rotational Split Level Shear Tester, ASTM Stand. Number D 6682-08. (n.d.).

[17] U. Zafar, C. Hare, A. Hassanpour, M. Ghadiri, Drop test: A new method to measure the particle adhesion force, Powder Technol. 264 (2014) 236–241.

Appendix A: Project Gantt Chart

Main Tasks	Sub Tasks	Time Scale (months)
		1 2 3 4 5 6 7 8 9 10 11 12 13 14 15 16 17 18 19 20 21 22 23 24 25 26 27 28 29 30 31 32 33 34 35 36
Source materials		
Size & shape analysis		
Flowability measurement with shear cell	Assessment of optimum pre-shear protocol	D1
	Establishing lower limit of operation	D2
Uniaxial compression	Establishing lower limit of operation	D3
Ball indentation	Hardness measurement and constraint factor determination	
	Statistical analysis of parameters influencing *C*	D4
Packing fraction assessment for all techniques, using XRT		
Surface energy measurement by drop test method		
Mechanical property measurement by nanoindentation		

1 Introduction and Program Summary

Segregation model development holds promise for translation of academic research into industrial practice. Two significant issues that hamper the applicability of these models in industry, however, are (1) the inherent difficulty in measuring segregation rates (especially in an experimental setting) for validation purposes and (2) the significant dearth of validated scale-up studies for these models. In this renewal project, we seek to continue on our path toward alleviating these two shortcomings of segregation research through a combined theoretical, computational, and experimental program. The central hypothesis of this follow-on proposal is that by exploring a novel view of the interplay between granular rheology and segregation, we can introduce a new way of structuring segregation rate models that will make them inherently more scalable than any models previously reported. Moreover, by continuing to exploit our segregation model testing framework – developed in the first phase of our IFPRI program – we will continue to be at the forefront of validation of new and existing models both via computational and (especially) experimental means. Ultimately, This combined approach will yield (experimentally) validated segregation models – either via adoption from the literature or through new theoretical development – that can be incorporated into device-level transport equations in order to supply quantitative prediction of segregation at process scale.

The establishment of a direct connection between granular rheology and segregation has the potential to spur a substantial jump in our understanding of both fields and lead to a transformation in the way that particle flow research is conducted. Not only will the proposed research lead to a completely new class of segregation model, but the unequivocal observation of a regime change in segregation rate (see preliminary results developed in Year 2 of the current IFPRI effort) will allow for the rational design of strategies to mitigate segregation in industrial processing. Goals to be attained within this project include:

1. Use an analogy between granular rheology and segregation to develop inherently scalable models
2. Experimentally testing these models in a variety of prototypical granular flows
3. Test the scalable nature of the models via incorporation into device-scale transport equations

2 Background

There has been a tremendous focus in recent years on granular segregation problems, ranging from density-driven [1–3] to size-dependent [4–8] and even multi-modal [7, 9–13] segregation, and much has been learned about the mechanisms driving these phenomena; however, there has been little to no effort devoted toward examining the scaling of these models with respect to vessel size and/or granular flow regime. At the same time, significant inroads have been made in uncovering an understanding of granular rheology with the so-called $\mu(I)$ model [14, 15] gaining substantial traction. Despite these parallel strides, to our knowledge, no study has been focused at connecting these two seemingly disparate fields of study. Our follow-on efforts in this IFPRI proposal will represent a unique approach to segregation study that will not only yield the first generation of inherently scalable segregation models (via direct incorporation of granular rheology concepts), but also will exploit the success of our novel segregation model testing framework to allow an unprecedented level of validation for these models.

In the first phase of our project (the first three years) we introduced and developed a segregation validation framework based on the the work of Shi *et al.* [16]. That is, Shi *et al.* [16] noted that the use of periodic flow perturbations could be used to thwart segregation in a material-independent way. Instead of completely halting segregation, however, in the proposed segregation model validation framework we note that *when the perturbation frequency is close to the inverse of the segregation time*, competition between the segregation and perturbations will lead to a "unique" steady state distribution. Thus, one can measure the resulting steady-state (or "equilibrium") distribution of particles in order to evaluate the accuracy of the *dynamic* models of segregation. This shift toward a single steady state measurement over a series of dynamic measurements vasts simplifies experimental (and computational) validation of these models.

Our project will, again, involve a combination of theoretical development, computational modeling, and

experimental validation. Computations will be based on the well-known Particle Dynamics (PD or DEM) approach to granular flows whereby each individual particle may be modeled as a unique entity so that particle properties can be varied in a trivial way.

3 Proposed Work

First we outline the overall tasks/milestones of the proposed program, along with a tentative timeline. Next, we discuss relevant preliminary results. Where necessary we follow with additional details for task completion.

3.1 Overview of the Project Goals and Tasks (with timeline)

Each of the proposed goals will involve a combination of theoretical development, Particle Dynamics (PD or DEM) modeling and/or experimental validation. Specific goals of this project, along with some associated sub-tasks, can be categorized as follows:

1. *"Ideal Solution" Segregation: single intruder studies (Year 1-2)*

1.a) perform complementary studies – both computational and experimental – of intruder segregation driven by density over a wide range of Inertia number (I): Our preliminary results (discussed in detail below) show a dramatic, never-before-reported transition in segregation behavior that mimics that of granular flow rheology (where changes in stress response are seen with changes in the value of the Inertia Number I – a number which characterizes the relative importance of inertia and confining stress [14]). Our results to date are extensive enough and our proposed model appears accurate enough that a full-scale investigation of the connection between (single-intruder) segregation and flow rheology is warranted. Thus far, we have studied this problem only computationally and then only in flows designed to capture only homogeneous shear. A "full-scale" investigation will involve experiments that complement our existing results as well as simulations on more typical (non-homogeneous) shearing flows.

1.b) perform complementary studies of size-segregation over a wide range of Inertia number (I): As size segregation is often considered to be more industrially relevant than density segregation, it is critically important to test whether a similar transition may be observed; as discussed below, a regime change can have tremendous impact for industrial practice. We expect that this portion of the project will be considerably more involved than Goal 1a as it has been shown that the segregation direction can change with flow conditions (which we will correlate with I) and that there is asymmetry [17] with respect to a small intruder in a bed of large particles and vice versa.

1.c) examine the effect of cohesion on segregation rates (intruder studies) as well as rheological transitions (with I): While the impact of cohesion on the *extent* of segregation was originally described theoretically by our group [18–20] (among others [21, 22]), the effect of cohesion on the *rate* of segregation has never been formally studied. As with Goal 1a, we have interesting preliminary results that suggest a simple scale shift can account for the impact of cohesion on the rate of density segregation. This work has not yet been confirmed experimentally, nor has the effect of cohesion on regime changes been tested.

2. *Segregation Flux Studies: concentration-dependent segregation (Year 2-3)*

2.a) examine concentration effects on density segregation: It is expected that, as in the case of a single intruder, a similar regime transition in segregation rate will be observed; however, as the density dependence in our preliminary results differs from the tradition approach, we expect subtle differences to become evident as the local average density changes. Theoretically capturing this dependency (and experimentally/computationally validating it) will be crucial to translation of our results to industrial practice.

2.b) examine concentration effects on size segregation: Concentration effects for size segregation will dramatically impact the local solids fraction; thus, it is likely that any observed regime effects from the single intruder studies will be altered by varying concentrations.

3. *Scale-up studies (Year 3)*

3.a) we will incorporate our most promising models from the previous goals into a device-scale transport

equation and compare to simple industrially-relevant flows: An important point to note is that, to our knowledge, none of the existing transport equations allow for changes in granular rheology. Thus, our choice of whether we use an Ottino/Leuptow [8,23] model or, alternatively, a Gray [13] model will be based on which model can most easily be modified to accept varying rheological and segregation models. Also, **communication with IFPRI collaborators will be critical in this task as we will require both guidance as to the most beneficial flows to examine as well as help in obtaining device-scale experimental data**.

3.2 Relevant Preliminary Results

The most successful density segregation model to date was set forth by Tripathi and Khakhar [2]. They begin with a force balance on a single dense/heavy particle within a sheared bed of lighter particles to get

$$0 = F_w - F_b + F_d \tag{1}$$

where F_w is the weight of the heavy particle, F_b is the buoyant force, and F_d is the particle drag force. Taking the particle drag force to have a Stokesian form, they assume

$$F_d = \beta\pi\eta d_p v_{seg} \tag{2}$$

where η is the particle bed "viscosity", d_p is the particle diameter, β is a constant, and v_{seg} is the segregation velocity. Solving this equation for v_{seg} suggests that the segregation velocity will vary linearly with the "effective heavy particle weight" ($(F_w - F_b)$ or $(V_p * g * (\rho_h - \rho_l))$ where V_p is the volume of a particle, g is the acceleration due to gravity and ρ_i is the density of the heavy (h) and light (l) particles, respectively). Thus a simple expression for v_{seg} may be written as

$$v_{seg} = \frac{d_p^2(\rho_h - \rho_l)}{\beta_s \eta} \tag{3}$$

where β_s is a modified constant.

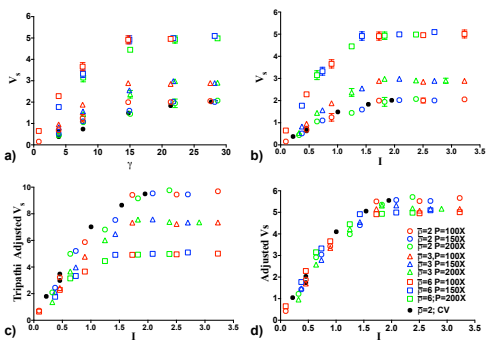

FIGURE 1: Segregation velocity under varying conditions of shear rate, density ratio, and boundary conditions. (a) The raw segregation velocities (in particle diameters per second) are plot vs the imposed shear rate. (b) Her we replot the raw segregation velocity as a function of inertia number. Note that the varying boundary conditions (i.e., for several different confining pressures and constant volumes) all collapse onto individual curves corresponding to different density ratios. Panels (c) and (d) test both the traditional and new density scaling, respectively, and show that a new density scaling law is required to collapse all of the examined data.

In all previous work reported in the literature a model like that of Equation 3 assumes that the granular flow may be assumed to be "rate independent" (i.e., stress is independent of the shear rate $\dot{\gamma}$), so that $\eta \propto \frac{1}{\dot{\gamma}}$ and we can write

$$v_{seg} = \frac{d_p^2\dot{\gamma}(\rho_h - \rho_l)}{\beta_\tau} = \frac{d_p^2\dot{\gamma}\rho_l(\bar{\rho} - 1)}{\beta_\tau} \tag{4}$$

where β_τ is a constant that captures the (constant) shear stress and $\bar{\rho}$ is the density ratio.

By relaxing the assumption that all segregating flows operate in the rate-independent regime (i.e., allowing our flow to extend to the so-call "intermediate regime", for example), we note that the Inertia number, I, is a better independent variable for correlating changes in segregation velocity (see Figure 1). Using the inertia number also allows us to capture – for the first time – the observation that the segregation rate saturates in much the same way that the effective friction is seen to saturate (at high inertia numbers) in $\mu(I)$ rheology [14, 15]. Additionally, by incorporating the effect of an intruder pushing through a less-dense medium we are able to build a uniquely accurate scaling law for dilute density segregation (see Figure 1d).

Perhaps the most industrially significant conclusion that can be made from our novel observation of a segregation regime change can be understood by considering the impact of *increasing processing rate*.

Under conventional (segregation) wisdom, it should make little to non difference if one were to increase the rate at which solids are processed because, while the time available for segregation will decrease, it was thought that the rate of segregation would correspondingly increase. However, based on our results, if one drives the system into the "saturated rate" regime they could obtain a **decreasing** extent of segregation with increasing processing rate. Thus, based on our findings, it is possible that one can *design* processes that are driven rapidly enough (i.e., at high enough processing rates or values of I) that the extent of segregation becomes effectively negligible.

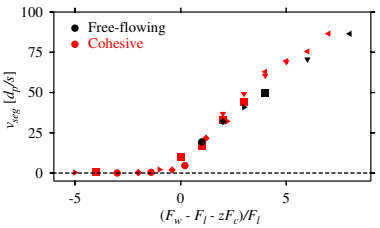

FIGURE 2: A plot of the segregation velocity measured in an idealized (computational) shear flow versus the effective heavy particle weight. Note that our newly proposed model for cohesive segregation agrees quantitatively with these results.

Another relevant suite of preliminary results concerns the impact of interparticle cohesion on the segregation rate. If we assume that the cohesive force acts opposite to that of gravity (with the limit that it cannot make the net weight "negative"), we can modify the balance equation of Tripathi and Khakhar [2] to give

$$0 = W_h - W_l - zf_l + c\pi\eta d_p v_{seg} \tag{5}$$

where W denotes the particle weight, z is the average coordination number, f_l is the capillary force of an individual bridge (so that the net cohesive force is $F_c = zf_l$), c is a constant, η is the particle bed "viscosity", d_p is the particle diameter, and v_{seg} is the segregation velocity. Solving this equation for v_{seg} suggests that the segregation velocity will vary linearly with the "effective heavy particle weight" ($W_h - W_l - zF_c$). As can be seen in Figure 2, this hypothesis seems to be supported by our computational results to date.

A critical unique observation of this preliminary work is that the rate of density segregation can be dramatically reduced even in the case of relatively small values of the Granular Bond Number (Bo_g) [24] (i.e., degree of cohesion), due to the impact of the coordination number in Eqn. 5. That is, even for flows that would normally be considered "non-cohesive" (i.e., $Bo_g < 1$), we can get substantially reduced segregation. This can have a dramatic industrial impact as it may be possible that cohesion could be used as a means of reducing segregation while it still remains small enough to not negatively impact overall flowability.

3.3 Experimental Details

In much of our proposed experimental testing/development of segregation models, we plan to use both a tumbler mixer experiment and a plane shear apparatus (discussed below) to validate our models. Specifically, the plane shear apparatus will be used for single "intruder" experiments, while both the (baffled and unbaffled) tumbler and a "rotating" version of the plane shear apparatus will be used for "mixtures" (where there is an appreciable amount of each component so that we may examine concentration effects).

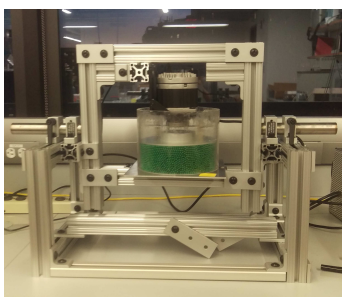

FIGURE 3: Plane shear apparatus. The cell height, imposed load, and shear rate can all be independently varied. Additionally, the experiment can be run in "perturbation mode" where the cell is periodically rotated with respect to gravity.

The intruder experiments (and simulations) will be used to assess the form of the segregation velocity expressions *in the absence of concentration effects*. That is, while the exact dependence of the segregation rate on the concentration of each species may be complex (particularly for the case of size segregation, where packing will be affected), one could argue that the most rapid segregation should happen in the limit that one small (or heavy) particle is trickling through a bed of large (or lighter) beads. The periodic plane shear flow apparatus (see Figure 3) consists of a vertical annular space that can be filled with particles. While the base and the inner and outer (side) walls of the annulus are fixed, the annular ring-shaped lid — which is free to move vertically to allow bed dilation and can accommodate weights in order to vary the effective pressure at the boundary — can be moved via a computer-controlled stepper motor.

shear only affects powder in the vicinity of the rotating "lid". Isn't most of the powder static? Does this matter?

Additionally, the central (horizontal) axis will allow the bed to be periodically inverted so that the direction of the segregation can be perturbed as a specified rate.

Our (concentration-dependent) mixture experiments will make use of both the plane shear apparatus as well as a tumbler mixer. In the context of our plane shear apparatus, this device can also be used in "perturbation mode" whereby we will alternate the sense of gravity periodically in order to achieve direct forcing of our system at a prescribed frequency. By incorporating centrally-located baffles in our tumbler mixer, we can effectively vary the perturbation frequency by changing either the rotation rate and/or the tumbler (or particle) size. A combination of image analysis and direct particle counting will be used as analytical techniques for our experimental studies. The particles to be used will include glass, cellulose acetate, acrylic, and stainless steel. For size segregation studies we will employ varying sizes of these materials; for density segregation, these materials will be used unmodified.

We should note that for cohesive, density segregation we must employ surface modification techniques similar to those in Ref [25]. That is, it is critical that the wetting angles of the materials are well-controlled when employing liquid bridge cohesion, yet varying the material density while maintaining similar surfaces is difficult. To alleviate this issue we have tested a modification of the method of Ref [26] whereby we use a Stober-like method to modify the surface of cellulose acetate (and stainless steel) beads with a (very) thin layer of silica. Preliminary tests of this method not only reduce the wetting angle of the cellulose acetate beads for roughly 40^o to 20^o, but also will allow further surface modification if necessary.

Is the affect of non-capillary cohesion the same as capillary? Does the length scale of the force matter?

3.4 Computational Details

The computational approach will employ DEM modeling in three geometries: a tumbler mixer (both with and without centrally-located baffles), a periodic plane shear geometry, and a "perfect shear" system obtained via a modification of the effective gravitational force on the particles (see Ref. [27]). Particle properties in the simulations will mimic those of our experimental materials whenever possible to facilitate direct comparison.

3.5 "Ideal Solution" Segregation: single intruder studies

In the case of "ideal solution" segregation, the role of concentration becomes immaterial and one can expect to examine "pure" segregation in the limit of zero concentration of intruding species. As such, this section of the work is devoted exclusively to examining the value and form of segregation *velocities*.

3.5.1 Density-based Intruder Studies

Our profound results outlined in Section 3.2 represent an extensive preliminary *computational* study; however, much remains to be done in this area. The most pressing of tasks will be the experimental validation of the computational results obtained thus far. For this portion of the task we will use our newly constructed (reversible) plane shear apparatus in both the traditional and "perturbation" mode. This device is designed to allow operation either in a mode that leads to a constant volume or constant pressure boundary condition, thus varying the inertia number should be readily attainable. Therefore, just as reported in our preliminary computational results, we will (experimentally) examine a variety of density ratios, shear rates, and confining pressures in order to directly observe the density segregation regime change in a physical flow.

In addition to a plane shear flow, it has been shown in Ref. [28] that the inertial number increases quite dramatically with an increase in a chute flow's (or presumably also a tumbler mixer's) inclination angle. As such, we will repeat – both experimentally and computationally – our conditions of varying density ratio for a host of chute flows and tumbler flows in an attempt to observe the regime transition in more industrially relevant flows. It should be noted that it is unlikely that we can measure the shear rate and/or pressure effectively within the experimental studies; thus, we will match our simulations to the experiments as closely as possible so that we can translate our computational measurements as well as possible to their corresponding experimental counterparts.

3.5.2 Size-based Intruder Studies

It is generally well accepted that size segregation is more industrially relevant than density segregation; therefore it is critically important to test whether a similar regime transition may be observed in size segregation. It is expected that this portion of the project will not only address the existence of a regime change, but also formalize the conditions under which the segregation direction can change with flow conditions (by correlating it with I). This will represent a dramatic step forward in the rational design of industrial practices that might mitigate segregation. It should be noted that a very early question to be addressed is exactly how to redefine the inertia number in the case of systems with varying size. As a first attempt we will adopt the approach of Ref. [28] where an average local density (here, size) is used.

As with density segregation, our initial computational results will focus on idealized systems both from the standpoint of including solely a small number of intruders, but also due to the fact that they will have simple, homogeneous shear. As such, our first series of simulations will be very similar to recent work from the Wassgren group [27], albeit with a focus on varying the Inertia number. Particles of varying (smaller) size and the same density will be sheared within our Lees-Edwards computational geometry for a variety of shear rates and confining pressures. Additionally, we will also incorporate particles of varying (larger) size as a means of testing rheological impact on segregation asymmetry [17]. The plane shear experimental apparatus will be used in both the traditional and perturbation mode as a means of validating computational observations. Finally, depending on the level of success obtained in capturing high inertia numbers in tumblers and chute flows during Task 3.5.1, we will conclude this portion with similarly industrial-focused flows.

3.5.3 The Effect of Cohesion in "Ideal Solution" Segregation

We plan to examine the impact of inertia number on cohesive segregation rates, the impact of cohesion on size segregation, and experimentally validate these results. As with much of the proposed work, our first task in this sub-topic will be to experimentally validate the preliminary computational results obtained. Since we will examine exclusively liquid-induced cohesion, and as mentioned in Section 3.3, the major difference between cohesive and non-cohesive experiments (other than the inclusion of a small amount of interstitial moisture) will lie in the necessity of surface modification for density segregation. As we have shown in previous work, we are well suited to performing cohesive segregation experiments [19,25]. We will use this expertise to examine the effect of inertia number on both density and size segregation with the additional control variable of Granular Bond number. The overall approach – that is, what variable will be varied and what apparatus will be used – will directly mimic the non-cohesive counterparts discussed above.

3.6 Segregation Flux Studies: concentration-dependent segregation

While our approach to concentration-dependent segregation – in both density-based and size-based segregation – will be critically important to the overall success of the project (due to the necessity of this aspect for industrial translation of our work), the overall computational and experimental approach will mirror the tasks already outlined in the previous sections with the additional control variable of the mass (or number) fraction of segregating species to be used. It is expected that, as in the case of a single intruder, regime transitions in segregation rate will be observed; however, the exact definition of the inertia number will need to be modified (as in Ref. [28]) due to local variations in both particle density and size. Also, as our preliminary results have suggested that the overall packing fraction plays a significant role in the regime transition, we expect that size-segregation, in particular, will have a more complicated dependence on the overall concentration of the segregating materials (as particles of varying size can sometimes pack more efficiently than those of uniform size, although not *always* [29]).

As in our previous tasks, we will begin with computational studies in an idealize homogeneous shear flow and work our way through both experimental validation as well as more industrially-relevant flows (such as chute and tumbler geometries).

Not much about process-scale segregation.

References

[1] D V Khakhar, J J McCarthy, J M Ottino, and T Shinbrot. Transverse Flow and Mixing of Granular Materials in a Rotating Cylinder. *Phys. Fluids*, 9:3600–3614, 1997.

[2] Anurag Tripathi and D. V. Khakhar. Density difference-driven segregation in a dense granular flow. *Journal of Fluid Mechanics*, 717:643–669, feb 2013.

[3] Yi Fan and K. M. Hill. Shear-induced segregation of particles by material density. *Physical Review E*, 92(2):022211, 2015.

[4] S B Savage and C K K Lun. Particle Size Segregation in inclined chute flow of cohesionless granular solids. *J. Fluid Mech.*, 189:311–335, 1988.

[5] V Dolgunin. Segregation modeling of particle rapid gravity flow. *Powder Technology*, 83(2):95–103, may 1995.

[6] Yi Fan and K. M. Hill. Phase Transitions in Shear-Induced Segregation of Granular Materials. *Physical Review Letters*, 106(21):218301, may 2011.

[7] J. M. N. T. Gray and C. Ancey. Multi-component particle-size segregation in shallow granular avalanches. *Journal of Fluid Mechanics*, 678:535–588, jun 2011.

[8] Conor P. Schlick, Yi Fan, Paul B. Umbanhowar, Julio M. Ottino, and Richard M. Lueptow. Granular segregation in circular tumblers: theoretical model and scaling laws. *Journal of Fluid Mechanics*, 765:632–652, 2015.

[9] JW Chew, DM Parker, and CM Hrenya. Elutriation and species segregation characteristics of polydisperse mixtures of Group B particles in a dilute CFB riser. *AIChE Journal*, 59(1), 2013.

[10] G. G. Pereira and P. W. Cleary. Radial segregation of multi-component granular media in a rotating tumbler. *Granular Matter*, oct 2013.

[11] Brenda Remy, Johannes G. Khinast, and Benjamin J. Glasser. Polydisperse granular flows in a bladed mixer: Experiments and simulations of cohesionless spheres. *Chemical Engineering Science*, 66(9):1811–1824, may 2011.

[12] Suman K. Hajra and D. V. Khakhar. Radial segregation of ternary granular mixtures in rotating cylinders. *Granular Matter*, 13(4):475–486, mar 2011.

[13] J.˜M.˜N.˜T. Gray and C. Ancey. Particle-size and -density segregation in granular free-surface flows. *J. Fluid Mech.*, 779:622–668, 2015.

[14] G D R Midi. On dense granular flows. *The European physical journal. E, Soft matter*, 14(4):341–65, aug 2004.

[15] J. M. N. T. Gray and A. N. Edwards. A depth-averaged -rheology for shallow granular free-surface flows. *Journal of Fluid Mechanics*, 755(2014):503–534, 2014.

[16] Deliang Shi, Adetola A Abatan, Watson L Vargas, and J J McCarthy. Eliminating segregation in free-surface flows of particles. *Physical Review Letters*, 99:148001, 2007.

[17] K. Van Der Vaart, P. Gajjar, G. Epely-Chauvin, N. Andreini, J. M N T Gray, and C. Ancey. Underlying Asymmetry within Particle Size Segregation. *Physical Review Letters*, 114(23):1–5, 2015.

[18] I Figueroa, H Li, and J J McCarthy. Predicting the impact of adhesive forces on particle mixing and segregation. *Powder Technology*, 195(3):203–212, 2009.

[19] Hongming Li and J.J. McCarthy. Cohesive particle mixing and segregation under shear. *Powder Technology*, 164(1):58–64, may 2006.

[20] H Li and J J McCarthy. Phase diagrams for cohesive particle mixing and segregation. *Physical Review E*, 71:21305, 2005.

[21] A Samadani and A Kudrolli. Segregation Transitions in Wet Granular Matter. *Phys. Rev. Lett.*, 85:5102–5105, 2000.

[22] D Geromichalos, M M Kohonen, F Mugele, and S Herminghaus. Mixing and condensation in a wet granular medium. *Physical Review Letters*, 90:168702, 2003.

[23] Conor P. Schlick, Yi Fan, Austin B. Isner, Paul B. Umbanhowar, Julio M. Ottino, and Richard M. Lueptow. Modeling segregation of bidisperse granular materials using physical control parameters in the quasi-2d bounded heap. *AIChE Journal*, 61(11):1524–1534, 2015.

[24] Steven T. Nase, Watson L. Vargas, Adetola a. Abatan, and J.J. J McCarthy. Discrete characterization tools for cohesive granular material. *Powder Technol.*, 116(2-3):214–223, may 2001.

[25] H Li and J J McCarthy. Controlling Cohesive Particle Mixing and Segregation. *Phys. Rev. Lett.*, 90:184301, 2003.

[26] R. A. Zoppi and M. C. Gonzalves. Hybrids of cellulose acetate and sol-gel silica: Morphology, thermomechanical properties, water permeability, and biodegradation evaluation. *Journal of Applied Polymer Science*, 84(12):2196–2205, jun 2002.

[27] N. Khola and C. Wassgren. Correlations for shear-induced percolation segregation in granular shear flows. *Powder Technology*, 288:441–452, 2016.

[28] Anurag Tripathi and D. V. Khakhar. Rheology of binary granular mixtures in the dense flow regime. *Physics of Fluids*, 23(2011), 2011.

[29] Melissa H. Lash, Jahnelle C. Jordan, Laura C. Blevins, Morgan V. Fedorchak, Steven R. Little, and Joseph J. McCarthy. Non-Brownian Particle-Based Materials with Microscale and Nanoscale Hierarchy (highlighted article). *Angewandte Chemie International Edition*, 54:5854–5858, 2015.

1 Proposal Summary and Reviewer Comments

The proposed work for the second phase of the "Prediction of Segregation" will build on accomplishments made in the first phase, which have been disseminated in a published article in *AIChE Journal* [1] and a manuscript under review for *Physical Review Letters* (attached as an Appendix). Specifically, in these works, we have established a direct connection between granular rheology and segregation that has the potential to spur a substantial jump in our understanding of both fields and, ultimately lead to a transformation in the way that particle flow research is conducted. Not only has our phase I work led to a completely new class of (density) segregation model, but we plan to continue to expand this work to size, shape, and cohesive systems in phase II. Moreover, the inherently scalable models that we are developing will allow for the rational design of strategies to mitigate segregation in industrial processing. As articulated in our original renewal proposal, the specific goals to be attained within this project include:

A. Use an analogy between granular rheology and segregation to develop inherently scalable models
B. Experimentally testing these models in a variety of prototypical granular flows
C. Test the scalable nature of the models via incorporation into device-scale transport equations

Upon review by IFPRI, the following comments were raised regarding our phase II plans:

1. "members are much more interested in size segregation"
2. "Everyone eagerly anticipates your foray into cohesion"
3. "IFPRI wants experimental demonstration that your approach works for size segregation; The need for experimental validation in industrially-relevant experiments was repeated by several members"

In this document we address each of these comments and introduce several sets of preliminary results that we have put together since we submit our renewal proposal.

2 Response to Reviewer Comments

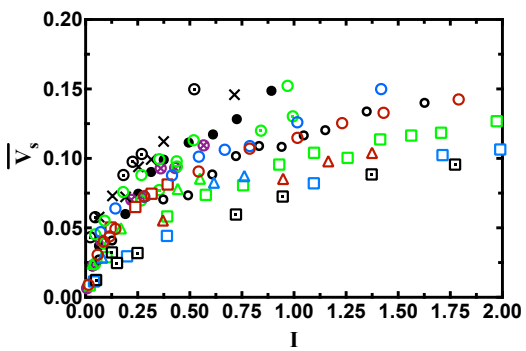

FIGURE 1: Segregation velocity as a function of size-rescaled Inertia number. Note that, while our preliminary analysis does not yet collapse our data onto one master curve, it is clear that we observe a "segregation saturated regime" in much the same way that we did for density-driven segregation.

While we have modified our proposed scope of work slightly in response to these insightful comments, we have also already begun some of the work proposed for phase II and believe that they will alleviate some concerns of the members. Here we give a detailed response and discussion on each point.

2.1 Response to Comments 1 (and partially 3): On Size Segregation

Size segregation has always been seen as a critical next step for phase II of the proposal. As size segregation is often considered to be more industrially relevant than density segregation, it is critically important to test whether a similar transition in segregation rate may be observed; as discussed above, a regime change can have tremendous impact for industrial practice. Thus far, we have begun our "single-intruder" studies of size segregation. In this portion of the project, we examine how a very dilute solution of small particles segregates in a shear flow dominated by larger beads.

As with our work on density segregation, we think that an approach to segregation rate model building that is focused on dimensional analysis and analogy between granular rheology and segregation will yield a comprehensive model. We are excited to report that our preliminary results show a similar "saturated" regime for segregation at high Inertia numbers (see Appendix for density discussion).

2.2 Response to Comment 2: On cohesion

As we have argued before, our group are pioneers in the control of particle mixing and segregation and and have firmly established ourselves as the world-leaders in this area [2]. In particular, we have enjoyed unprecedented success in controlling segregation in cohesive granular flows ranging from gravity-dominated [3–6] to shear dominated [7] to gas-solid flows [8]. As discussed in the renewal proposal we have observed significant progress in modeling the impact of cohesion on segregation rate (due to density) in preliminary simulations (see Fig. 2, reprinted from our proposal).

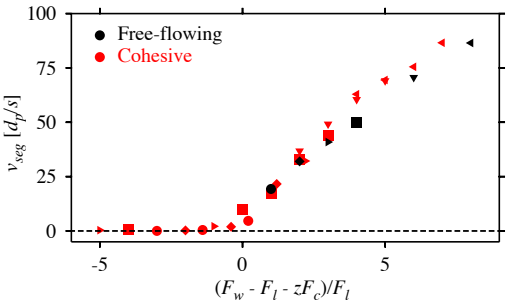

FIGURE 2: A plot of the segregation velocity measured in an idealized (computational) shear flow versus the effective heavy particle weight. Note that our newly proposed model for cohesive segregation agrees quantitatively with these results.

As a refresher, we assume that the cohesive force acts opposite to that of gravity (with the limit that it cannot make the net weight "negative"), we can modify the balance equation used in both Ref. [9] as well as the Appendix, to give

$$0 = W_h - W_l - zf_l + c\pi\eta d_p v_{seg} \tag{1}$$

where W denotes the particle weight, z is the average coordination number, f_l is the capillary force of an individual bridge (so that the net cohesive force is $F_c = zf_l$), c is a constant, η is the particle bed "viscosity", d_p is the particle diameter, and v_{seg} is the segregation velocity. Solving this equation for v_{seg} suggests that the segregation velocity will vary linearly with the "effective heavy particle weight" $(W_h - W_l - zF_c)$. As can be seen in Figure 2, this hypothesis seems to be supported by our computational results to date.

As the model for this segregation approach is built entirely within the framework of our current density-driven model (see Appendix), we believe that a similar degree of success can be expected in capturing density segregation for particles ranging from fully free-flowing to cohesive.

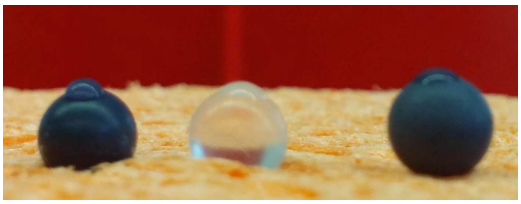

FIGURE 3: Preliminary tests of surface modification of "generic" materials. Notice that the wetting angle can be made completely uniform – regardless of base material – when we use this technique.

We should caution that examining size-driven segregation in cohesive systems will be significantly more complex and can only be attacked toward the conclusion of phase II (without significant increases in manpower). That is, cohesion/size will be complicated by the following considerations: a) our size theory is still under development and will be a primary focus of phase II; b) size will require that we not only include a cohesive force that opposes motion (as in the density case above), but also will necessitate that cohesion actively promote mixing of differing size particles (see our previous work in Ref. [4]).

It is likely that for both density and size-based cohesive segregation studies, we will use our newly-developed technique of surface modification in order to carefully control the wetting angles of the materials (as we did in Ref [4]). Our technique is a modification of the method of Ref [10] whereby we use a Stober-like synthesis to modify the surface of cellulose acetate (and stainless steel) beads with a (very) thin layer of silica. As one case see in Figure 3, preliminary tests of this method not only reduce the wetting angle of the cellulose acetate beads for roughly 40^o to 20^o, but also will allow further surface modification if necessary.

2.3 Response to Comment 3: On particle size and experimental focus

We have addressed our strong focus on size-based segregation in phase II of the proposed work in an earlier section of this document. Here, we further detail our experimental efforts to date (on shape-driven segregation) as well as the experiments proposed for phase II.

At the present time there are no currently proposed segregation models that incorporate shape in any way. To date, we have performed a series of experiments focused on segregation of axisymmetric shapes embedded as "intruders" within a background flow of spheres. As suggested in previous reports from our phase I efforts, we use axisymmetric materials (specifically, cylinders with varying aspect ratios) and compare their tendency to segregate

when blended with spheres of varying sizes. Our preliminary approach is to treat the segregation loosely akin to size-driven segregation whereby we assign an "effective size" to the non-spherical shape. At present, it appears that taking a ratio of the projected areas of the particles is the most effective method of correlating our experimental results (see Figure 4). Interestingly, the proper area to use for our non-spherical particles appears to *not* be linked to a specific orientation of the cylinder, but instead is an angular average of the projected area.

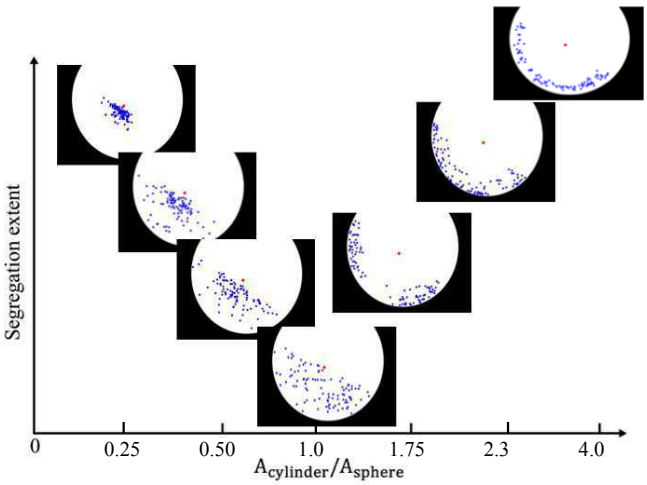

FIGURE 4: Shape-based segregation experiments. At present we have performed a variety of "intruder" studies whereby we track the periodic location of non-spherical intruders within a tumbler filled with spheres. Correlating our results with the relative projected area of the particles seems to work well as a predictive tool. The red dot is a spacial reference point used for quantification of the mixing extent, while the blue point represent the location where the non-spherical intruder has been found.

As one can see from our preliminary work on surface modification and shape segregation, our group is committed to experimental study/validation comprising a significant portion of the phase II project. As was described in the renewal proposal, we have constructed – and begun testing – a plane shear apparatus to be used to validate our models. As the models are all built based on dimensionless quantities, we expect scale-up to be captured largely as a native consequence of the model structure. Obviously, the device geometry introduces additional dimensionless numbers (at a minimun the dimensionless size of the device – required for geometric scale-up). We will use the plane shear apparatus with a variety of particle sizes in order to explore several orders of magnitude of geometric scaling, while carefully monitoring the validity of existing model as the model-specific scaling variables change with geometric scaling.

We expect to use the plane shear apparatus in two modes: a native mode and a perturbation mode. We primarily use the native mode for single "intruder" experiments, while we have designed the "perturbation" or "rotating" mode so that it can be used for "mixtures" (where there is an appreciable amount of each component so that we may examine concentration effects). The experiments on mixtures will make use of our recent "segregation testing framework" built and verified in phase I [1].

Finally, we have begun to explore the possibility of collaborating with an experimental specialist. In particular, we are in discussion with Professor Kimberly Hill from the University of Minnesota who is an expert in granular segregation experiments. We are most interested in making use of Dr. Hill's "split bottom cell" which is a shear device that allows control of both pressure boundary conditions as well as the distribution of shearing within the mixing device. We anticipate that the controlled variation of the local shear rate will result in specific concentration profiles that will allow a sensitive probe of our segregation models (when incorporated into simple transport equations).

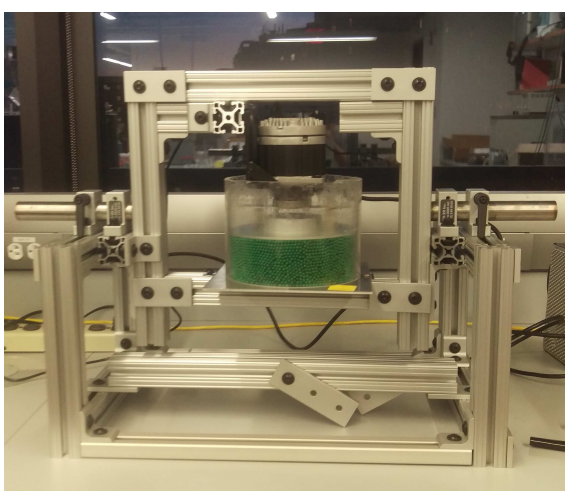

FIGURE 5: A picture of our plane shear experimental apparatus. The cell height, imposed load, and shear velocity can all be independently varied. Additionally, the experiment can be run in "perturbation mode" where the cell is periodically rotated with respect to gravity (note the bearings along a horizontal axis).

References

[1] Siying Liu and J J Mccarthy. Validating Segregation Rate Models. *AIChE Journal*, in press:1–25, 2017.

[2] J.J. McCarthy. Turning the corner in segregation. *Powder Technology*, 192(1):137–142, jun 2009.

[3] H Li and J J McCarthy. Phase diagrams for cohesive particle mixing and segregation. *Physical Review E*, 71:21305, 2005.

[4] H Li and J J McCarthy. Controlling Cohesive Particle Mixing and Segregation. *Phys. Rev. Lett.*, 90:184301, 2003.

[5] I Figueroa and J J McCarthy. Using Janus Particles to Control Mixing and Segregation of Adhesive Particle Systems. *Industrial & Engineering Chemistry Research*, 49(11):5204–5214, 2010.

[6] I Figueroa, H Li, and J J McCarthy. Predicting the impact of adhesive forces on particle mixing and segregation. *Powder Technology*, 195(3):203–212, 2009.

[7] Hongming Li and J.J. McCarthy. Cohesive particle mixing and segregation under shear. *Powder Technology*, 164(1):58–64, may 2006.

[8] K Jain, D Shi, and J J McCarthy. Discrete Characterization of Cohesion in Gas-Solid Flows. *Powder Technol.*, 146(1):160–167, 2004.

[9] Anurag Tripathi and D. V. Khakhar. Density difference-driven segregation in a dense granular flow. *Journal of Fluid Mechanics*, 717:643–669, feb 2013.

[10] R. A. Zoppi and M. C. Gonzalves. Hybrids of cellulose acetate and sol-gel silica: Morphology, thermomechanical properties, water permeability, and biodegradation evaluation. *Journal of Applied Polymer Science*, 84(12):2196–2205, jun 2002.

Appendix

A Transport Analogy for Segregation and Granular Rheology

Siying Liu and Joseph J. McCarthy*
Department of Chemical and Petroleum Engineering
University of Pittsburgh
Pittsburgh, Pennsylvania 15261
(Dated: April 26, 2017)

Here we show a direct connection between density-based segregation and granular rheology that can lead to unique insight into both problems. Our results exhibit a dramatic transition in the rate of segregation during simple shear that occurs at $I \sim 0.5$ and exactly mimics a coincident regime change in flow rheology. We propose scaling arguments that support a packing fraction criterion for this transition that can both explain our segregation results as well as unify existing literature studies of granular rheology [1–3]. By recasting a segregation model in terms of rheological parameters we establish a novel approach that not only collapses results for a wide range of conditions, but also yields a direct relationship between the coordination number, z, and the segregation velocity. Moreover, our approach predicts the precise location of the observed regime change/saturation. This suggests that it is possible to rationally design process operating conditions that lead to dramatically lower segregation extents. These observations can have a profound impact on both the study of granular flow/mixing as well as industrial practice.

Segregation [4] is a costly phenomenon that has garnered research for decades [5–7]. In contrast, the study of dense phase granular rheology has only recently gained traction, but significant inroads have been made [1–3, 8–11]. Despite these parallel strides, only a tenuous connection has been proposed [12] between these two seemingly disparate topics and no work has focused on building a formal analogy, despite the synergistic advantages that analogies have afforded [13] in a variety of fields [14–17].

It is generally accepted [18–20] that the scaling of gravity driven density segregation is proportional to the density difference between species as well as to the local value of the shear rate within the flow (although segregation in the absence of gravity has been shown to be more complex [21, 22]). This simple phenomenological scaling results in just three relevant dimensionless groups – for segregation velocity: $\bar{v}_s = v_s/(\sqrt{gd_p})$, shear rate: $\bar{\gamma} = \dot{\gamma}\sqrt{d_p/g}$, and density: $\bar{\rho} = \rho_h/\rho_l$, where g is the acceleration due to gravity and d_p is the particle diameter; however, it does not account for the impact of varying boundary conditions (specifically, confining pressure, P), thus it does not readily allow direct coupling between granular flow rheology and the segregation rate. In this Letter, we examine a simplified "ideal solution" segregating flow whereby isolated dense intruders segregate as a function of a host of rheological variables. By explicitly accounting for the confining pressure, we make a more direct connection between rheology and segregation. In this way, we not only shed light on how rheological-segregation coupling may be modeled, but also uncover a direct analogy between measurements of rheological variables and the resulting segregation rate.

A recent survey of density-based segregation models [23] found that a successful phenomenological model for the density-driven segregation velocity has been set forth by Tripathi and Khakhar [19]. They begin with a force balance on a single dense particle in a medium of light particles to get

$$0 = F_w - F_b + F_d \tag{1}$$

where F_w is the weight of the dense particle, F_b is the buoyant force, and F_d is the particle drag force. Taking the particle drag force to have a Stokesian form, they assume

$$F_d = \beta\pi\eta d_p v_s \tag{2}$$

where η is the particle medium viscosity, d_p is the particle diameter, β is a constant, and v_s is the segregation velocity. Assuming that the drag force and net particle weight are in balance, after simplification, yields an expression for v_s which may be written as

$$v_s = \frac{g d_p^2(\rho_h - \rho_l)}{\beta_s \eta} \tag{3}$$

where β_s is a modified constant, g is the acceleration due to gravity, and ρ_i is the density of the heavy (h) and light (l) particles, respectively. In order to recover the previously mentioned scaling, one assumes that the stress, τ, within the granular flow is shear rate independent so that we can write

$$\eta = \frac{\tau}{\dot{\gamma}} \propto \frac{1}{\dot{\gamma}}. \tag{4}$$

Based on the above equations, we recover the frequently used scaling results that: (1) v_s is proportional to the shear rate $\dot{\gamma}$; and (2) at a constant shear rate the segregation velocity, v_s, should scale as $(\rho_h - \rho_l)$.

To test these predicted scaling relations, yet at the same time allow variation of flow boundary conditions, we employ the discrete element method (DEM) to examine a wall-driven periodic plane shear cell. A schematic of the simulated 3D plane shear flow system is shown in Fig. 1 and details of the simulation parameters may be found in the supplementary materials. Periodic boundaries are used in both the x and z directions. In most trials, the majority of the particles have the same (light) density of $\rho_l = 1300 kg/m^3$, material properties that roughly match cellulose acetate, and an average radius of 4.5 mm with a 10% particle size distribution to prevent crystallization. In some cases we examine the impact of varying particle diameter over a range from $d_p =$ 6.0 mm - 18 mm in 3.0 mm increments. For all simulations eight uniform heavy intruders (which have the same radius as the light particles, but with varying heavy density, ρ_h) are randomly placed in the system. Three different ρ_h values are used (2700 kg/m^3, 3900 kg/m^3, and 7900 kg/m^3), along with corresponding material properties that roughly match glass, "heavy glass", and stainless steel, respectively. The top and bottom walls (shown as black in Fig. 1) are roughened with particles and the top wall is given varying masses in order to examine the effect of confining pressure (P). Alternatively, several trials were run at constant volume fraction (i.e., fixed height, h) where we measured the time-average of the pressure at the top wall (rather than prescribing the confining pressure). Shearing velocity is varied from 0.1-4.0 m/s (0.1, 0.5, 1, 2, 3, 4 m/s) while the bottom wall remains static. To obtain a nearly homogeneous shear flow, fins made of wall particles are attached to both the top and bottom walls, and in most simulations we employ a modified gravitational field whereby (net) gravitational forces act only on the heavy intruders (similar to the approach of Ref. [24]). The particle bed is deep enough (15 particle diameters) that the segregating intruders reach a steady segregation velocity under all examined conditions. In a small number of simulations full gravity effects are included, however, due to shear localization in these cases we perform all calculations based on the local value of the shear rate (and only measure the segregation velocity while in the sheared region).

In Figure 2 we show the dimensionless segregation velocity obtained for the average of the heavy intruders for three different density ratios under a range of boundary conditions (confining pressures vs fixed volumes and our modified gravity field vs full gravity), particle diameters, and shear rates. In Figure 2a, which shows the variation of $\bar{v}_s$ with dimensionless shear rate ($\bar{\gamma}$), we note that there are roughly three groups of curves – corresponding to each of the three density ratios; however, it is clear that there are a number of issues with this naive scaling. First, there is a systematic variation in the value of $\bar{v}_s$ for differing boundary conditions, whereas higher pressures and/or the constant volume cases result in a routinely

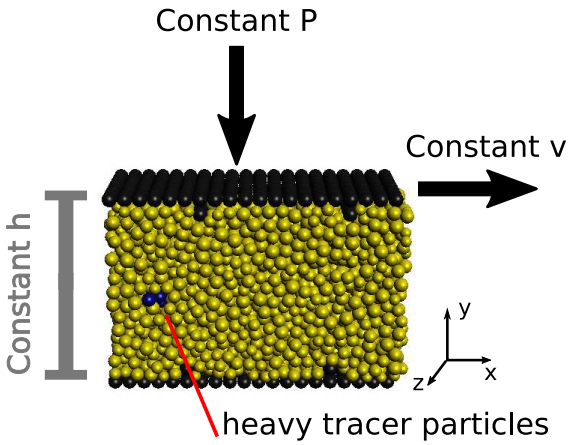

FIG. 1. Schematic of the simulated plane shear geometry. The 3D flow is periodic in both the streamwise (x) and transverse (z) directions. Blue (dark) particles are heavy intruders while yellow (light) particles are lower density particles. We employ either constant pressure or constant volume boundary conditions.

smaller value of the segregation velocity. Second, when varying the particle diameter, we notice a qualitatively different shape to the scatter plot (it does not appear to pass through the origin, for example). Finally, when including the full effects of gravity, our segregation velocity values are uniformly lower than for the corresponding shear rates in modified gravity cases and ultimately the segregation rate saturates at dramatically larger values of the dimensionless shear rate.

In order to fix these issues with the scaling, and as a first step toward connecting segregation to granular rheology, in Figure 2b we instead plot $\bar{v}_s$ against a different dimensionless shear rate, that of the Inertia number (I). The Inertia number [1], given as $I = \dot{\gamma} d_p \sqrt{\frac{\rho}{P}}$, relates the timescale of shearing to the timescale of consolidation and has been a staple of constitutive model development in recent years [3, 9–11]. We note that I is a better independent variable for correlating changes in segregation velocity as the scatter from pressure (and constant volume) variation is now eliminated in the higher density ratio (triangle and square) trials. Moreover, the low density ratio (circle) case now collapses results not only for varying boundary conditions, but also for varying particle diameter and for both full and modified gravity cases (note that the modified gravity case uses the average bed pressure and the local shear rate in the calculation of I). Using the Inertia number allows us to capture, for the first time, a clear observation that the segregation rate saturates (Figure 2b) at a specific value of I in much the same way that the effective friction (μ_{eff}) is seen to saturate (at high Inertia numbers) in $\mu_{eff}(I)$ rheology [1, 25]. Also, we note that, while our $\bar{v}_s$ results now collapse onto three curves regardless of particle size and boundary condition, the relevant scaling for density ra-

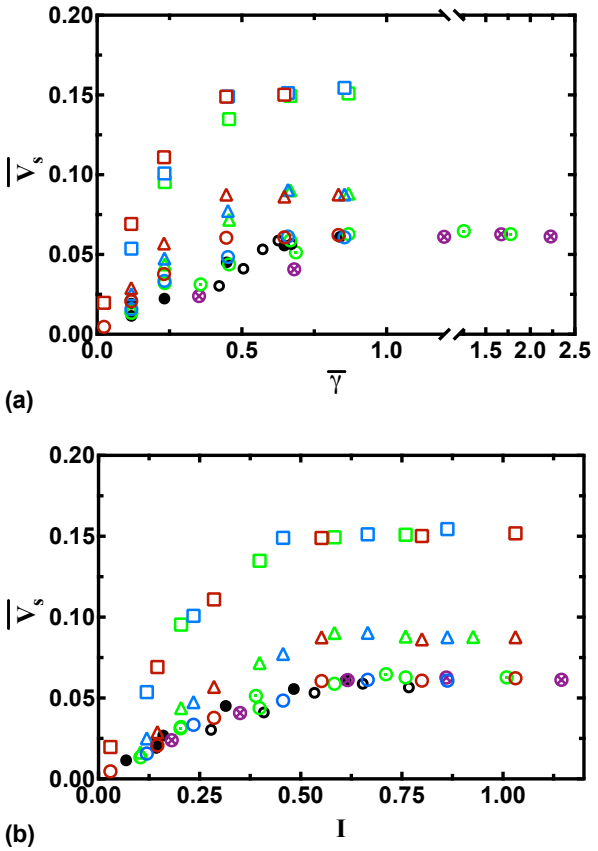

FIG. 2. Segregation velocity under varying conditions of shear rate, density ratio, particle diameter, and boundary conditions. Differing colors represent boundary conditions (constant pressures 78 Pa – red, 117 Pa – blue, 156 Pa – green; constant volume – solid circles; full gravity effects – dotted and crossed circles) while shape represents density ratio (circle - $\bar{\rho} = 2$; triangle - $\bar{\rho} = 3$; square - $\bar{\rho} = 6$). While most particles are 9.0 mm in diameter, the thick-walled open circles represent a range from 6.0 mm - 18.0 mm. (a) The dimensionless segregation velocities are plot versus the shear rate made dimensionless with $\sqrt{g/d_p}$. (b) In this panel we have replot the $\bar{v}_s$ as a function of Inertia number (I). Note that the varying boundary conditions all collapse onto individual curves corresponding to different density ratios.

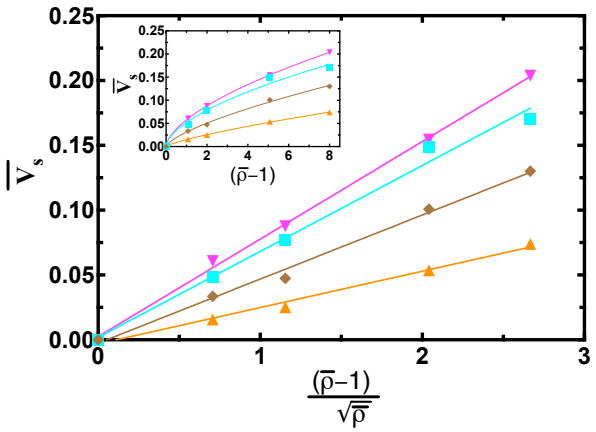

FIG. 3. Variation of dimensionless segregation velocity with varying density at fixed values of the Inertia number (with values ranging from 0.11 - 0.82). The inset shows the traditional scaling of the segregation rate with the dimensionless density difference. Note that, in contrast to previous studies, we find a power law relationship with exponents that range from 0.6 - 0.75. In contrast, when we plot the segregation velocity versus our newly proposed density scaling, we obtain straight lines.

tio is not captured in this plot. This scaling is examined next.

Turning to the impact of the density ratio, one can note that using the traditional density scaling suggested from Eqn. 3, fails to collapse the data (that is, the plot in Figure 3(inset) does not lead to a straight line). This is particularly evident when one re-scales the results from Figure 2b and examines the saturated segregation regime (i.e., for values where $I > 0.5$; see Supplementary Information). If we relax the assumption that all segregating flows operate in the rate-independent regime and instead develop a scaling relation for the local viscosity near a segregating particle, we can recast Equation 3 and not only recover the proper density relationship (Figure 3, motivated below), but also establish a direct analogy between granular flow rheology and the segregation velocity.

We start by choosing a characteristic stress scale in the neighborhood of the heavy intruder(s) as the quantity $\tau_{char} \sim \rho_h g d_p$. If we similarly take the local shear rate to be related to a characteristic collisional velocity, v_{coll} (to be identified later), divided by the particle diameter we obtain

$$\eta \sim \frac{\rho_h g d_p}{v_{coll}/d_p}. \tag{5}$$

For a heavy intruder, a density dependence of the collisional velocity, v_{coll}, arises due to the fact that the intruder must undergo repeated collisions with the lighter "background" particles. By performing a conservation of energy balance around a colliding particle [26], we obtain a post-collision characteristic velocity given as $v_{coll} \sim v_o \left(\frac{\rho_h}{\rho_l}\right)^{1/2}$ where v_o may be thought of as the pre-collisional characteristic velocity. Combining these expressions, we can write an equation for the viscosity near a heavy intruder particle that is segregating within a granular fluid as

$$\eta \sim \frac{\rho_h g d_p^2}{v_o \left(\frac{\rho_h}{\rho_l}\right)^{1/2}}. \tag{6}$$

This simple model suggests a modification of the density scaling from what is traditionally used whereby

$$v_s \sim \frac{v_o(\bar{\rho}-1)}{\sqrt{\bar{\rho}}}. \tag{7}$$

As a direct test of this scaling, we plot the measured segregation velocity as a function of this new density scaling for fixed values of the Inertia number (see Figure 3). Note that each set of results examined lies on a straight line whose slope is a function of the Inertia number chosen.

In order to more fully realize the form of Eqn. 7, we finally examine the characteristic (pre-)collisional velocity, v_o. Obviously, in the absence of interactions with neighboring particles the characteristic velocity of a falling intruder would scale as $\sqrt{d_p g}$ (motivating the choice of dimensionless scaling thus far used). If we argue that the characteristic velocity varies from this value solely due to interactions with neighboring particles, we can write that the number of interactions with neighbors per unit time is captured by the product of the coordination number, z, and the shear rate – $z\dot{\gamma}$ (note that z has been shown to be a function of the Inertia number [3, 11]). We note that, in our results, the average coordination number per particle follows a power law $z \sim I^{-a}$ – as discussed in Ref. [8] – however, as seen in Figure 4(a), we find two regimes where $a = 1/3$ and 1 for I values below and above 0.5, respectively. We note that this transition point is coincident with the saturation location of both the effective friction coefficient, μ_{eff}, and the segregation velocity. Finally, if we limit the effective number of neighbor interactions to those that occur faster than the consolidation time-scale, $t_c = d_p(\rho_l/P)^{1/2}$, we obtain a choice of v_o that is given by

$$v_o \sim (\sqrt{d_p g})z\dot{\gamma}t_c = (\sqrt{d_p g})zI. \tag{8}$$

Combining Eqns. 7 with 8 and recovering the constants from previous equations yields an expression for the dimensionless segregation velocity as

$$\bar{v}_s = \frac{v_s}{\sqrt{d_p g}} = \frac{z(\bar{\rho}-1)}{\beta_n\sqrt{\bar{\rho}}}I. \tag{9}$$

Thus, by using our new scaling, and determining a relationship between the collision frequency and inertia number (I), we yield a closed form equation for segregation velocity that includes only a single parameter, β_n. Figure 4 shows the relationship between segregation velocity (scaled with our new density relation) and I for all simulation conditions studied and includes a line corresponding to Equation 9 with $\beta_n = 0.16$.

It is interesting to note that the location of the segregation velocity (and μ_{eff} and z) transition corresponds to the value of I where the solid packing fraction decreases below a value of roughly $\phi \approx 0.52$ (see Supplementary Information). This value of the packing fraction is characteristic of a simple cubic lattice of equal sized spheres. While the rheological transition from linear $\mu_{eff}(I)$ to saturated μ_{eff} has been reported at varying values of I in the literature [1, 3, 8] (perhaps due to non-local effects [9]), examining these transitions in light of this packing fraction observation one notes that a simple cubic solids' fraction criterion would identify this critical I value irrespective of whether the system is 2D [1, 2] or 3D [3]. Regardless of the origin of this transition, here we show that recasting our data in light of the In-

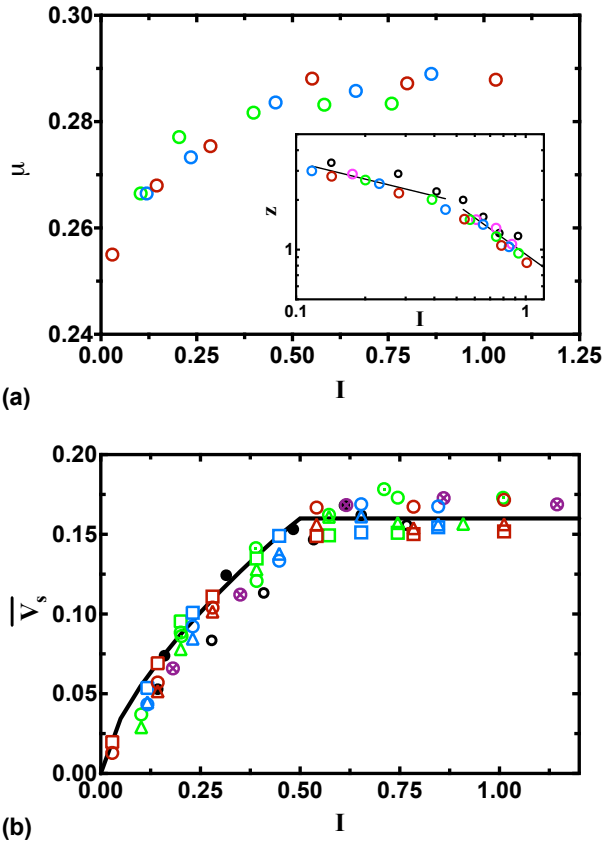

FIG. 4. Rheology and segregation in a sheared cell system under varying conditions of shear rate, density ratio, particle diameter and boundary conditions (symbols explained in Fig. 2). (a) This panel shows how the effective friction coefficient changes with the Inertia number. The inset shows the variation of the coordination number with I. Note that both rheological quantities display a regime change near a value of $I = 0.5$. Panel (b) shows the dimensionless segregation velocity rescaled with our proposed density scaling (Eqn. 7) and plot against I. Note that all results fall on a master curve regardless of gravitational condition, boundary condition, or other process parameters. The included line represents the model proposed in Eqn. 9.

ertia number collapses our results onto a single master curve for a wide variety of process variables, boundary conditions, and gravitational conditions and allows us to recognize – and predict the location of – a novel regime where the segregation rate saturates. This observation could have significant industrial importance as it could enable, for the first time, the rationale design of industrial processing methods that could lead to dramatically reduced segregation extents. Moreover, this work highlights that density-based segregation is not only coupled to the underlying flow rheology in shearing geometries, but that a true analogy exists whereby determination of the relationship between the coordination number and I, that is obtaining $z(I)$, can lead directly to a quantitative expression for the segregation velocity (and likely vice versa).

We wish to acknowledge the support of the International Fine Particle Research Institute (IFPRI) for partial funding of this work.

* jjmcc@pitt.edu

[1] G D R Midi. On dense granular flows. *The European physical journal. E, Soft matter*, 14(4):341–65, aug 2004.

[2] Pierre Jop, Yoãl Yoël Forterre, Olivier Pouliquen, Pierre Jop, and Yoãl Yoël Forterre. A constitutive law for dense granular flows. *Nature*, 441(7094):727–730, 2006.

[3] Ryan C. Hurley and José E. Andrade. Friction in inertial granular flows: competition between dilation and grain-scale dissipation rates. *Granular Matter*, 17(3):287–295, 2015.

[4] Julio M Ottino and Richard M Lueptow. Materials science. On mixing and demixing. *Science*, 319(February):912–913, 2008.

[5] R L Brown. The Fundamental Principles of Segregation. *Inst. Fuel*, October:15–19, 1939.

[6] J C Williams. The Segregation of Powders and Granular Materials. *Fuel Soc. J.*, 14:29–35, 1963.

[7] JM M Ottino and DV V Khakhar. Mixing and segregation of granular materials. *Annual Review of Fluid Mechanics*, 32:55–91, 2000.

[8] Frédéric Da Cruz, Sacha Emam, Michaël Prochnow, Jean Noël Roux, and François Chevoir. Rheophysics of dense granular materials: Discrete simulation of plane shear flows. *Physical Review E - Statistical, Nonlinear, and Soft Matter Physics*, 72(2):1–17, 2005.

[9] Ken Kamrin and Georg Koval. Nonlocal constitutive relation for steady granular flow. *Physical Review Letters*, 108(17):1–5, 2012.

[10] Emilien Azema and Farhang Radjai. Internal structure of inertial granular flows. *Physical Review Letters*, 112(7):1–5, 2014.

[11] E. Degiuli, J. N. McElwaine, and M. Wyart. Phase diagram for inertial granular flows. *Physical Review E - Statistical, Nonlinear, and Soft Matter Physics*, 94(1):1–11, 2016.

[12] François Guillard, Yoël Forterre, and Olivier Pouliquen. Scaling laws for segregation forces in dense sheared granular flows. *Journal of Fluid Mechanics*, 807:R1, 2016.

[13] H M Jaeger and S R Nagel. Physics of the Granular State. *Science*, 255(5051):1523–1531, 1992.

[14] Osborne Reynolds. On the Extent and Action of the Heating Surface of Steam Boilers. *Proceedings of the Literary and Philosophical Society of Manchester*, 14:1–5, 1874.

[15] Allan P Colburn. Relation between Mass Transfer (Absorption) and Fluid Friction. *Industrial & Engineering Chemistry*, 22(9):967–970, 1930.

[16] Ivo R. Peters, Sayantan Majumdar, and Heinrich M. Jaeger. Direct observation of dynamic shear jamming in dense suspensions. *Nature*, 532(7598):214–217, 2016.

[17] Dapeng Bi, Jie Zhang, Bulbul Chakraborty, and Robert P Behringer. Jamming by shear. *Nature*, 480(7377):355–358, 2011.

[18] D V Khakhar, J J McCarthy, J M Ottino, and T Shinbrot. Radial segregation of granular mixtures in rotating cylinders. *Phys. Fluids*, 9:3600–3614, 1997.

[19] Anurag Tripathi and D. V. Khakhar. Density difference-driven segregation in a dense granular flow. *Journal of Fluid Mechanics*, 717:643–669, feb 2013.

[20] Hongyi Xiao, Paul B Umbanhowar, M Ottino, and Richard M Lueptow. Modelling density segregation in flowing bidisperse granular materials. *Proc.R.Soc.A*, 472:20150856, 2016.

[21] MY Louge, JT Jenkins, H Xu, and BÖ Arnarson. Granular Segregation in Collisional Shearing Flows. *Mechanics for a New ...*, 2002.

[22] Yi Fan and K. M. Hill. Shear-induced segregation of particles by material density. *Physical Review E*, 92(2):022211, 2015.

[23] Siying Liu and J J Mccarthy. Validating Segregation Rate Models. *AIChE Journal*, in press:1–25, 2017.

[24] N. Khola and C. Wassgren. Correlations for shear-induced percolation segregation in granular shear flows. *Powder Technology*, 288:441–452, 2016.

[25] J. M. N. T. Gray and A. N. Edwards. A depth-averaged -rheology for shallow granular free-surface flows. *Journal of Fluid Mechanics*, 755(2014):503–534, 2014.

[26] J R de Bruyn and a M Walsh. Penetration of spheres into loose granular media. *Canadian Journal of Physics*, 82(6):439–446, 2004.

Nonlocal rheology tests in intermediate flows

Karen Daniels, NC State University
Nathalie Vriend, Cambridge University

Research Plan

The aim of this collaboration is to perform an additional test of the two nonlocal rheologies [Kamrin and Koval 2012, Bouzid et al. 2013] using a faster flow (intermediate flow, higher inertial number *I*) than is available in the annular Couette cell at NC State. Three different but complementary experiments will be conducted at NC State (PI: Daniels, PhD-student Zhu Tang) and Cambridge (PI: Vriend, PhD-student Amalia Thomas), using identical custom-made 2D photoelastic particles. This material allows for the direct measurement of the contact forces on each particle [Daniels, Puckett, Kollmer 2017], combined with particle tracking analysis for dynamical properties. Contact-force measurements can be time-averaged and coarse-grained to provide the necessary stress fields at the boundaries of the materials and both laboratories have expertise in running the open-source code (https://github.com/jekollmer/PEGS), written at NC State, to resolve contact forces.

The lab at Cambridge has an existing chute-flow apparatus (see Figure 1) and imaging system that can be slightly modified to provide similar data to what Zhu Tang is already taking in the annular flow geometry at NC State.

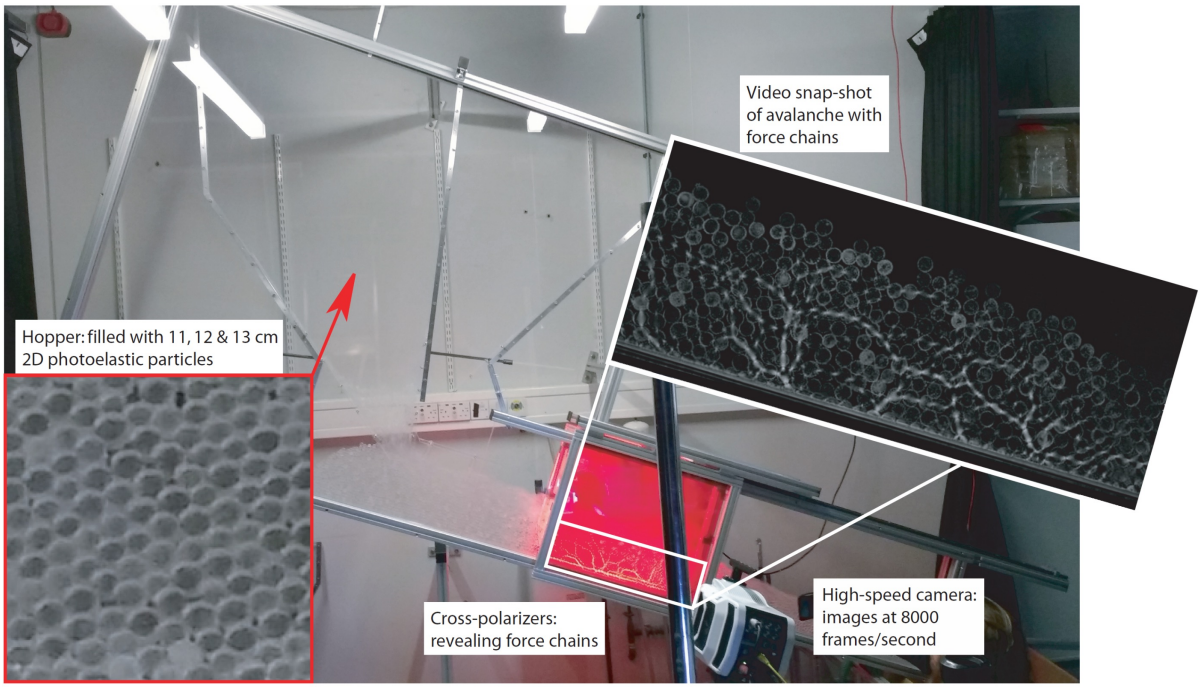

Figure 1: Photo of Cambridge chute flow apparatus, containing bespoke, superior-quality birefringent photoelastic particles (11 - 13 cm diameter, but other sizes available). It is a 3.5m x 4m experiment with two hoppers (allows for mixtures) and a 2m-long avalanche channel. Bottom left: photoelastic particles, middle right: movie still from an 8000 fps movie, showing the presence of dynamic contact forces and force chains, captured during the short-lived collisions present in avalanches.

The requirement, in all cases, is to make measurements of both the time-averaged downstream $u(r)$ and cross-slope $v(r)$ velocity profile and their fluctuations $u'(r)$ and $v'(r)$, normal stress field $P(r)$, and tangential stress fields $\tau(r)$ within the chute flow. The

measurements can be analysed as continuum fields by coarse-graining the experimental data, resulting in continuously spatially varying fields. An example measurement of the downstream velocity u(r) as a function of downstream distance, for both a rough (glued half-particles) and smooth base, is giving in figure 2. Of note is that the rough base flow thins considerably, but continuously increases linear shear value. The smooth flow on the other hand only changes slightly with downstream position, including in a roughly constant shear above a thin (~2-3 particle diameter) boundary layer.

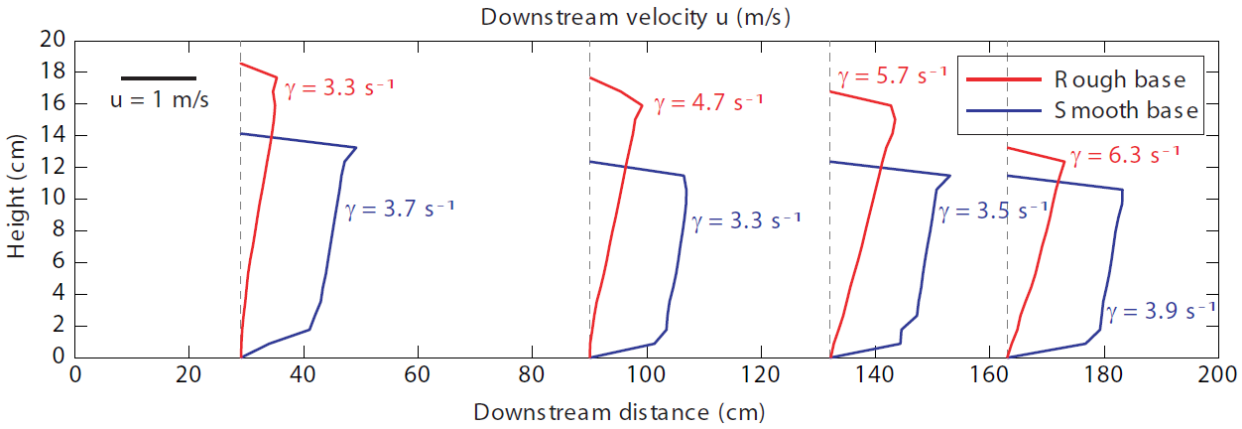

Figure 2: Sample measurement of *v(r)*, performed on a smooth vs. rough base.

By coarse-graining the 2D particle area, a coarse-grained density (or equivalent packing fraction) can be determined as a function of depth. Initial results provide a coarse-grained density of 1050 kg/m^3 and a typical shear rate of 3.5 s^{-1}. The pressure and shear stress can be determined from the stress tensor on every particle, obtained with resolving the stresses and force chains in a procedure outlined above and explained in figure 3.

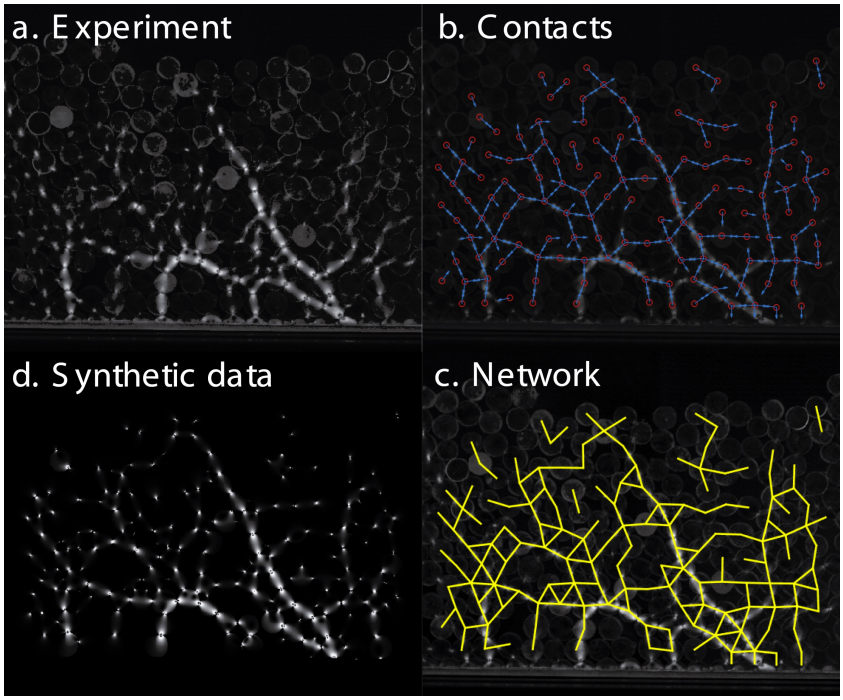

Figure 3: (a) Experimental snap-shot of movie, displaying instantaneous force chains, (b) contacts identified, (c) force network, (d) synthetic data resolved from a least-squared algorithm.

We are planning to conduct this calculation to get accurate measurements of the confining pressure. Here however, we can estimate the pressure assuming a hydrostatic pressure increase in the flow:

$$P = \rho g \cos(\theta)(h - z)$$

By taking a typical height of the flow of 15 cm, an average particle diameter of 1.2 cm, and an inclination of 20 degrees, the inertial number can be estimated as $I = 10^{-1}$. Given that I_0 can be calibrated experimentally, and has been measured as 0.02 – 0.2 for different particles, we expect to be in the inertial and collisional regimes.

By placing inserts in the existing channel, we can vary the angle of the chute by 5 – 10 degrees in each direction, therefore tuning the value of *I*. It is likely that an additional calibration measurement (to obtain μ_s) will be beneficial to the project. This will be performed in a plane shear cell at NC State, as sketched out in figure 4.

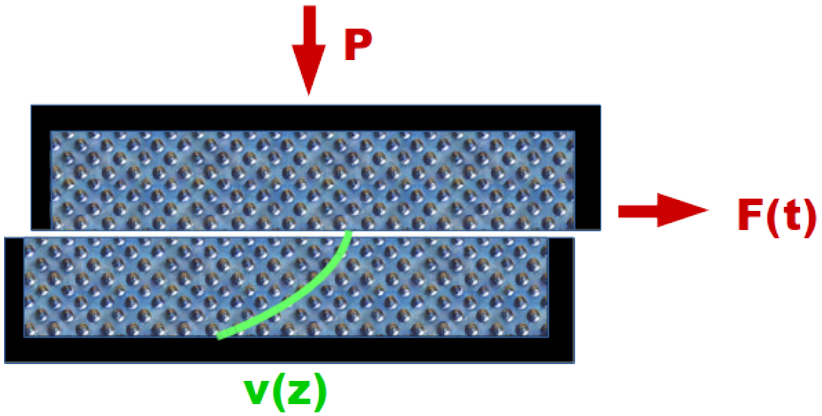

Figure 4: (a) Schematic of plane shear apparatus, to be constructed at NC State. It will contain the same photoelastic particles shown in Figure 1. The velocity profile will be measured for known confinement and pulling force.

The strength of this proposal is that identical custom-made photoelastic particles are used in three different experiments, probing different regimes in inertial number *I*. Amalia Thomas will travel to NC State in November to work with Zhu Tang to conduct the plane shear experiments (figure 4) and calibrate the photoelastic particles in the existing NCSU rheometer. In March, Zhu Tang will travel to Cambridge to work alongside Amalia to perform analysis on the chute-flow experiments (which are being conducted as part of a separate existing project).

When all data is collected, the two groups will work together to analyze the results and test the applicability of the two nonlocal theories. For the theories to succeed, both experiments will need to be modelled by a single set of 3 rheological parameters that are associated with this set of photoelastic particles. The parameters will be determined by the plane shear cell, and tested in the chute flow. By having a fast/slow pair of experiments, the tests will be particularly valuable. As time permits, the chute flow can also be run more slowly, but still with a free surface. This could be done either by lowering the angle of the channel (tricky given the mounting, but possible with inserts) or roughening the base (easier, through the use of inserts of different patterns and sizes).

References

Mehdi Bouzid, Martin Trulsson, Philippe Claudin, Eric Clément, and Bruno Andreotti. “Nonlocal Rheology of Granular Flows across Yield Conditions.” *Physical Review Letters.* **111**, 238301 (2013)

Karen E. Daniels, Jonathan E. Kollmer and James G. Puckett. "Photoelastic force measurements in granular materials" *Review of Scientific Instruments*. **88**, 051808 (2017)

Ken Kamrin and Georg Koval. “Nonlocal Constitutive Relation for Steady Granular Flow.” *Physical Review Letters.* **108**, 178301 (2012)

Budget

- 2 week visit of graduate student Amalia Thomas to NC (~ November 2017), to perform plane shear experiments: $2k
- 2 week visit of graduate student Zhu Tang to Cambridge (~ March 2018), to perform nonlocal analysis to chute flow data: $2k
- Nathalie Vriend and Amalia Thomas travel to annual IFPRI meeting in Edinburgh: $1k
- Additional hardware to modify chute apparatus in Cambridge: $2k
- Additional hardware to create plane shear apparatus in NC: $3k

Total Cambridge portion: $5k
Total NC portion: $5k